N77-32870

HARVARD COLLEGE OBSERVATORY

60 GARDEN STREET   CAMBRIDGE, MASS.

Final Report for NASA Contract NASW-2938

for the Development and Test of

Photon-Counting Microchannel

Plate Detector Arrays

for use on Space Telescopes

November 1976

J. Gethyn Timothy
Harvard College Observatory
60 Garden Street
Cambridge, MA., 02138

Introduction

Following the termination of the hardware phase of the Skylab Apollo Telescope Mount (ATM) instrument program the microchannel array plate (MCP) detector development program was continued under a separate contract from the Marshall Space Flight Center (MSFC). This contract, however, did not cover labor costs and consequently the development program came to a halt early in 1976 when the Harvard College Observatory (HCO) in-house funds for salaries were exhausted. At this time our proposal to NASA headquarters for the continuation of the program was accepted and contract NASW-2938 was issued with a period-of-performance from 8 March to 30 June 1976. The funds for this contract were accordingly used to cover in-house and subcontractor labor costs and to procure additional items of hardware not covered by the MSFC contract.

The following sections of this final report describe in detail the status of the MCP detector development program as of 30 June 1976 and outline the requirements for the continuation of the program.

2. Status of the MCP detector development program

Microchannel array plates (MCP's) offer a number of significant advantages over alternative photoelectric image-intensifying systems, such as the Digicon or the Intensified Charge Coupled Device (ICCD), particularly when operation in space is a consideration. Among the unique characteristics of the MCP's are:

- *Photon counting capability.*

- *Low applied potential ($\sim$2.5 kV).*

- *High gain (10^6 to 10^8 electrons per pulse).*

- *Can use opaque photocathodes (high quantum yields at ultraviolet wavelengths).*

- *Can operate in a windowless configuration.*

- *Rugged with high immunity to vibration.*

- *High immunity to external magnetic fields.*

- *High immunity to high-energy charged particle background at orbital altitudes.*

- *No cooling of multiplier required for photon counting.*

- *Direct development of channel electron multiplier (CEM) flown successfully on sounding rockets, orbiting satellites, and interplanetary spacecraft.*

- *Currently used extensively by military in low light level imaging systems.*

In order to exploit these capabilities we have initiated a development program to produce photon-counting detection systems which utilize the full sensitivity, dynamic range and photometric stability of the MCP's. Our MCP detection systems are

based on three fundamental and unique components:

1. *Feedback-free MCP's* which produce a high gain and a saturated output pulse-height distribution with a stable response over a wide range of ambient pressure. The performances of these devices scale directly from those obtained with conventional channel electron multipliers (CEM's).

2. *Multi-anode readout arrays* mounted in proximity focus with the output face of the MCP. The spatial resolution is defined solely by the geometry of the electrodes in the anode array with all output data coded in a digital format. The associated electronics operate at high speed with low power consumption. Multi-layer electrodes have been produced to provide information from a very large member of spatial elements without a commensurate increase in the complexity of the associated electronics.

3. *Multi-layer ceramic headers* to provide the electrical interface between the anode array in a sealed detector tube and the associated electronics. The headers form the basis of an exceptionally rugged modular tube assembly with a very high vacuum integrity. Furthermore, the multi-layer construction permits a wide variety of anode arrays to be accommodated with the same output connector format.

The current state of progress with the development of each of these components is described in detail in the following sections.

Feedback-free MCP's

The concept of combining the secondary-emissive dynode with the resistive potential-divider chain in an electron multiplier was first proposed by Farnsworth[1] in 1930. Since that time there have been many attempts to produce continuous-dynode multipliers, but it was not until 1956 that the first succesful results were obtained by Goodrich and Wiley[2] with the magnetic electron multiplier (MEM). However, the MEM has a number of disadvantages, particularly the large magnet structure and the limitation on gain imposed by ion-feedback problems arising from the straight geometry of the continuous-dynode strip. The continuous channel electron multiplier (CEM), which does not require a magnetic field to focus the secondary electrons, was first developed by Goodrich and Wiley[3] in 1958. Parallel development of the CEM was undertaken by Bendix Inc. (later Galileo Inc.) in the United States and by Mullard Ltd. in England from 1960 onwards.

The basic CEM consists of a semiconducting glass channel having an internal diameter of a few mm and a length-to-diameter ratio of the order of 50:1. The channel has a resistance of about 10^9 Ω, and the semiconducting inner surface can be used as the photocathode at EUV and soft X-ray wavelengths. A photon

or charged particle striking the wall of the channel releases an electron that is accelerated along the channel axis and drifts across to strike the wall with sufficient energy to release secondary electrons. This process is repeated throughout the length of the channel, the output pulses with an amplitude of the order of 10^6 to 10^8 electrons being collected at the anode. The gain is limited by the effects of space charge within the channel and the output pulse-height distribution has a quasi-Gaussian form. The resolution of the output pulse-height distribution can thus be defined as $R=\Delta G/\overline{G}$, where $\Delta G=$full width at the half-height of the distribution and $\overline{G}$ = modal gain value; resolutions of the order of 30 - 50% are typically obtained. The channel is curved to inhibit the acceleration of positive ions towards the cathode where they can initiate further avalanches and hence produce spurious output counts.

Since the performance of the CEM depends primarily on the length-to-diameter ratio of the channel and not on the absolute physical dimensions, the CEM can be reduced in size to a limit set by the available glass technology. Large numbers of these microchannels can then be assembled in a billet to form a microchannel array plate (MCP). Since each channel is an independent photomultiplier, the MCP is a detector with an imaging capability similar to that of a photographic plate, but with sufficient sensitivity to permit photon counting. However,

a basic problem with the operation of conventional MCP's is
that the microchannels have a straight geometry and are prone
to ion-feedback instabilities at high operating potentials
and high ambient pressures. For this reason the gain of a
single plate is generally limited to about 10^4, and the
device can be operated only at pressures below 10^{-6} Torr. It
is nevertheless possible to couple two MCP's in cascade, as
described in the publications in section 4 of this report.
MCP's can be obtained with the microchannels set at any bias
angle with respect to the face of the plate in the range from
$0 - 25^{\circ}$; hence a multiplier can be constructed with suitable
bias angles and plate orientations so that positive ions are
trapped at the interface between the two plates. The total
voltage across the plates can then be increaed to the level
at which a saturated output pulse-height distribution is
obtained.

We have earlier evaluated the performances of cascaded
MCP's at EUV wavelengths and have found the output pulse-height
distributions to be greatly inferior to those of conventional
CEM's.[4] Consequently, we have also investigated techniques
to eliminate the problems of ion feedback. The angled-field
MCP produced by Galileo, Inc., shows promise but suffers from
problems of gain reduction because of the accumulation of
space charge on the insulating strips in the channel wall used
to establish the angled electrostatic field.[5] Accordingly,

as the first step in our development program we obtained the first samples of MCP's in which the microchannels are curved to inhibit ion feedback in an identical manner to that employed in a conventional CEM.

. The degree of curvature required to inhibit ion feedback in a microchannel was determined in a series of tests at Mullard Ltd. It was found that 75-90% of the feedback ions are produced in the output 30% of the microchannel length.[6] Consequently, for the gains normally employed in MCP image intensifiers (10^3 to 10^4), a J-configuration microchannel with steep curvature at the output end would appear to be sufficient to effectively eliminate ion feedback. C-configuration or S-configuration microchannels, analogous to conventional CEM's will, of course, be required for use at the higher gain levels (10^6 to 10^8) required in pulse-counting detection systems. The practical realization of the curving process was first achieved at LEP[7] in France and preliminary results have been reported in the literature.[8] The facilities for quantity production of these devices have been constructed at Mullard Ltd. in England, with pilot production currently under way.

To date we have evaluated sample units of MCP's with both J- and C-configuration microchannels, the results of these tests will be described in the literature in the near future[9] now that publication permission has been given by Mullard Ltd. We are currently the *only* group in the United States working with these devices and can summarize the main results of our

investigations as follows.

First, in order to completely eliminate ion-feedback a curvature along the entire length of the microchannel is required. Consequently, a more steeply curved C-configuration of the form shown in Figure 1, or ideally an S-configuration, will provide the optimum MCP performance. It can be seen in Figure 2 that the curving process does not in any way affect the cross-sectional uniformity of the microchannels, the open area remaining at about 65%.

The high-voltage characteristic obtained when the C-plate was illuminated with extreme ultraviolet photons at a wavelength of 584 $\overset{o}{A}$ is shown in Figure 3. The dark count from the entire plate was extremely low until the onset of ion-feedback at 2400V, the dark count rate at 2300V being equivalent to 3×10^{-2} count s^{-1} mm^{-2}. It can be seen in Figure 4 that a good saturated pulse height distribution was obtained when the MCP was illuminated by a beam of 584 $\overset{o}{A}$ photons incident normal to the input face of the plate with only a small tail of low-amplitude pulses caused by multiple reflections with the microchannels. We attribute this excellent performance to both the increased length-to-diameter ratio of the microchannels and to the effect of the relatively large 12° bias angle at the input face of the plate.

The dynamic range of the MCP is limited by the high resistance of the microchannels since the gain of the MCP will be reduced at high count rates because of the inability of

C-PLATE MCP

80:1 LENGTH-TO-DIAMETER RATIO

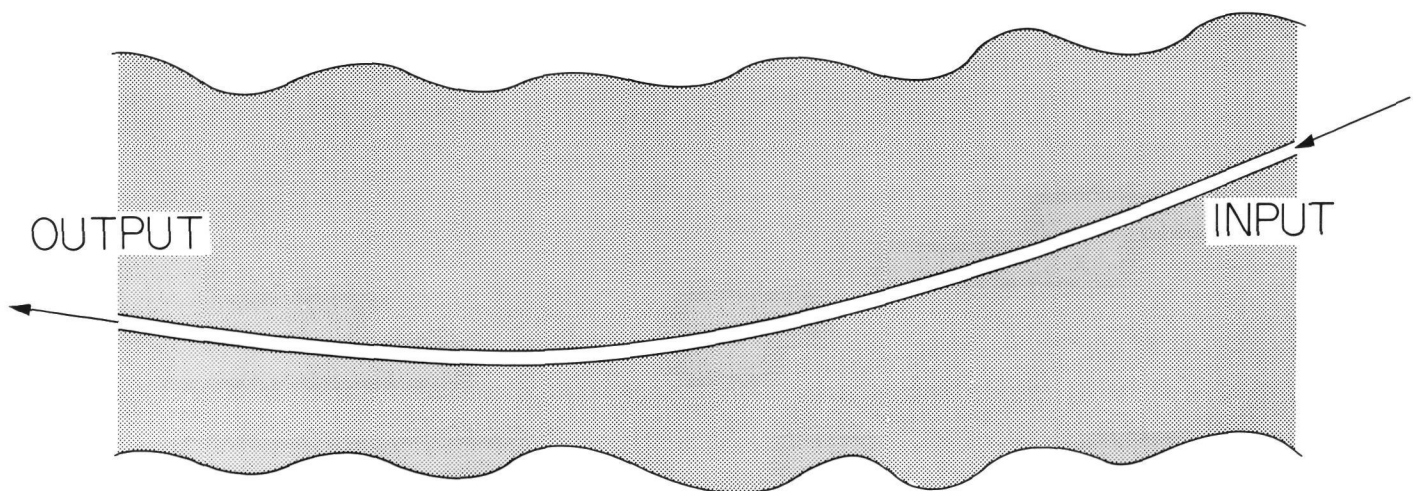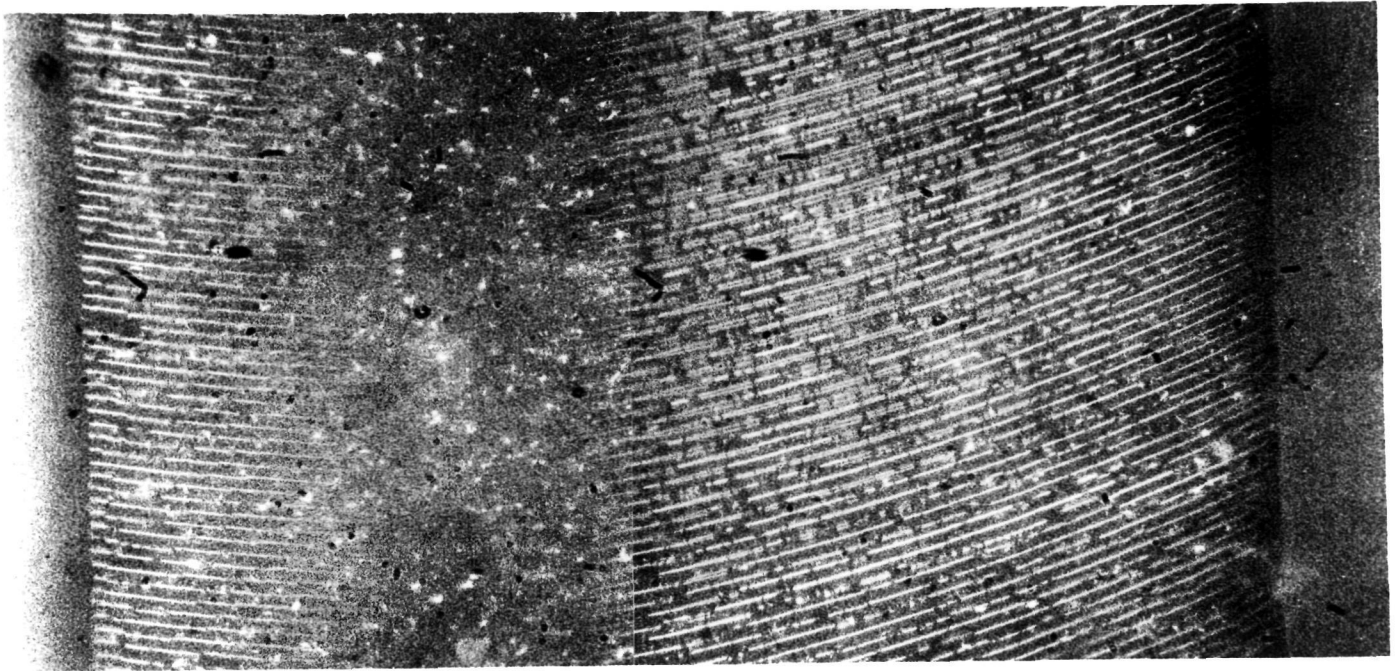## 12.5 μ CHANNELS

OUTPUT

INPUT

Figure 1. C-plate MCP (side view of plate). Nominal length-to-diameter ratio 80:1, effective length-to-diameter ratio 100:1, allowing for curvature of the microchannels.
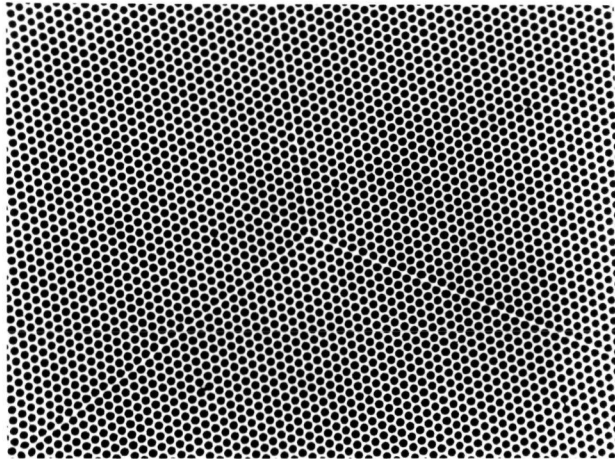
C-PLATE MCP

80 : 1   LENGTH-TO-DIAMETER RATIO
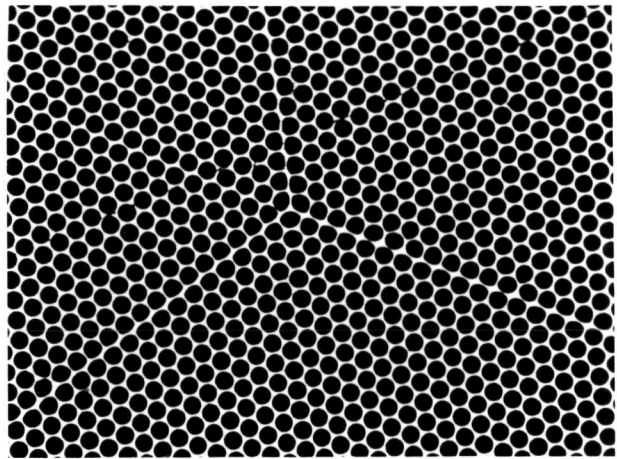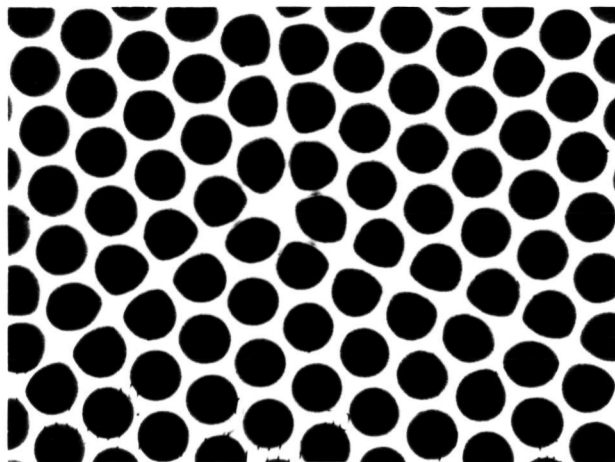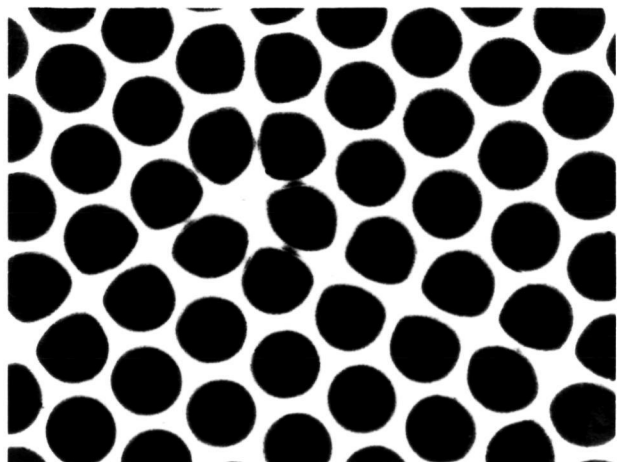
12.5 μ CHANNELS

Figure 2.   Face of C-plate MCP.

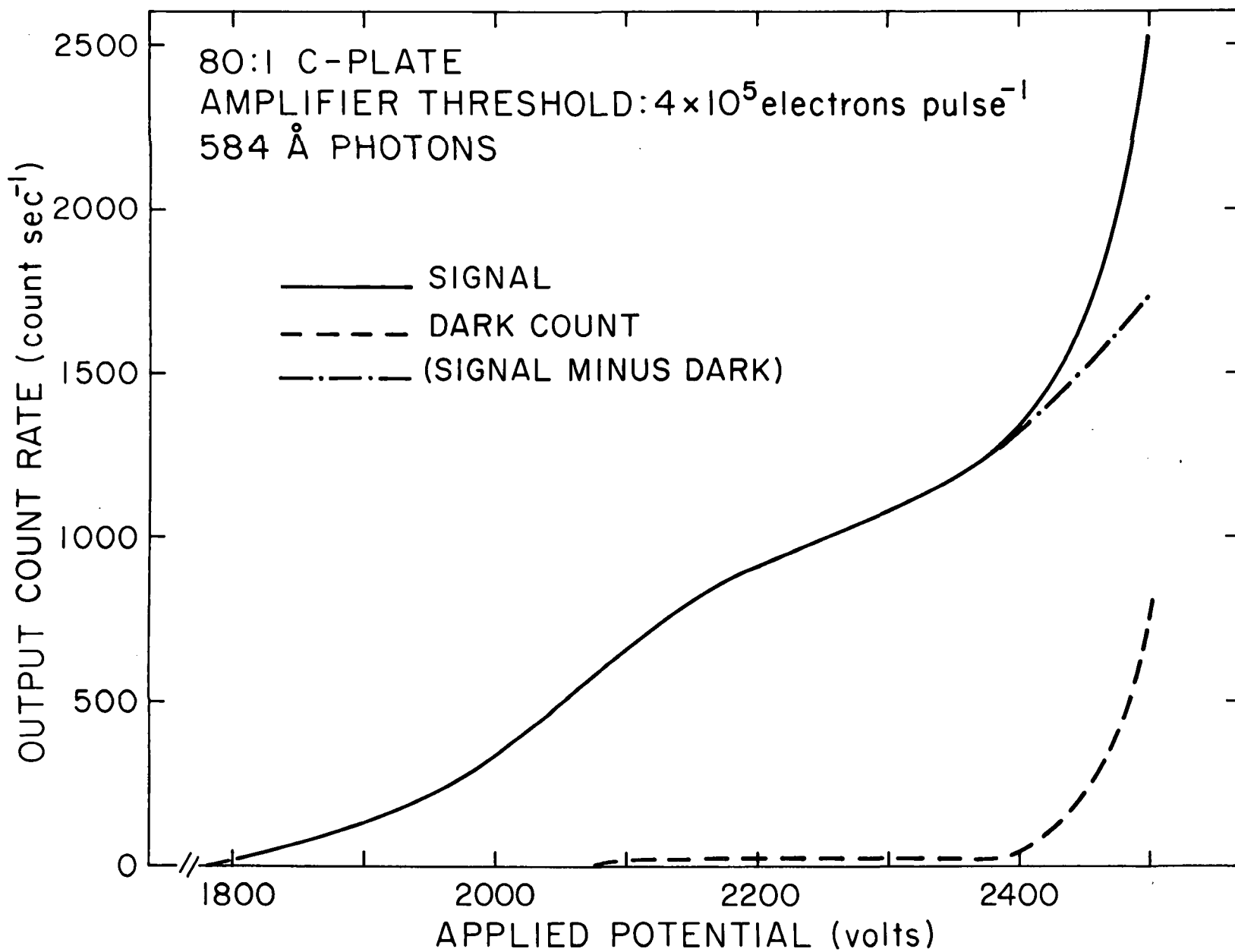Figure 3. High-voltage characteristic of C-plate MCP. Illuminated area of plate 6.8 mm^2. Total area of plate contributing to the dark count 573 mm^2. Pressure 2 x 10^{-7} Torr.
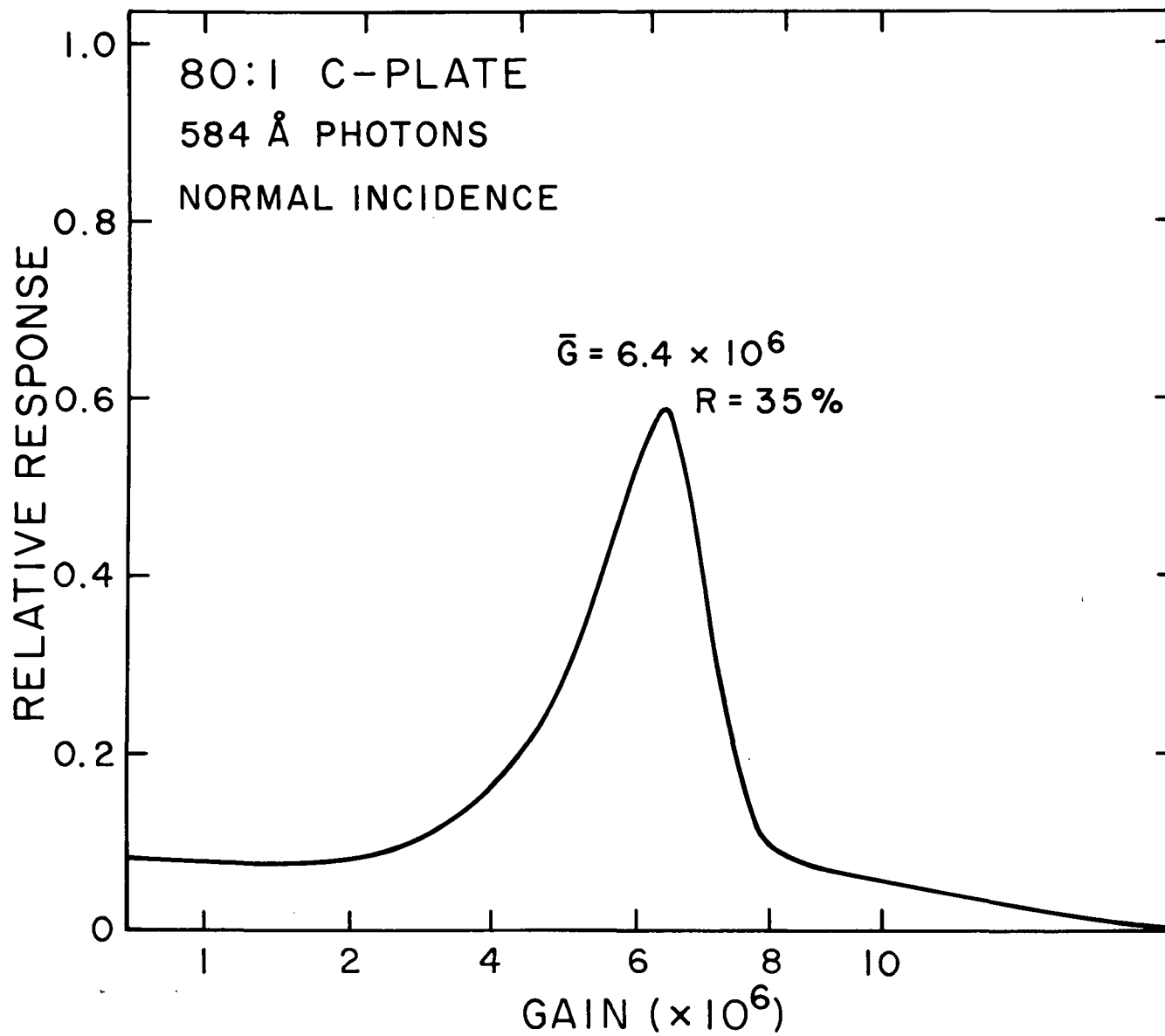
Figure 4. Output pulse-height distribution for C-plate MCP at an applied potential of 2300V. Pressure 2 x 10^-7 Torr.

the walls of the microchannels to supply charge. In order to overcome this problem we have evaluated the performances of high-conductivity MCP's (R<200 M Ω for 27-mm diameter plate). These tests are still proceeding; however, we have already established that we can maintain a linear response to count rates in excess of 10 count. s^{-1} (Poissonian arrival) for a 30 x 300 (micron)^2 pixel.

We will continue to evaluate the effect of the conductivity of the MCP's on the dynamic range as a factor of major importance. Our goal is to obtain a performance level of a 10% loss of signal at count rates in excess of 500 count. s^{-1} (Poissonian arrival) for a 30 x 300 (micron)^2 pixel, referenced to an amplifier threshold of 2 x 10^5 electrons. pulse^{-1}.

A number of factors play a critical role in determining the maximum count rate of the MCP. First, it is essential to suppress ion-feedback since even though it is possible to discriminate against the low-amplitude feedback pulses in the electronics there will be a significant current drain at the output end of the microchannel. In addition, we find that approximately 50% of the output charge is collected by the electrode on the output face of the MCP which is allowed to penetrate the microchannels to a depth of about one channel diameter. This technique called 'endspoiling' is used to collimate the output electron cloud when the MCP is used at low gain (10^3 to 10^4) in a proximity-focused image intensifier.

Since the endspoiling does not have a focusing effect on the space-charge saturated electron cloud it will be necessary to determine experimentally the amount of end-spoiling needed to minimize the collection of charge when the MCP is operated in a pulse-counting mode.

As the result of tests of MCP's having resistances ranging from about 140 M Ω to 5000 M Ω we have established that the gain in a curved microchannel, is to a first order, independent of the conductivity and dependent solely on the physical length. This is a critically important result since it means that the performances of the feedback-free MCP's operated in a space-charge saturated mode scale directly from those of conventional CEM's. The gain of the MCP's will thus lie in the range 10^6 to 10^7 for microchannels with diameters of the order of 10 to 50 micron and length-to-diameter ratios of the order of 100:1. This gain is more than adequate for our pulse-counting readout systems and, furthermore, corresponds to a charge density in the microchannel of the same order as that in a CEM. We can accordingly expect the lifetime characteristics of a feedback-free MCP to be at least equal to those of a CEM in terms of a total accumulated count per unit area.

We are currently awaiting delivery of the first MCP's with S-configuration microchannels that are being produced to our specifications by Mullard Ltd. (purchased through Amperex, Inc.). The evaluation of these MCP's will be the prime task in the

continuing development program. In addition, we expect to obtain feedback-free MCP's from a second and U.S. manufacturer, namely Galileo Electro-Optics Corp., Sturbridge, MA.

Multi-anode readout arrays

In order to exploit the full sensitivity, dynamic range and photometric stability of the MCP, it is necessary to employ pulse-counting readout systems working directly at the output of the plate. A number of systems of this type have been described in the literature;[10,11,12] however, these systems have been designed to employ a limited number of amplifiers, two for a one-dimensional array and four for a two-dimensional array, and consequently have significant limitations in terms of dynamic range. A sophisticated version of this type of readout system, employing a considerably larger number of amplifiers (34), to increase the dynamic range has been developed for use in the X-ray imaging detector on the NASA HEAO-B spacecraft.[13] The published performance data for these readout systems show them to be highly efficient for applications where very low signal levels are obtained, such as galactic X-ray astronomy. In order to record the high signal levels obtained from laboratory ultraviolet and soft X-ray sources or from telescopes for solar or stellar observations at ultraviolet and visible wavelengths a detection system with larger dynamic range is required. This type of detector can in principle have the required dynamic range; however, this has not

yet been demonstrated although a modification for this purpose
is currently under study.

We are currently developing photon-counting detector arrays
of high dynamic range, employing discrete anodes in proximity-
focus at the output of the MCP, in which each anode (i.e. picture
element) is connected to an individual amplifier and counting
circuit. In this type of readout system the spatial resolution
is defined by the geometry of the anode electrodes rather than
by charge-amplitude division or timing-discrimination networks
in the data-handling electronic circuits. The advantages of
simpler electronic circuits operating at high speed and low
power are thus traded for increased complexity in the fabrica-
tion of the anode array.

The *discrete anode* system, however, has its own limitations
in that the total number of picture elements (pixels) is limited
to about 500 by the currently available electronic and ceramic
technologies. To overcome this limitation we have recently
designed a novel readout system, which can be produced in a
variety of two-dimensional and extended one-dimensional formats,
and with which photometric data from (n x m) pixels are read
out with a total of (n + m) amplifier and discriminator circuits.
The *coincidence-anode* readout system employs two sets of
orthogonal linear anodes (row and column), insulated from each
other, but exposed to the output face of the MCP. The output
charge from the MCP is divided between the row and column
anodes at the intersection where the event occurs, allowing the

spatial location to be identified by the coincident arrival of pulses on the appropriate row and column anodes. The readout-array can be laid out in a full two-dimensional format, or can be "unfolded" to produce an extended linear array which is ideally suited for spectroscopy. Details of the breadboard units of both types of readout system are described in the publications in section 4 of this report.

We are currently well under way with the production of prototype sealed photon-counting detector arrays employing feedback-free MCP's and examples of both the discrete-anode and the coincidence-anode readout systems. The operating characteristics of the two multi-anode MCP detector arrays are listed in table 1. Since both detector tubes must be sealed each anode array is being fabricated as an integral part of a multi-layer ceramic header and is described in detail in the next section.

The (10 x 10)-pixel array (see Figure 11) is being produced initially to meet the requirements of Air Force Cambridge Research Laboratories (AFCRL). However, the 1.2 x 1.2 mm^2 pixel format is ideal both for parametric studies of MCP per-formances and for investigating photocathode deposition tech-niques. Consequently, we are also employing units of this type as part of the NASA development program in addition to fabricat-ing the (2 x 1024)-pixel array (see Figure 14). Furthermore, many of the required characteristics of the data-handling and display electronics are common to both types of detector array.

Table 1   Operating Characteristics of Prototype MCP Detector Arrays

a) **100-Pixel Discrete-Anode Array**

Number of Pixels: 10 x 10

Number of Amplifiers: 100

Pixel Dimensions: 1.2 x 1.2 mm^2

Dynamic Range: 10% loss of count rate at 5 x 10^4 count. s^{-1}. pixel^{-1} (Poissonian arrival)

Photocathode: CsI (opaque)

Window: MgF$_2$

Quantum Efficiency: >30% at 1216 Å

Wavelength Range: 1160 to 1900 Å

b) **(2 x 1024)-Pixel Coincidence-Anode Array**

Number of Pixels: 2 x 1024

Number of Amplifiers: 160

Pixel Dimensions: 30 x 300 µ^2 (Two linear arrays of 1024 pixels separated by 1mm)

Dynamic Range: 10% loss of count rate at >10 count. s^{-1}. pixel^{-1} (Poissonian arrival) Total count rate from array 10^5 count. s^{-1} (1 µs pulse-pair resolution)

Photocathode: Bialkali (opaque) or trialkali

Quantum Efficiency: >10% at 4000 Å

*Wavelength Range: 3000 to 6000 Å (bialkali)
         <3000 to 8000 Å (trialkali)*

Consequently, we have constructed a general purpose laboratory data-recording and display system, based on an existing MAC-16 minicomputer, which can accommodate both the (10 x 10)-pixel discrete-anode array and the (2 x 1024)-pixel coincidence-anode array. A block diagram of this system, which will also be used to support the tests of the detectors at ground-based telescopes, is shown in Figure 5.

The output charge from the MCP is collected on a single electrode in the discrete-anode array. We have accordingly designed and built charge-sensitive amplifier and discriminator circuits capable of operating on a threshold charge output from a feedback-free MCP in the range from 2×10^5 electrons pulse^{-1} (3.2×10^{-14} C) to 4×10^6 electrons pulse^{-1} (6.4×10^{-13} C). The discriminator threshold can be varied between these limits by external control and the threshold level has been shown to be completely stable over the temperature range from 0 to 70° C. The basic amplifier and discriminator circuit, which has a quiescent power dissipation of 25mW and a pulse-pair resolution of 1μs, is shown in Figure 6. Minor modifications to this circuit have provided an increase in the pulse-pair resolution to 300 ns with an increase in the quiescent power dissipation of only 2mW to 27mW. This power consumption is an order of magnitude less than our earlier design based on conventional operational amplifiers. The circuits are easily fabricated using standard printed circuit techniques (see Figure 7), and the components are compatible with fabrication in thick-film hybrid format.
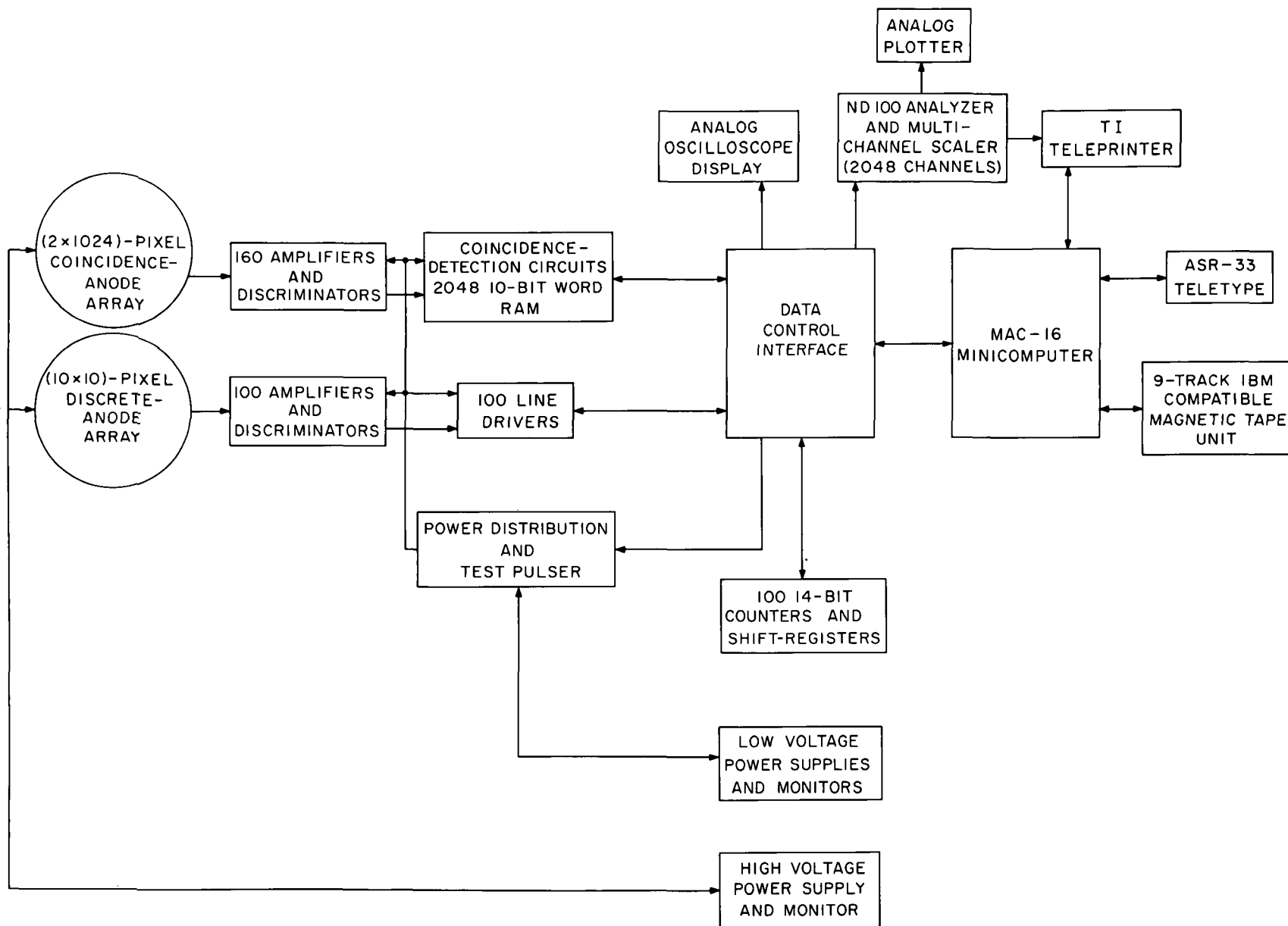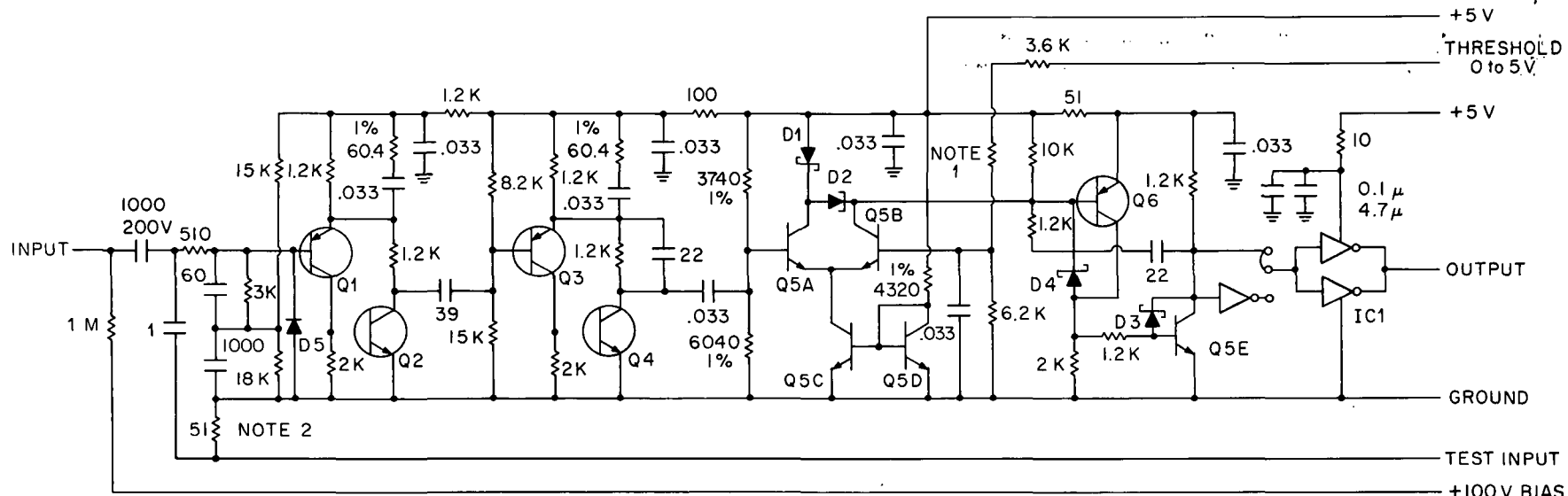
Figure 5.   Block diagram of laboratory data-handling and display system.

Q1,Q3,Q6 — 2N4917
Q2,Q4   — EN2369A
Q5   — CA3086
D1,D3,D4 — HP2800
D2   — IN4395B
IC1   — 74C901

NOTE 1 - SELECT FOR PROPER THRESHOLD

NOTE 2 - ONLY ONE 51 Ω TEST INPUT
         TERMINATION RESISTOR PER BOARD

Figure 6. Schematic of MCP charge-sensitive amplifier and discriminator circuit.

0.5 mm divisions

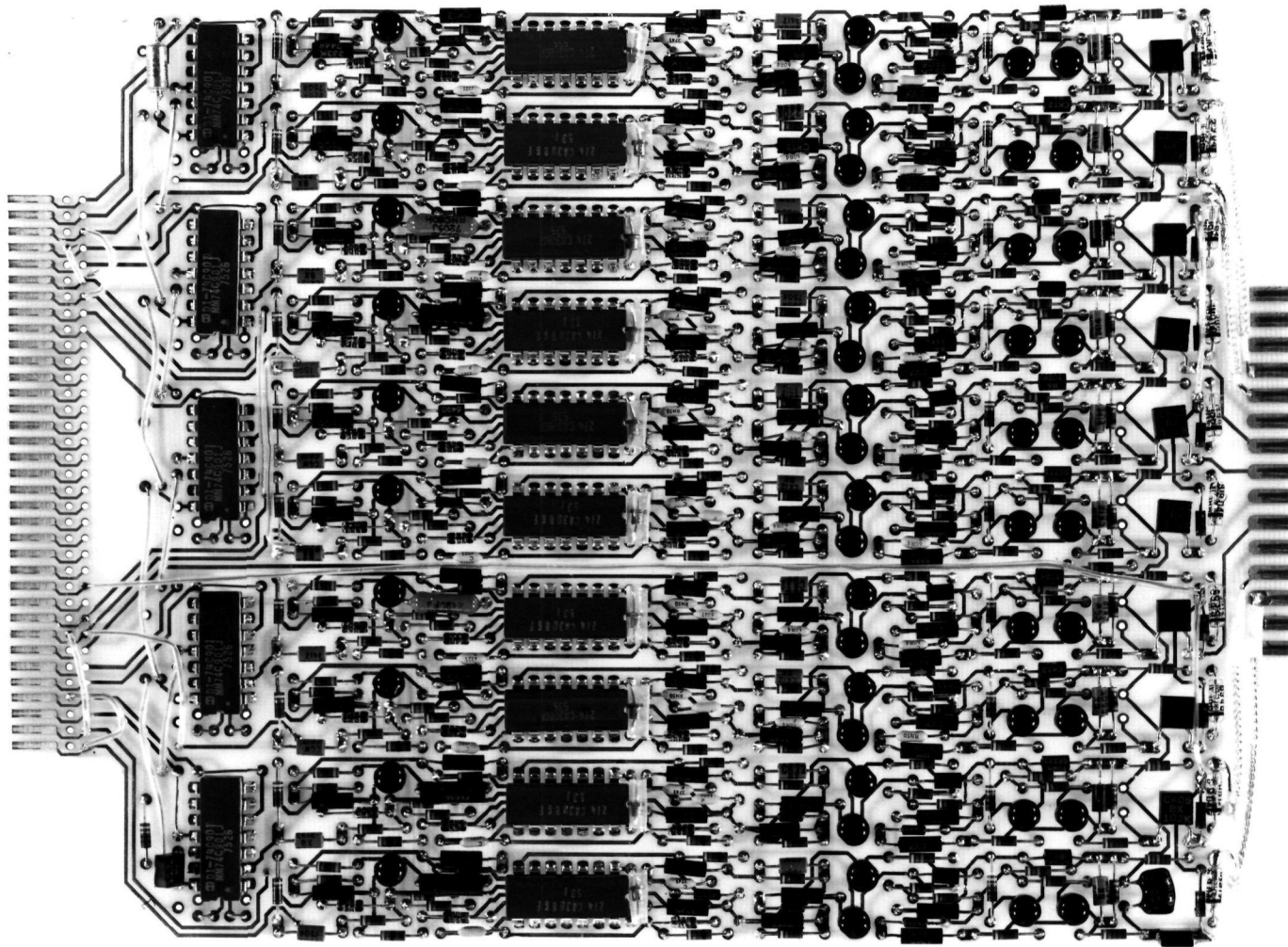10 20 30 40 50 60 70 80 90 100 110 120 130 140 150 160 170 180 190 200 210 220

Figure 7. Assembly of 10 MCP amplifier and discriminator circuits constructed with discrete components on a printed circuit board.

The reduction in size obtained with the production of 10 amplifier and discriminator circuits in hybrid format can clearly be seen in Figure 8. All circuits have so far been fabricated from discrete components and the production of thick film hybrid units has a high priority in the continuing program since each card is 0.1 inches thick allowing it to plug directly into the output connector in the multi-layer ceramic header (see Figure 11).

The output data from the (10 x 10)-pixel array are accumulatd in 100 14-bit counters and sequenced to the mini-computer for recording and display. The output data from the (2 x 1024)-pixel array are fed to a coincidence-detection and address-generation circuit and stored in a 2048 10-bit word Random Access Memory (RAM) (see Figure 9). The output from the RAM is then sequenced to the main computer on command. The RAM has been constructed using Silicon-on-Sapphire (SOS) C-MOS memory elements and the complete system occupies a volume of 9 x 4 x 7 inches^3 with a total power consumption of 5W (excluding amplifier and discriminator circuits). The integration of the RAM with the laboratory data-recording and display system will be one of the first tasks under the continuing program.

We have discovered, as a direct result of the detailed design work for the (2 x 1024)-pixel array, a method of producing very large arrays using the coincidence-anode read-out system. Briefly, we intend to use a fourfold coincidence

10 20 30 40 50 60 70 80 90 100 110 120 130 140 150 160 170 180 190 200 210 220 230 240 250 260 270 280 290 300
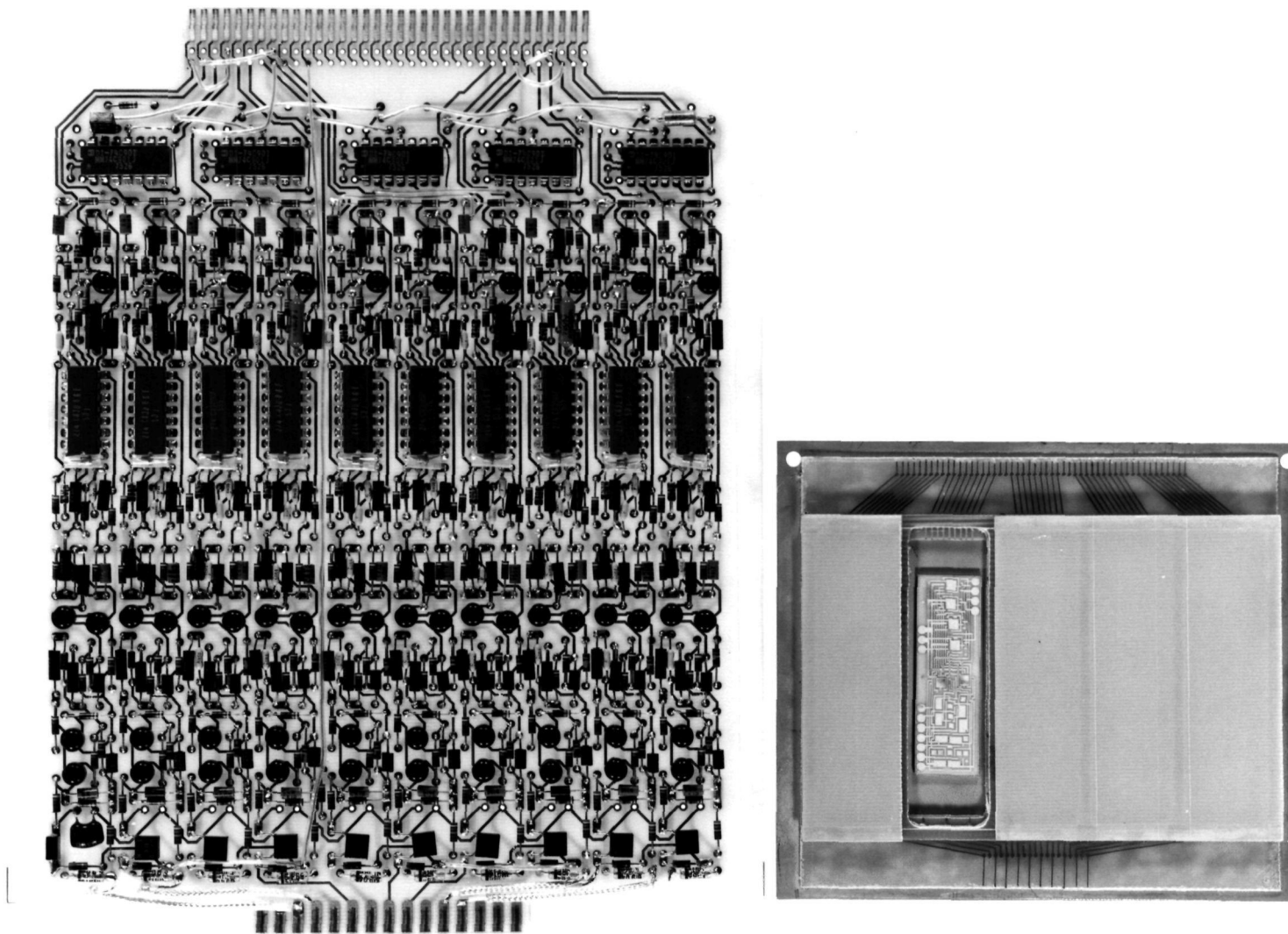

Figure 8. Comparison of layout of 10 MCP amplifier and discriminator circuits as presently constructed with discrete components and as planned in thick-film hybrid format.
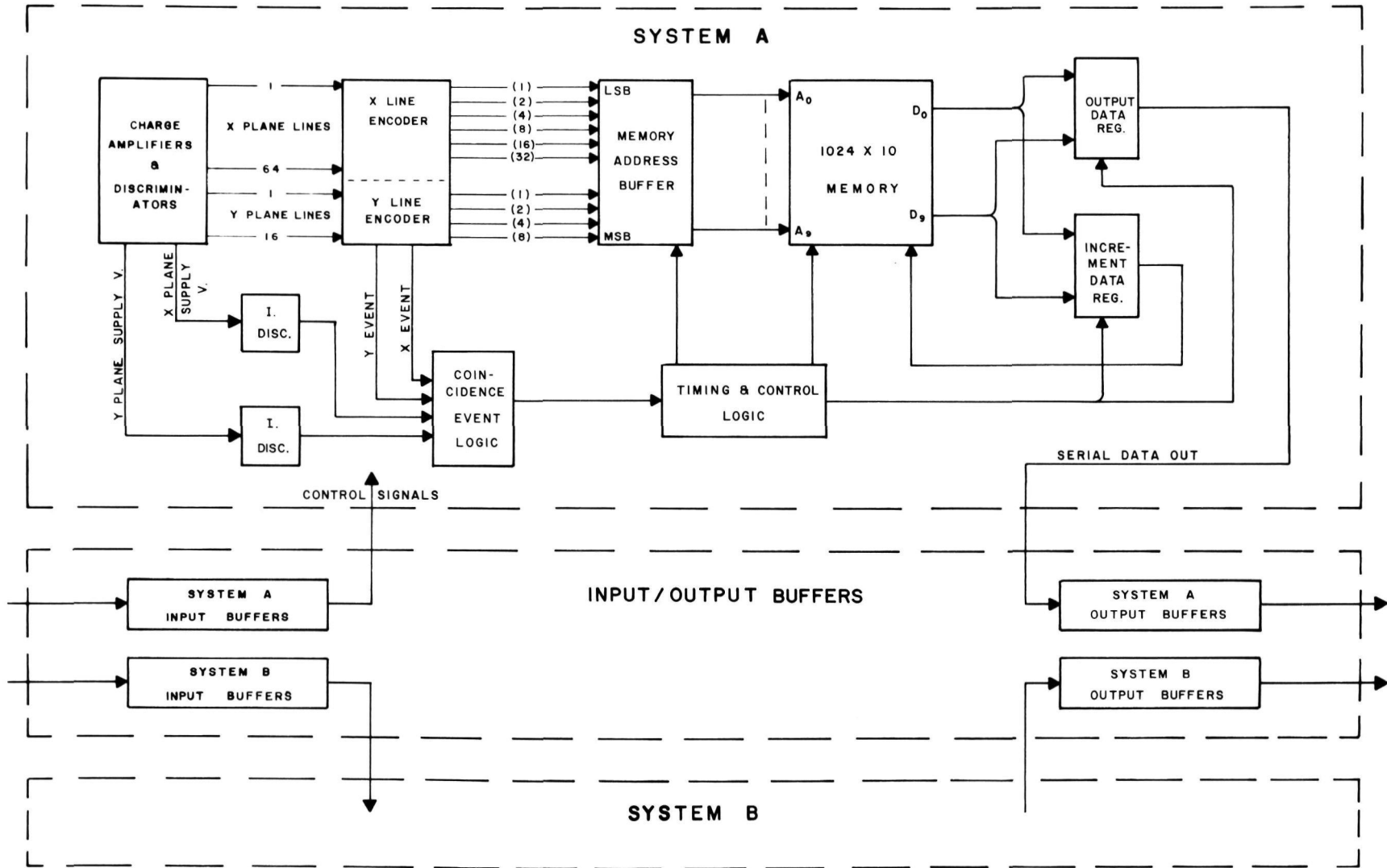
Figure 9. Block diagram of (2 x 1024)-pixel coincidence-anode detection system.

system in which (a x b x c x d) pixels are readout using
(a + b + c + d) amplifier and discriminator circuits. It
will be necessary to investigate the layout of the proposed
arrays in detail before we can exactly define the upper limit
on the size of such a system. The practical limits will be
set first, by the distributed capacitance in the array which
reduces the amplitude of the signal at the input of the
amplifier, and second, the interelectrode capacitance which
controls the level of crosstalk between adjacent pixels.
However, it is already clear from our preliminary investiga-
tions that it will be possible to build an array of greater
than (400 x 400) pixels with a spatial resolution of about
30 x 30 μ^2 using less than 160 amplifiers. For example a
(400 x 400)-pixel array will require a minimum of
(20 + 20 + 20 + 20) amplifiers. The cycle time of the
coincidence-detection, address-generation circuits and RAM
will be essentially identical to that for the (2 x 1024)-pixel
system, i.e. $\lesssim$1µs. A block diagram of the proposed (400 x
400)-pixel system is shown in Figure 10. Having been
informed by Raytheon Company that they expect the (400 x 400)-
pixel array to be easier to fabricate than the (2 x 1024)-
pixel array since fewer metallic layers are required, we
plan to immediately initiate the detailed design and
fabrication of this anode array as part of the continuing
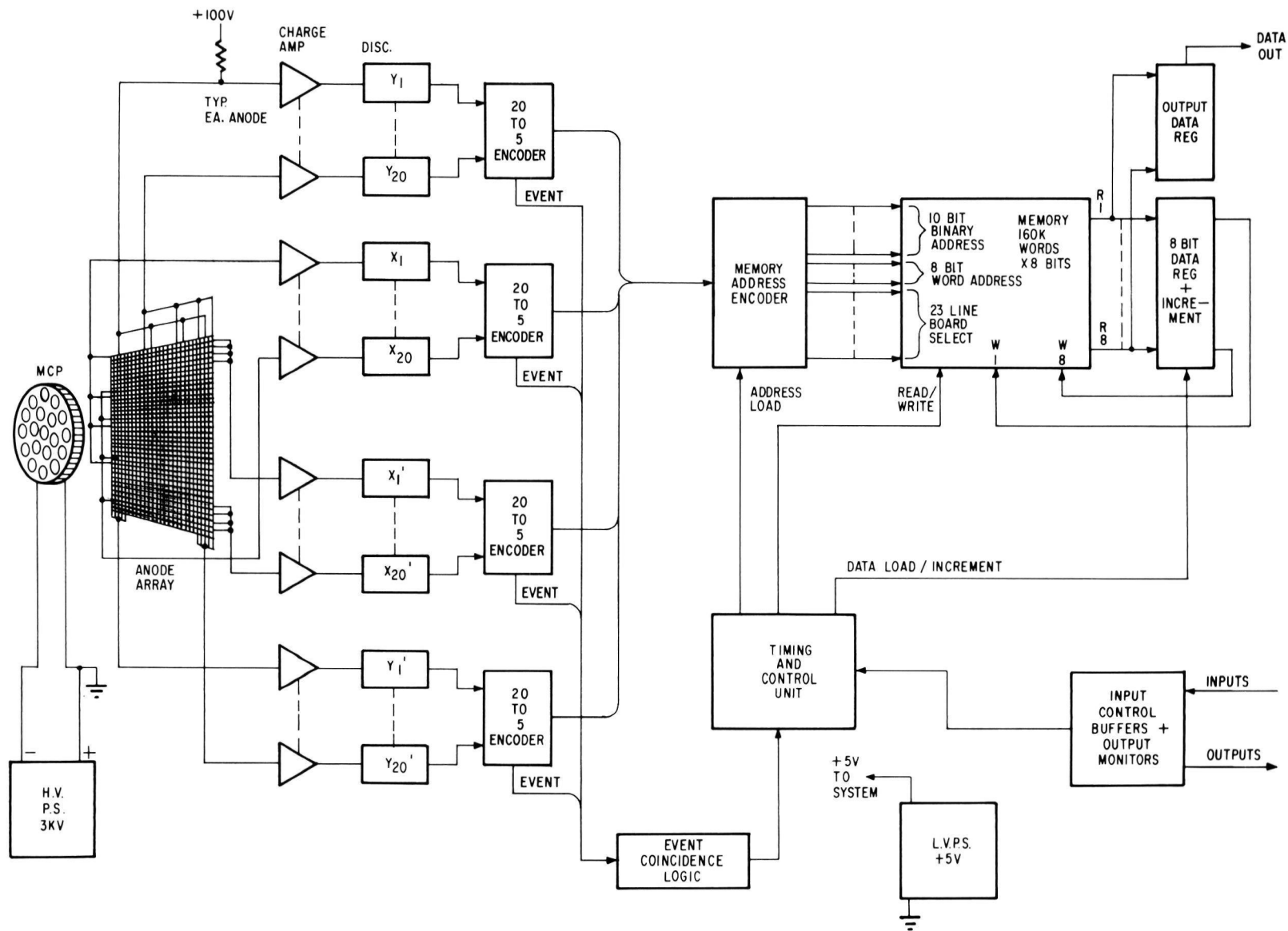program.

Figure 10. Block diagram of proposed (400 x 400)-pixel coincidence-anode detection system.
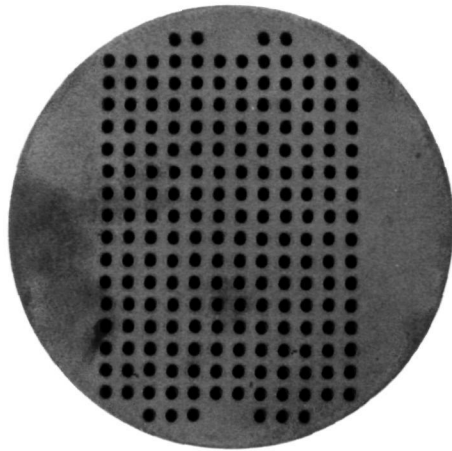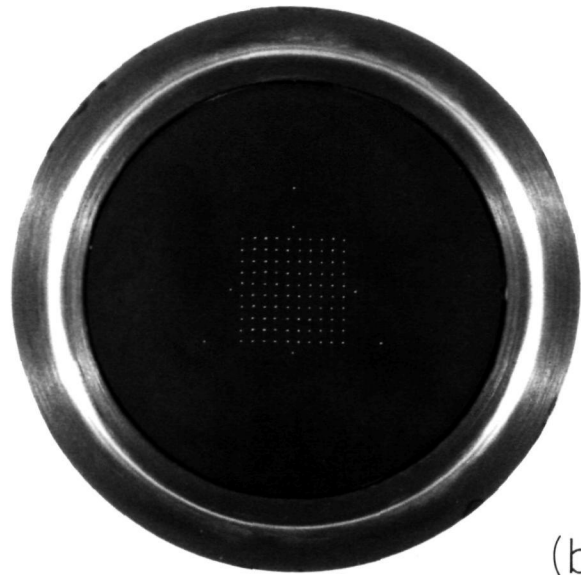
Multi-layer ceramic headers

The electrical interface between the anode array in the evacuated detector tube and the external electronics is a multi-layer ceramic header. Two types of headers have so far been fabricated, type I for the (10 x 10)-pixel discrete-anode array and type II for the (2 x 1024)-pixel coincidence-anode array. Both headers have a diameter of 2 inches, a thickness of 0.12 inches and identical output (airside) connector pin configurations, each header being laminated from eight ceramic wafers containing the via-holes and electrodes required to provide the conducting paths through the assembly. The layout of the electrodes has been designed to minimize the cross-capacitance and hence the cross-coupling of the output signals from the anodes. In the (10 x 10)-pixel array the anode dimensions are large enough to permit deposition directly on the type I header electrodes (see Figure 11). The type I header accordingly accommodates a total of 108 electrodes; 100 for the 10 x 10 pixel electrodes, 4 for guard electrodes, 1 for a 50-μ wide inter-pixel screening electrode and 3 for combined MCP support pads and output-face contact electrodes.

The proximity focus requirements dictate that a gap of 30 to 50μ be maintained between the output face of the MCP and the anode array. The vacuum side of the header was accordingly lapped to a flatness of better than 3μ prior to the deposition of the anode array. Furthermore, the thickness of the header was calculated to ensure that the deformation

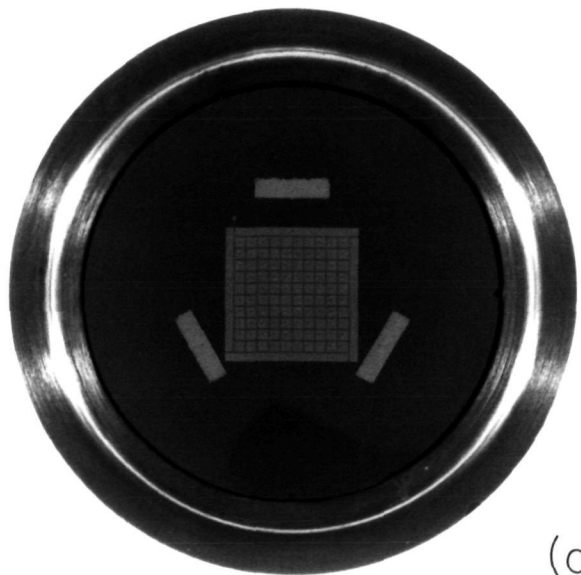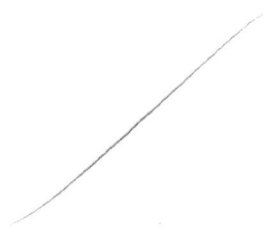60 70 80 90 100 110 120   60 70 80 90 100 110 120

(a)   (b)

(c)   (d)

TYPE I

100-ELECTRODE ARRAY

MULTI-LAYER CERAMIC HEADER

Figure 11. Type I multi-layer ceramic header.

a. Output electrodes in basic header.

b. Vacuum side electrodes with kovar flange attached.

c. Output connector sockets and guide pins attached.

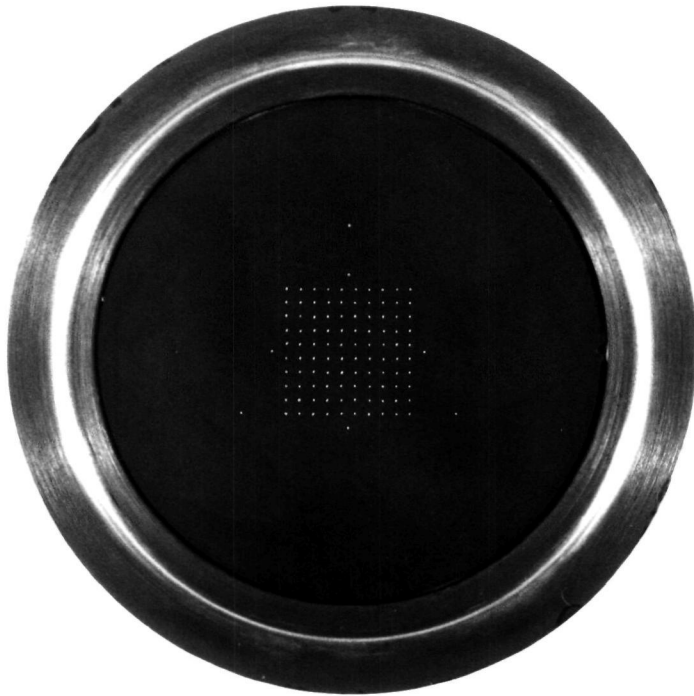d. Anode array and combined MCP connector and support pads deposited.

with one atmosphere of external pressure on a sealed tube does
not exceed 2 to 3μ at the center of the array. As a final pre-
caution, the MCP is mounted directly on three support pads
deposited on the header adjacent to the anode array. These
gold pads are about 35μ thick and are deposited on electrodes
in the header (see Figure 11) which are used to establish
the electrical connection to the electrode on the output face
of the MCP. The surface finish of the lapped header is of
sufficient smoothness to permit the deposition of the 50-μ thick
screening electrode between the pixel electrodes without breaks.

The precision of the (2 x 1024)-pixel coincidence-anode
array is such that it cannot be deposited directly on the
lapped surface of the ceramic header. Accordingly, this array
is deposited on a separate ultra-smooth ceramic substrate
which is subsequently bonded to the inside face of the type II
header. The vacuum-side electrodes in the type II header
(Figure 12) are therefore arranged in two annuli around the
inside edge allowing connections to be made by wire-bonding
between the header electrodes and pads on the periphery of
the anode substrate. The type II header accommodates a total
of 170 electrodes; 160 for the pixel electrodes, 2 for the
guard electrode, 3 for the combined MCP support pads and
output-face contact electrodes and 5 spares.

The (2 x 1024)-pixel coincidence-anode array is an
exceedingly complex structure comprising a total of six
conducting and insulating layers. The layout of the x- and
y-plane conducting electrodes is shown in Figure 13. The

Figure 12. Vacuum-side electrode configurations in type I and type II multi-layer ceramic headers.
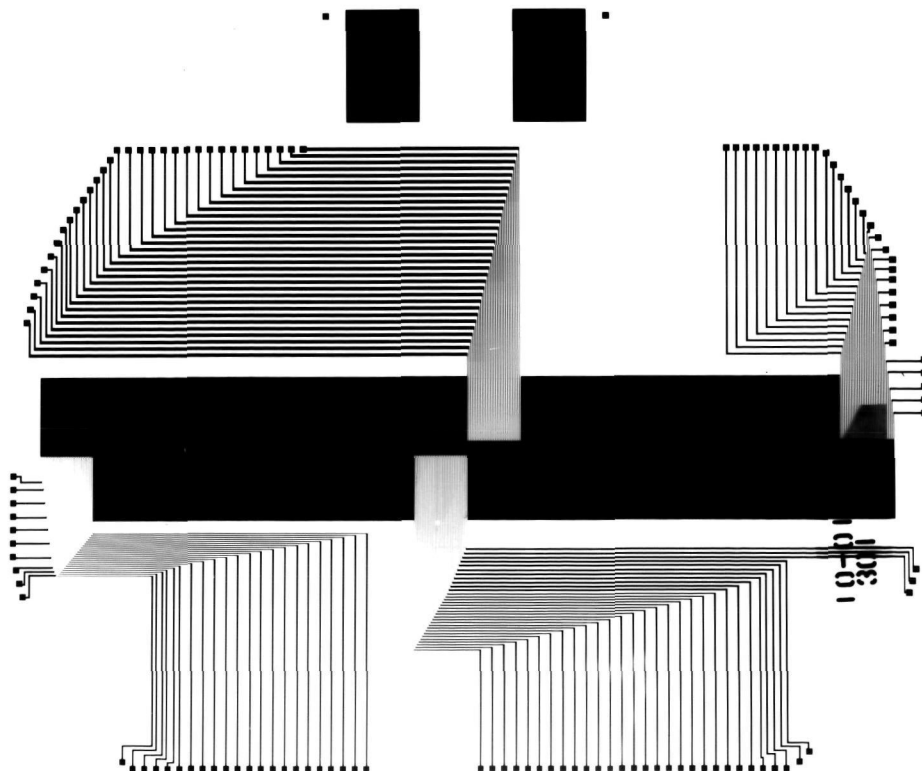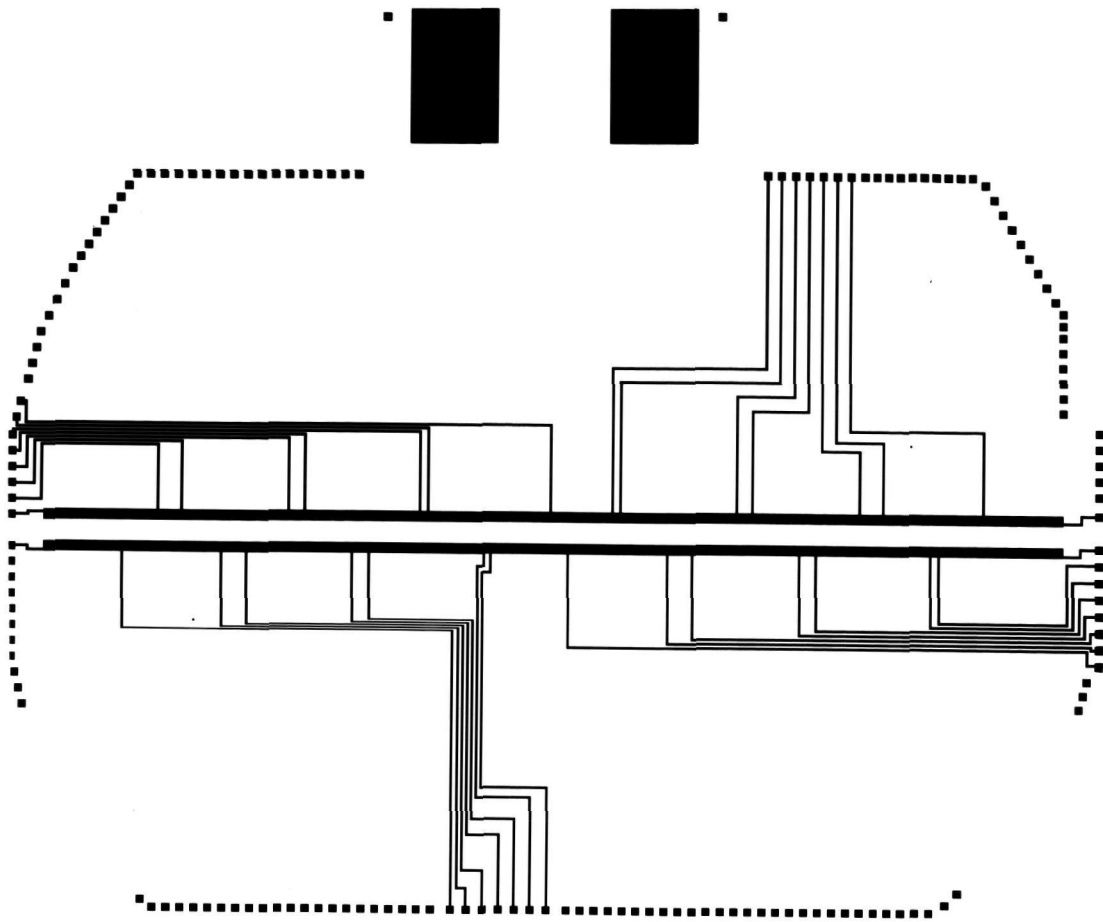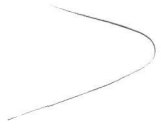
Figure 13.   Photographic masks for production of (2 x 1024)-pixel
coincidence-anode array.
                 a.   **x**-plane electrodes   b.   y-plane electrodes

64 y-plane electrodes which are approximately 20μ wide on 30-μ centers are however too fine to be resolved on a photographic print. The layout of the complete array on the ultra-smooth ceramic substrate is shown in the photograph of a deposition test unit in Figure 14. A number of units of the array have been fabricated and the techniques for deposition of the conducting electrodes and for etching the SiO_2 insulating layers have been perfected. A batch of production units is currently in process, the first two sets of electrodes having been produced with zero defects in a number of samples. Completion of the arrays is expected to require a further six to eight weeks and is subject to the allocation of additional funds in the continuing program.

A number of modular tube bodies have been fabricated and the first sealed tube employing the (10 x 10)-pixel discrete-anode array has been assembled. We are at present employing a demountable tube structure which permits cathode reprocessing and replacement of the MCP in a simple and cost-effective manner. The MCP mounting structure and header assembly is, however, common to both the demountable laboratory evaluation units and to the units which will subsequently be assembled for flight operation, as shown in the schematics in Figure 15. The overall dimensions of a typical flight detector package employing 100 amplifier and discriminator circuits in either discrete or hybrid format are shown in Figure 16. This package can accommodate the (400 x 400)-pixel array.
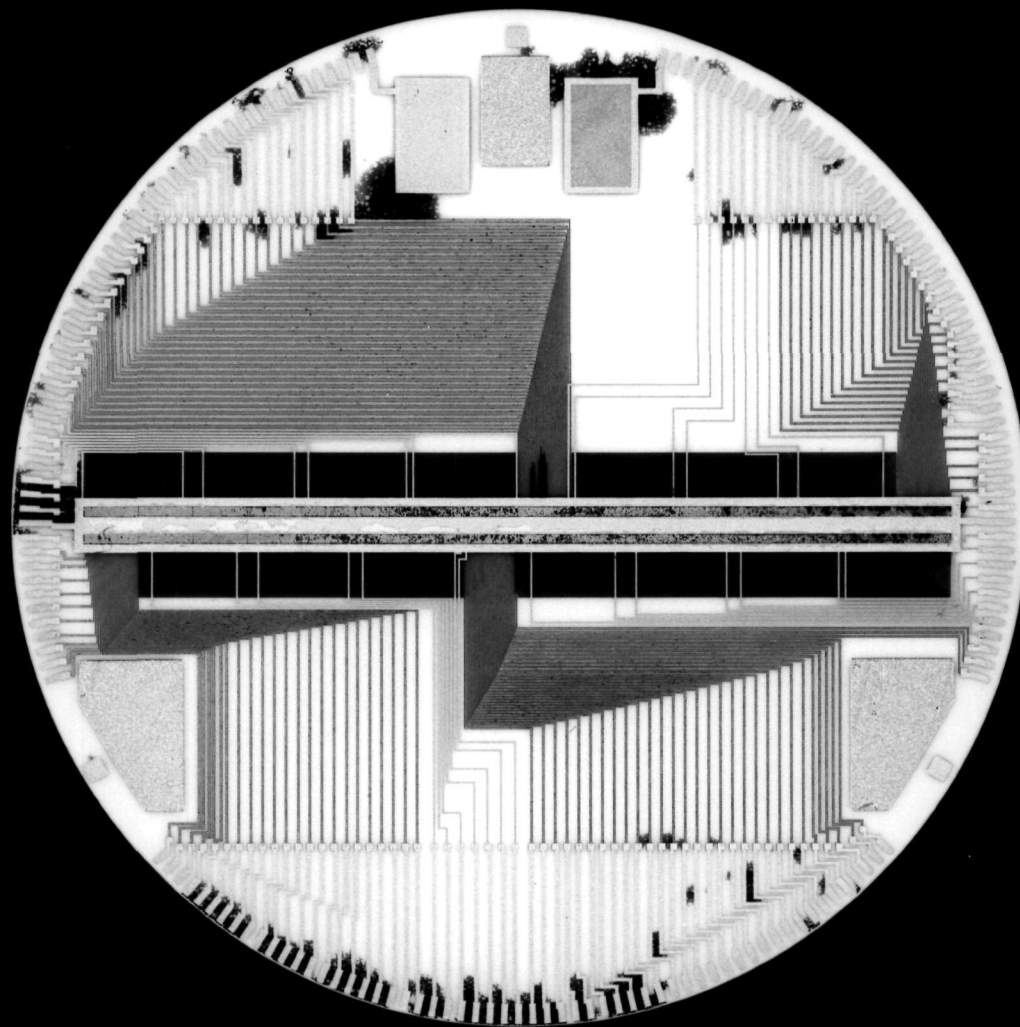
Figure 14. Deposition test unit of (2 x 1024)-pixel coincidence-
anode array. The two 1024-pixel linear arrays can be seen within the
guard electrode at the center of the array

HARVARD COLLEGE OBSERVATORY

PLATE NO. _____

NEGATIVE NO. _Tab-33G_
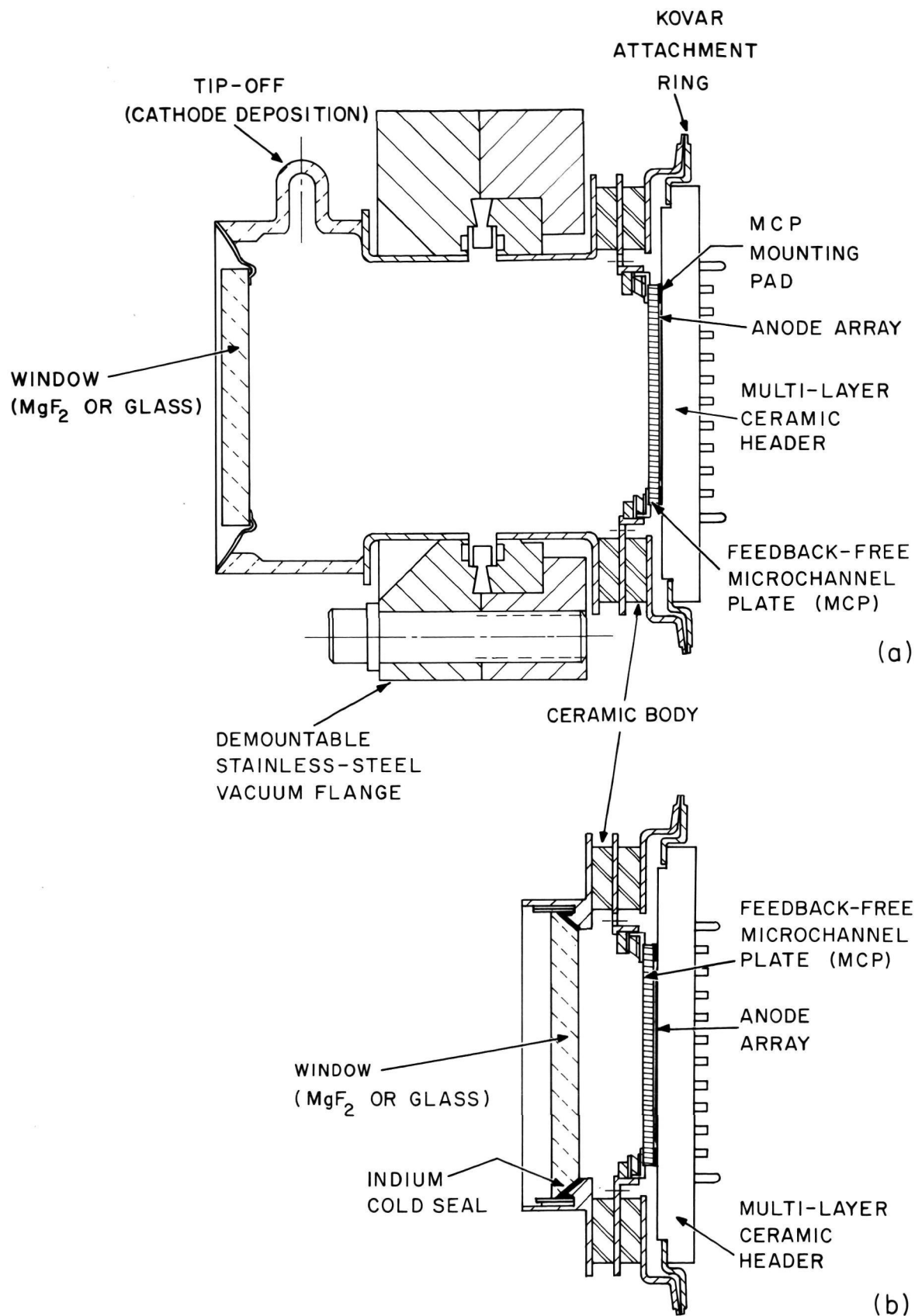
Figure 15.   Schematics of MCP detector tubes.
             a.   Demountable laboratory evaluation unit.
             b.   Flight unit.
             Photocathode is deposited on the input face of the MCP.

NEGATIVE NO. *7606·33 H*
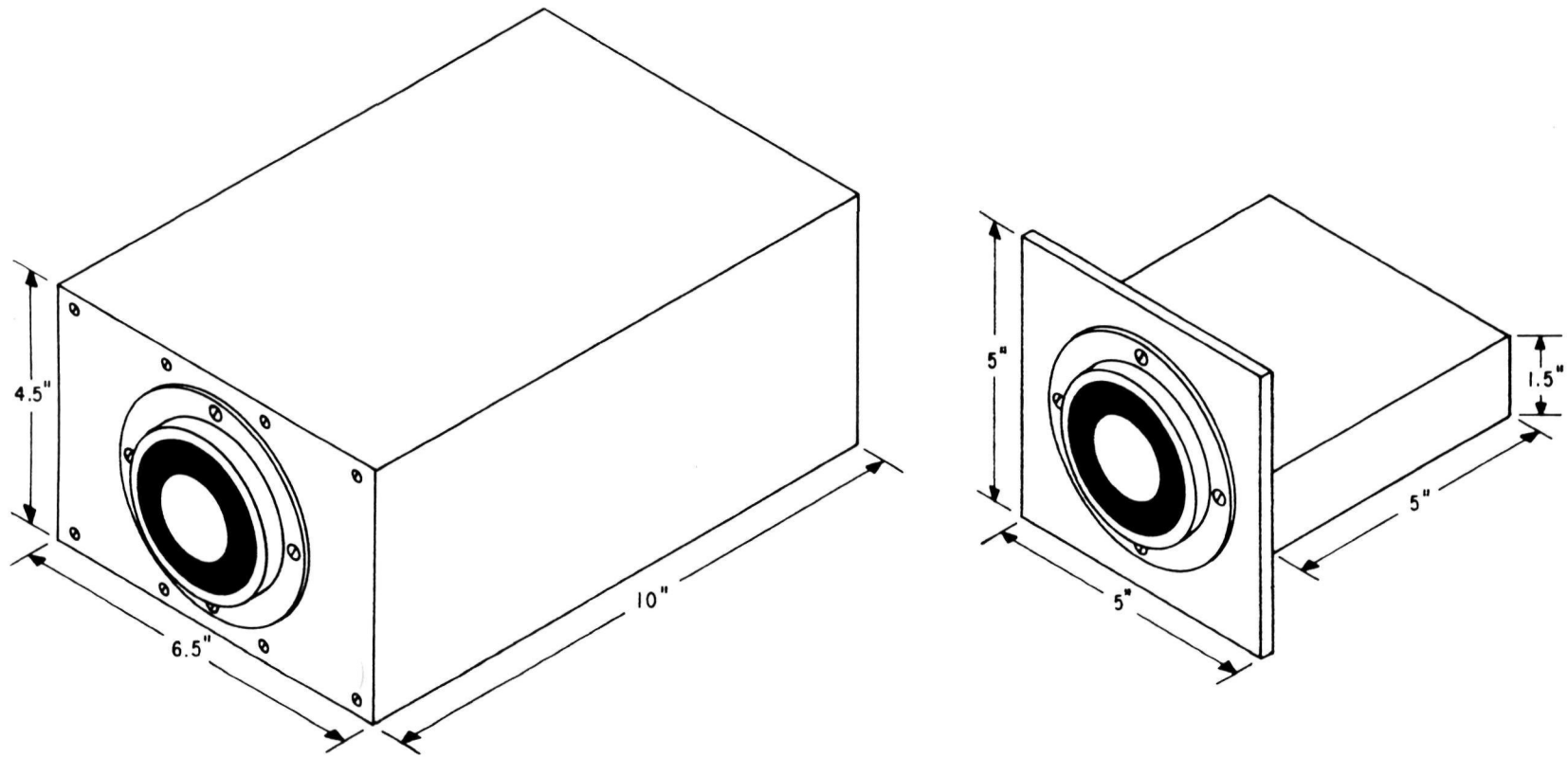
Figure 16.   Envelope dimensions for flight detector with 100
amplifier and discriminator circuits in discrete and hybrid formats.

HARVARD COLLEGE OBSERVATORY

PLATE NO.

NEGATIVE NO. 7606-23B

The layout of the demountable tube assembly is shown in Figures 17 and 18. An appendage ion-pump has been attached to this first tube in order to obtain quantitative information on the outgassing rates from the MCP during high-voltage turn-on and during bakeout. Since we are currently awaiting delivery of the S-plate MCP's, one of the existing C-plate MCP's has been installed in the tube for the purposes of a preliminary evaluation. The MCP is uncoated and will be stimulated with UV radiation from a mercury pen-ray lamp for these tests. Subsequently a CsI photocathode will be deposited on the face of the MCP for the UV version of the tube and a bialkali photocathode for the visible light unit. The use of a trialkali (S-20) photocathode will be investigated following the tests of the bialkali unit. The initial investigations of the visible-photocathode deposition techniques will be under-taken using the (10 x 10)-pixel array prior to the fabrication of the (2 x 1024)-pixel tube.

The first tube assembly has already demonstrated the electrical and mechanical integrity of the basic design. The resistance between an electrode in the anode array and the output connector socket is typically of the order of 1 ohm and no shorts between the anode array and the output face of the MCP have occurred as a result of the one atmosphere overpressure on the evacuated tube. Complete electrical tests of the assembled tube are planned to begin at the end of June. Consequently, after a year of intense effort with the development of the individual components of the detector assembly

Figure 17. Demountable tube assembly incorporating type I multi-layer ceramic header.
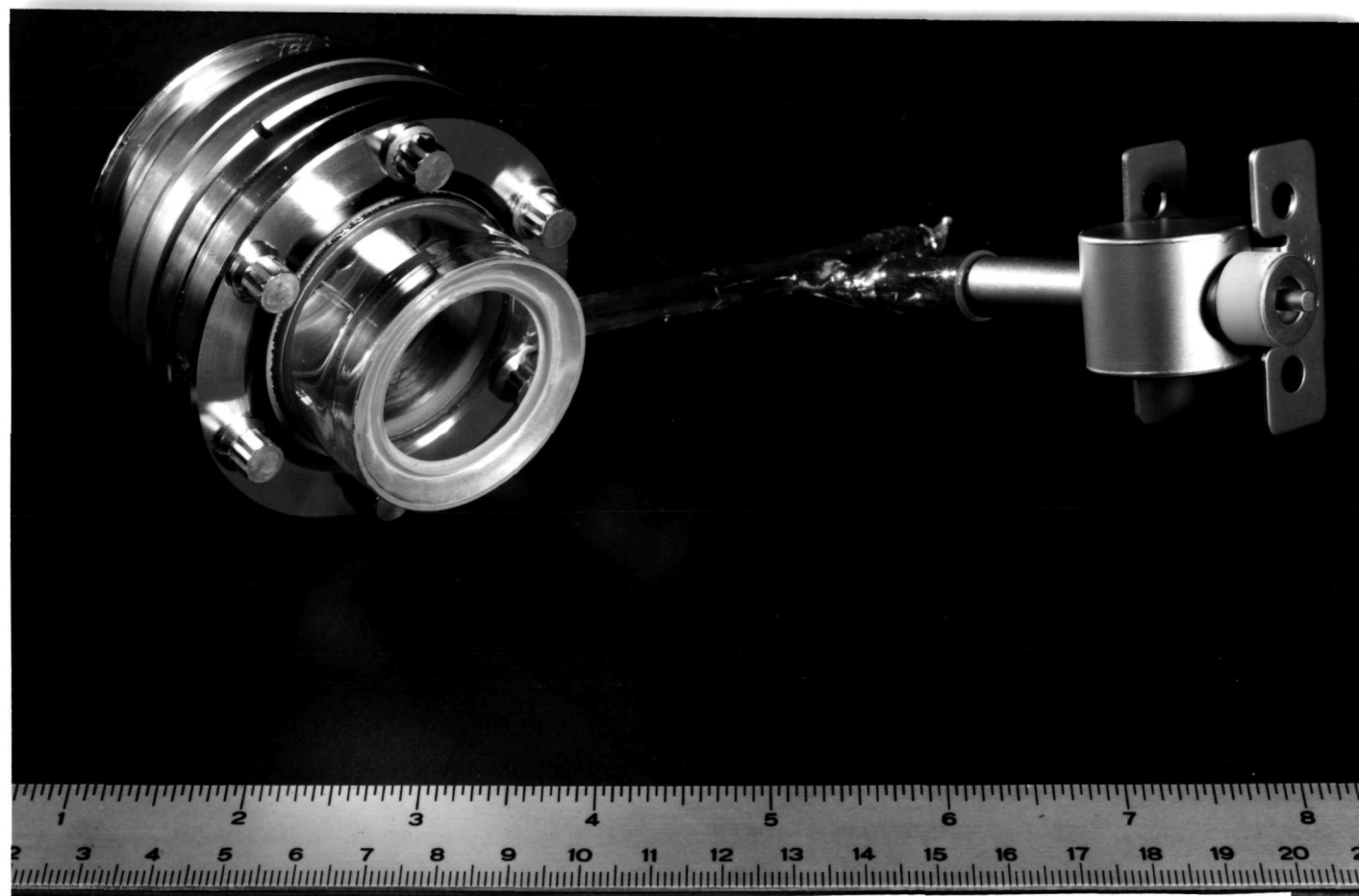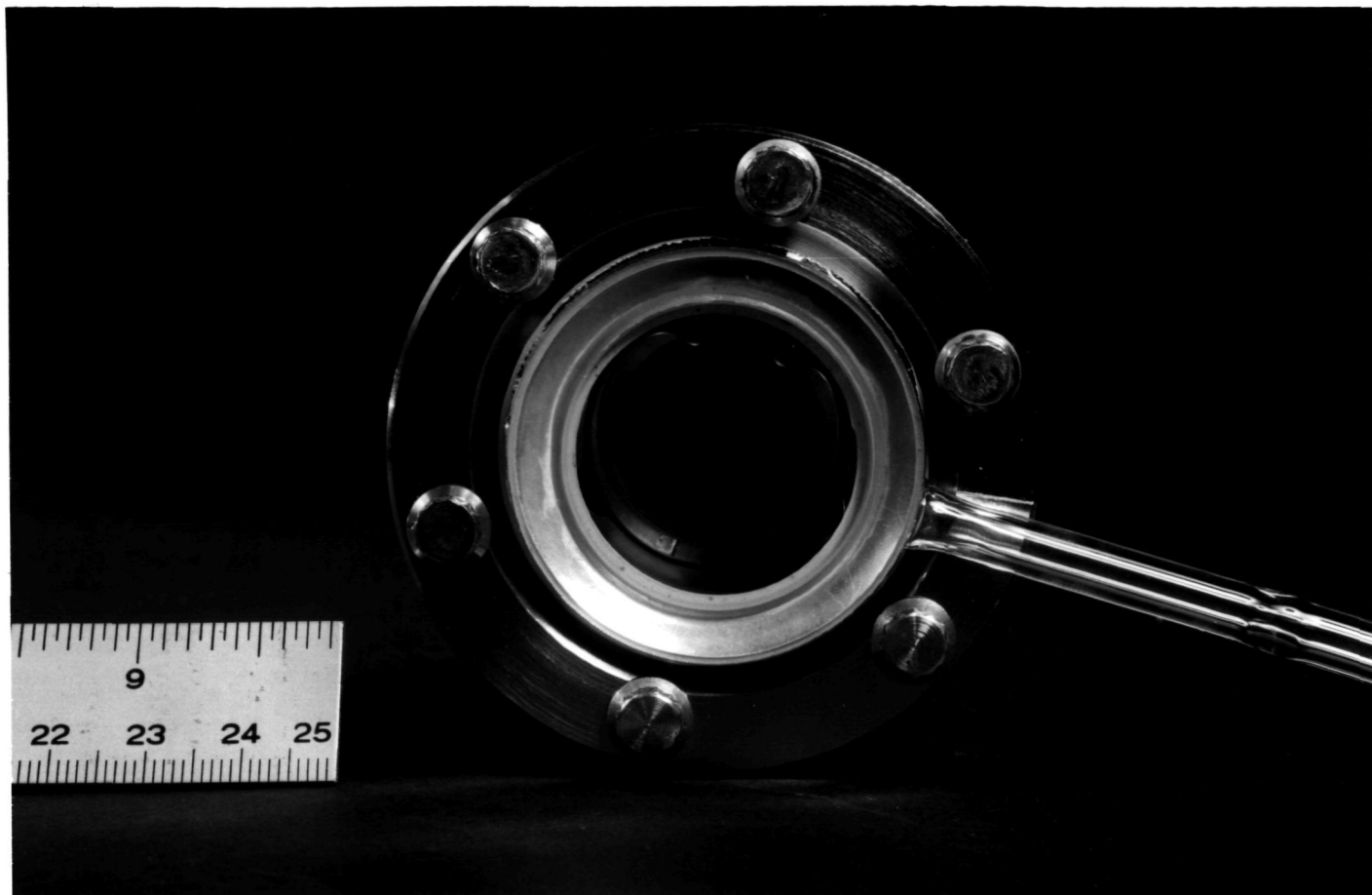
Figure 18.   Demountable UV tube assembly with MgF_2 window and appendage ion-pump for outgassing tests.

and the associated electronics, we are now ready to begin a detailed evaluation of each of the two prototype detection systems as an entity.

References (Section 2)

1. P.T. Farnsworth, US Patent 1 969 399 (1930).

2. G.W. Goodrich and W.C. Wiley, Rev. Sci. Instrum. 32, 846 (1961).

3. G.W. Goodrich and W.C. Wiley, Rev. Sci. Instrum. 33, 761 (1962).

4. J.G. Timothy and L.B. Lapson, Applied Optics 13, 1417 (1974).

5. J.G. Timothy, Rev. Sci. Instrum. 45, 834 (1974).

6. D. Washington, British Patent 1 352 732 (1974).

7. Laboratoires d'Electronique et de Physique Appliquee, 94450 Limeil-Brévannes, France.

8. J.P. Boutot, G. Eschard, R. Polaert, V. Duchenois, Proceedings of Sixth Symposium on Photo-electronic Image Devices, London, September, 1974.   To be published in Advances in Electronics and Electron Physics.

9. J.G. Timothy and R.L. Bybee, Rev. Sci. Instrum., in press, 1976.

10. J.M. Morton and W. Parkes, Acta Electronica 16, 85 (1976).

11. M. Lampton and F. Paresce, Rev. Sci. Instrum. 45, 1098 (1974).

12. G.M. Lawrence and E.J. Stone, Rev. Sci. Instrum. 46, 432 (1975).

13. E. Kellogg, P. Henry, S. Murray and L. Van Speybroeck,
     Rev. Sci. Instrum. <u>47</u>, 282 (1976).

3. Summary of results and outline of continuing program

The MCP detector development program suffered significant delays during the period through 30 June 1976 for the following reasons:

1. Delays in the fabrication of the multi-layer ceramic headers because of delamination and braze problems.

2. Late delivery of the S-plate MCP's.

3. Difficulties with the production of the photographic masks for the coincidence-anode array.

4. A funding gap caused by the late execution of the NASA headquarters contract.

5. Long lead times for the procurement of electronic parts.

In spite of these problems we and our subcontractors have made major progress toward the production of the prototype discrete-anode and coincidence-anode arrays as shown in the program chart in Figure 19. Although it was not possible to meet the original goal of testing an assembled MCP detector tube at a telescope the following tasks were completed:

1. *Test of the first feedback-free MCP's employing curved microchannels including reprocessing to increase the plate conductivity and retesting.*

2. *Design and construction of high-speed, low power amplifier and discriminator circuits for both discrete-anode and coincidence-anode readout arrays.*

3. *Design and construction of 2048 10-bit word low power Random Access Memory using SOS C-MOS integrated circuits.*

4. *Design and construction of a general purpose laboratory*

PROCURE J, C AND S PLATE MCPs — AMPERX INC. | CRL- 3 UNITS NASA 3 UNITS

PROCURE HEADERS (100 OUTPUT PINS) — CERAMIC SYSTEMS | CRL

DESIGN AND PRODUCE ARTWORK FOR ANODE ARRAY (10×10) — RAYTHEON INC. | CRL

DESIGN AND FABRICATE BREADBOARD CHARGE AMPLIFIER AND DISCRIMINATOR CIRCUITS — BBRC | CRL

EVALUATE PERFORMANCE OF J AND C PLATES — BBRC | NASA

LAP HEADERS (10×10) — CERAMIC SYSTEMS | CRL

PROCURE AMPLIFIER AND DISCRIMINATOR CARDS (MIN 20 CARDS) — BBRC | CRL (3) NASA (18)

EVALUATE PERFORMANCE OF S PLATES — BBRC/HCO | NASA

DEPOSIT ANODE ARRAY ON HEADER — RAYTHEON INC. | CRL

DESIGN AND FABRICATE TUBE BODIES — EMR | CRL

DESIGN AMPLIFIER AND TUBE MOUNTING STRUCTURE — BBRC | CRL

INTEGRATE TUBE BODY AND MCP WITH HEADER (10×10) — EMR | CRL

FABRICATE AMPLIFIER AND TUBE MOUNTING STRUCTURE (2 units) — BBRC | CRL/NASA

CONSTRUCT AND DEVELOP HARDWARE AND SOFTWARE FOR DETECTOR EVALUATION (100 CHANNELS) — HCO | HCO

TEST SEALED TUBE WITH UNCOATED MCP AT UV WAVELENGTHS (10×10) — HCO | HCO

PROCESS DEMOUNTABLE TUBE WITH CsI PHOTOCATHODE (10×10) — EMR | CRL

TEST DEMOUNTABLE TUBE IN SEALED CONFIGURATION AT UV WAVELENGTHS (10×10) — HCO | HCO

PROCURE HEADERS (160 OUTPUT PINS) — CERAMIC SYSTEMS | NASA

DESIGN AND PRODUCE ARTWORK FOR ANODE ARRAYS (2×1024) — RAYTHEON | NASA

MODIFY HARDWARE AND SOFTWARE FOR TEST OF (2×1024) COINCIDENCE ARRAYS — HCO/BBRC | NASA

PRODUCE ANODE ARRAYS ON POLISHED SUBSTRATE (2×1024) — RAYTHEON | NASA

INTEGRATE ANODE ARRAYS WITH HEADER (2×1024) (160 OUTPUT PINS) — RAYTHEON | NASA

INTEGRATE TUBE BODY AND MCP WITH HEADER (2×1024)(100 OUTPUT PINS) — EMR | NASA

TEST SEALED TUBE WITH UNCOATED MCP AT UV WAVELENGTHS (2×1024) — HCO | NASA

PROCESS TUBE WITH BIALKALI OR TRIALKALI PHOTOCATHODE (2×1024) — EMR | NASA

In process 1 June, 1976

TEST SEALED TUBE AT VISIBLE WAVELENGTHS IN LABORATORY AND/OR AT TELESCOPE (2×1024) — HCO | NASA

Figure 19. Development program for prototype discrete-anode and coincidence-anode MCP detector arrays.

data recording and display facility.

5. *Fabrication of the multi-layer ceramic headers. Major problems of ceramic delamination, pin warping and braze wicking were successfully overcome.*

6. *Fabrication of the (10 x 10)-pixel discrete-anode array on the multi-layer ceramic header.*

7. *Completion of artwork and deposition and etching tests for (2 x 1024)-pixel coincidence-anode array.*

8. *Assembly of the first sealed MCP detector tube.*

9. *Verification of the optimum geometry for charge division in a coincidence-anode array by means of additional laboratory tests with the breadboard (32 x 32)-pixel array.*

As the result of these accomplishments the prototype MCP detector tubes can now, for the first time, be evaluated as parts of a complete system. Accordingly the development program now has three specific and feasible objectives for the continuation of work in Fiscal Year 1977:

1. To develop the discrete-anode array in both open and sealed configurations to the point where units can be made available at a practical cost for use in both laboratory and space instrumentation.

2. To exploit the unique capabilities of the (2 x]024)-pixel coincidence-anode array in a series of scientific programs at ground-based telescopes, and at the same time test the array under actual conditions of scientific use.

3. To construct and evaluate the performance of a prototype coincidence-anode array having a very large number of pixels (in excess of 2×10^5) and formats of the type that are representative of the requirements for both photon-counting spectrometers and cameras on space telescopes.

The major events and milestones of the overall program are shown in Figure 20. In order to meet these program goals the following specific tasks need now to be undertaken:

1. *Evaluation of MCP's with S-configuration microchannels.*

2. *Completion of the (2 x 1024)-pixel anode arrays.*

3. *Production of the amplifier and discriminator circuits in thick-film hybrid format.*

4. *Laboratory and telescope evaluation of the sealed tubes.*

5. *Environmental tests of the sealed tubes. (Vibration, thermal, and radiation).*

6. *Design and initial fabrication of (400 x 400)-pixel coincidence-anode array.*

7. *Design and initial fabrication of (400 x 400)-pixel coincidence-detection and data-recording system.*

The funds necessary to complete these tasks have accordingly been requested from NASA under a continuation of the MSFC contract.
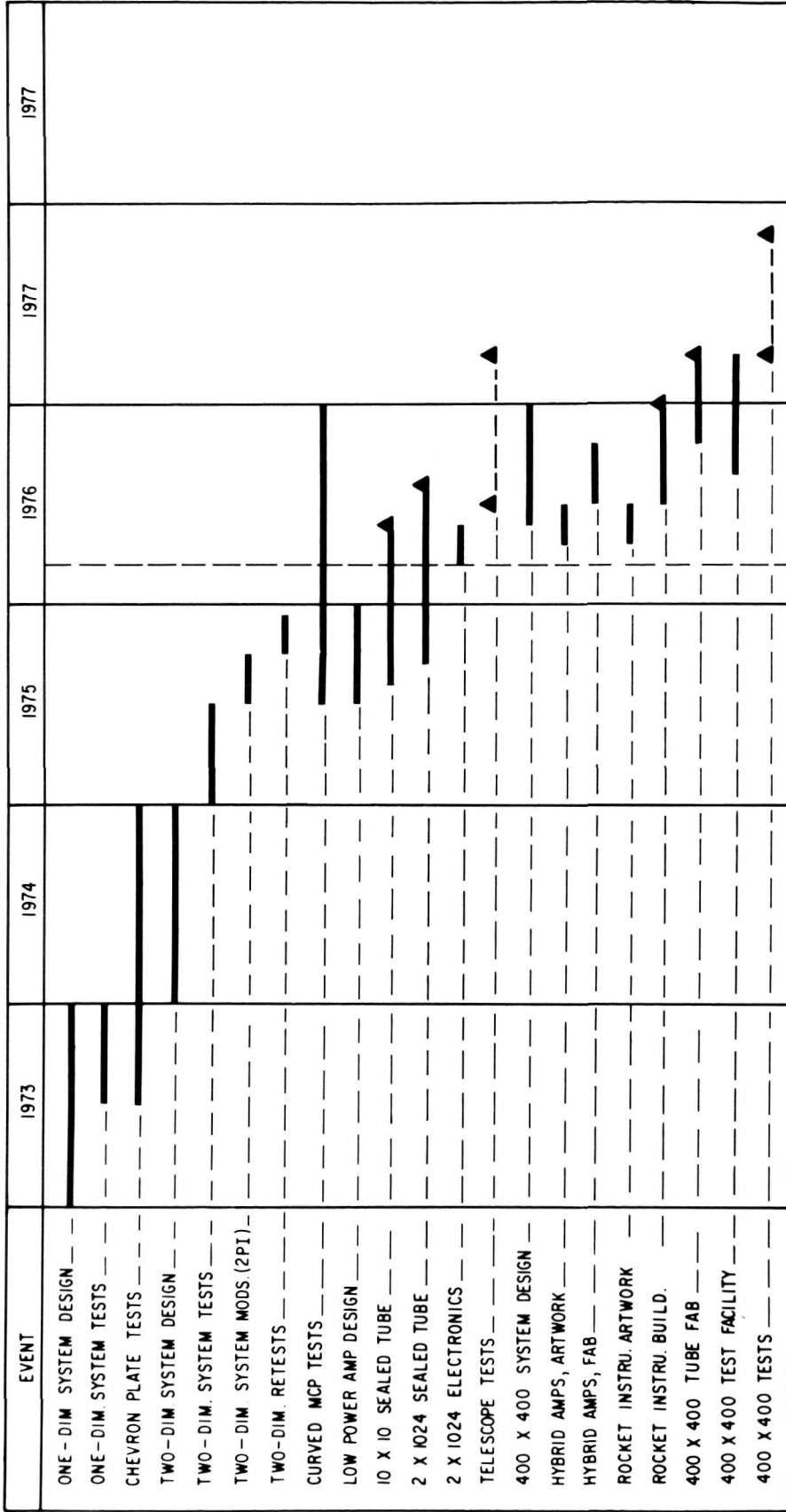
Figure 20. Major events and milestones for the MCP detector
development program.

4.   <u>Bibliography</u>

'One-dimensional photon-counting detector array for use at EUV and soft x-ray wavelengths'. J. G. Timothy and R. L. Bybee, Applied Optics <u>14</u>, 1632 (1975).

'Two-dimensional photon-counting detector arrays based on microchannel array plates.' J. G. Timothy and R. L. Bybee, Rev. Sci. Instrum. <u>46</u> 1615 (1975).

One-dimensional photon-counting detector array for use at EUV and soft x-ray wavelengths

J. G. Timothy and R. L. Bybee

The performance of a one-dimensional photon-counting detector array based on microchannel array plates has been evaluated in the laboratory over the wavelength range from 461 Å to 1216 Å. The output charge pulses from a set of cascaded microchannel array plates were collected on a proximity-focused anode array consisting of sixty-four linear electrodes 1.3 mm in length and 25 μm in width, set on 50-μm centers. Although the dynamic range of the detector array was severely limited by ion-feedback effects in currently available microchannel array plates, the theoretical spatial resolution of 50 μm was achieved with a detection efficiency at wavelengths below 800 Å equal to that of a conventional channel electron multiplier.

I. Introduction

Instruments for photometric studies at uv and x-ray wavelengths have traditionally been divided into two distinct classes: photographic and photoelectric. Photographic instruments, employing film as the detection system, have the great advantage of an image-storing capability. It is therefore possible to use this type of instrument to record a very large amount of data with a single exposure. However, photographic film has a number of major disadvantages. First, the sensitivity is considerably lower than that of a photoelectric detector; at uv wavelengths, where special emulsions are required, the quantum efficiency is typically about 1% that of a photoelectric detector. Second, the response is nonlinear as a function of the incident energy. Hence, photometric calibration is a difficult and time-consuming procedure, and the resulting accuracy is poor. Furthermore, the emulsion is sensitive to a very wide range of wavelengths; accordingly, the elimination of background fog levels is extremely difficult. Finally, the output signal is not electrical in character. The use of photographic film in space experiments on orbiting satellites thus implies either recovery (as in Skylab) or a complex onboard processing and video transmission system (as in the Lunar Orbiter Spacecraft).

Photoelectric instruments, on the other hand, are more sensitive, have a greater stability of response, and provide a linear output as a function of the incident energy. The output data format is also fully compatible with spacecraft data-handling and telemetry systems. However, since most photoelectric detectors do not have image-recording capabilities, the data must be read out sequentially, point by point. Consequently, the over-all speed of the system is considerably slower so that a photographic instrument, with all its inherent disadvantages, may be more efficient.

The SEC vidicon tube has been used extensively on sounding rockets and orbiting satellites to combine some of the advantages of both the photographic and the photoelectric detection techniques. Although this device has an image-recording capability and an electrical readout, it has major limitations in terms of dynamic range, stability of response, resolution, and photometric accuracy.

The recent development of the channel electron multiplier (CEM) and its miniaturization into the microchannel array plate (MCP) offers for the first time the possibility of fully combining the advantages of both the photographic and the photoelectric detection systems. The MCP can be operated as an image intensifier and has the potential of being developed to yield signal outputs superior to those of conventional photomultipliers. In particular, the MCP has a photon-counting capability and a negligible dark count rate.

These devices can operate stably and efficiently at extreme ultraviolet (EUV) and soft x-ray wavelengths in a windowless configuration or can be installed with a photocathode in a sealed tube for use at uv and visible wavelengths. This paper will describe the construction and performance of a one-dimensional photon-counting detector array based on the MCP and designated to operate over the wavelength range from about 20 Å to 1400 Å.

J. G. Timothy is with the Center for Astrophysics, Cambridge, Massachusetts 02138; R. L. Bybee is with Ball Brothers Research Corporation, Boulder, Colorado 80302.
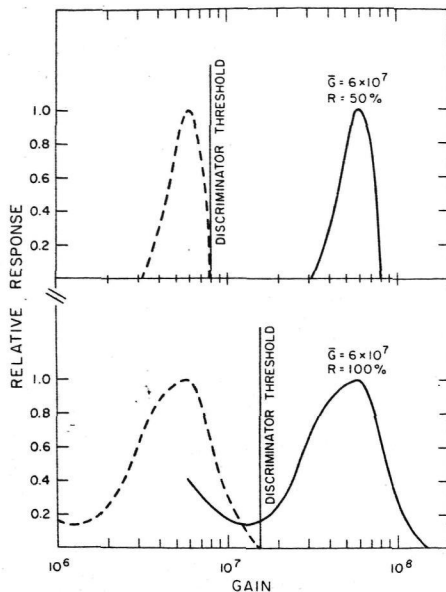
Fig. 1. Values of the discriminator threshold required to eliminate noise pulses resulting from 10% cross coupling between adjacent electrodes in an array for two different output pulse-height distributions. (Upper curve) conventional CEM. (Lower curve) two MCP's in cascade (Galileo BX 3040 plates).

II. Detector Array

A. Microchannel Array Plates

The mode of operation of the CEM and the MCP has been well described in the literature[1–5] and will not be considered in detail here. We should note, however, the characteristics of both the CEM and the MCP that are fundamental to the operation of these devices in photon-counting detection systems. The conventional CEM consists of a semiconducting glass channel having an internal diameter of a few millimeters and a length-to-diameter ratio of about 50:1. The resistance of the channel is typically of the order of 10^9 Ω and the channel is curved to inhibit the feedback of positive ions to the input where they can initiate spurious output pulses. With an accelerating potential along the channel greater than about 3 kV, the output pulse-height distribution has a saturated form, as shown in Fig. 1, in marked contrast to the exponential distribution obtained with conventional discrete-dynode multipliers. The resolution of the pulse-height distribution is defined as

$$R = \Delta G / \overline{G},$$

where ΔG is the full width at half-maximum and $\overline{G}$ the modal value of the gain. Typically, $\overline{G}$ has a value between 10^7 and 10^8, and R is of the order of 30–60%. The CEM can thus be used in a pulse-counting mode with the amplifier threshold set well below the level of the modal gain.

However, in the MCP it has not proved possible, so far, to inhibit ion feedback by curving the microchannels, although techniques are currently being developed to achieve this.[6] Consequently, the maximum accelerating potential that can be applied to a conventional MCP is about 1.5 kV, limiting the gain to 10^4 and producing an exponential output pulse-height distribution. A single array plate can therefore not be used in a pulse-counting mode. It is possible, nevertheless, to couple two array plates in cascade as shown in Fig. 2. By a careful selection of channel bias angles and plate orientation, we can produce a chevron multiplier[7] in which positive ions are trapped at the interface between the two plates. The over-all voltage across the plates can then be raised to the level at which a high gain and a saturated output pulse-height distribution are obtained. The output electron beam can then be collected with a proximity-focused anode array as shown in Fig. 2 to produce a photomultiplier with an image-recording capability.

B. Anode Array

The readout system generally employed with the MCP to date has been a visible-light phosphor coupled to either a vidicon tube or photographic film.[4] In this arrangement, the detected photon is converted to a pulse of electrons in the microchannel; these electrons are accelerated toward the phosphor and reconverted to visible photons, which are detected by either the vidicon photocathode or the photographic emulsion. Although the MCP can provide a gain of the order of 10^7, this system is cumbersome and has all the inherent disadvantages of either the photographic plate or the vidicon tube. The use of a self-scanning silicon photodiode array (Reticon) after a
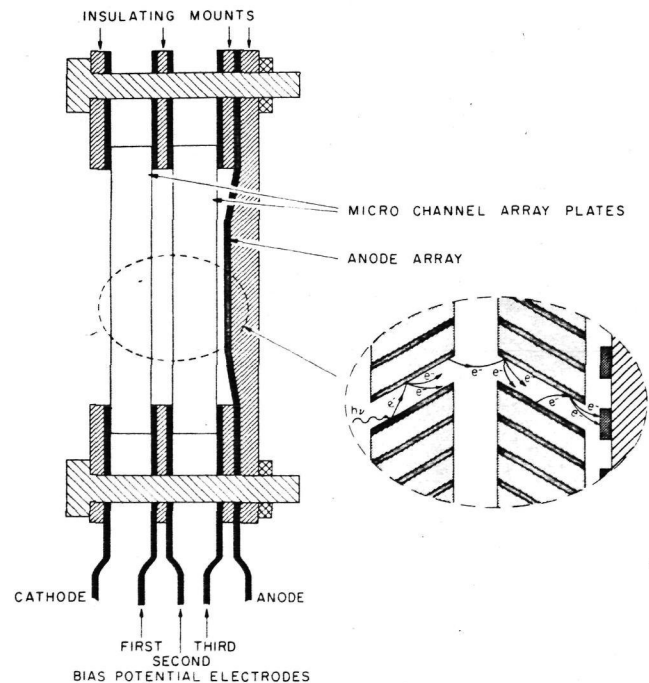

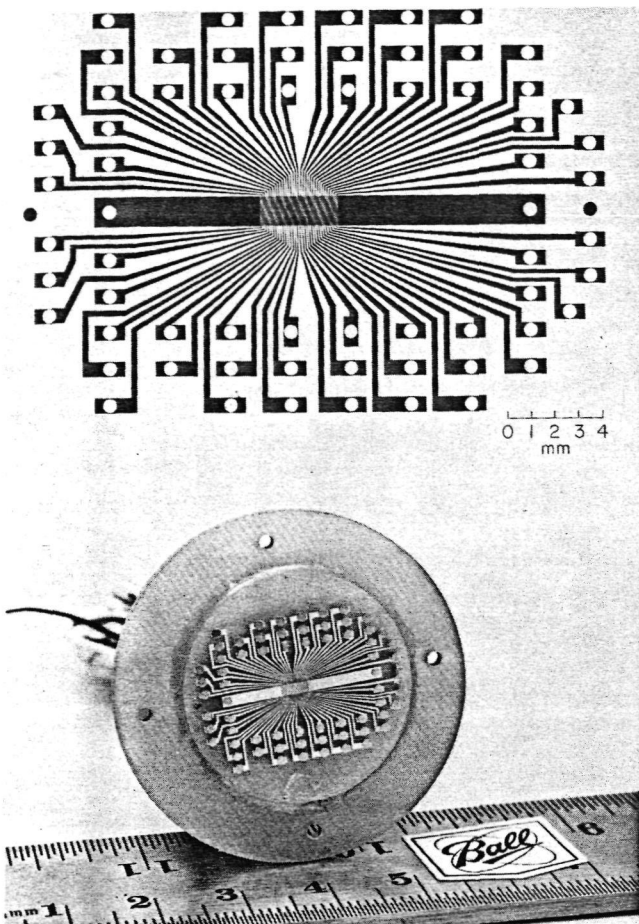Fig. 2. Schematic of detector array employing cascaded microchannel array plates.

Fig. 3. Sixty-four-element anode array: (a) photomask; (b) assembled array of gold-coated copper electrodes on a ceramic substrate.

literature,[12] but no performance details are available.

In order to demonstrate the feasibility of this approach, we have evaluated in the laboratory the performance of the breadboard sixty-four-element linear array shown in Fig. 3. A set of cascaded MCP's is coupled in proximity focus to an anode array consisting of sixty-four linear electrodes 1.3 mm in length and 25 μm in width, set on 50-μm centers. Each electrode in the array is connected by means of a charge-sensitive amplifier and discriminator circuit to the data handling and display circuits. The array was produced by photoreduction on a ceramic substrate, each conducting element consisting of a 5-μm thick copper electrode stabilized with a thin gold overcoat. The total capacitance between adjacent electrodes was kept below 0.5 pF in order to minimize the effects of charge coupling. The complete array is flat to better than 2.5 μm, allowing separations as small as 25 μm to be used between the array and the output of the MCP.

phosphor has recently been reported.[9] However, this is once again an analog detection system with a limited dynamic range. In order to exploit the full sensitivity, dynamic range and photometric stability of the MCP, it is necessary to employ pulse-counting readout systems working directly at the anode.

Several pulse-counting systems to read out spatial information at the anode of the MCP have been described in the literature.[10,11] However, these systems have been designed to employ a limited number of amplifiers, two for a one-dimensional array and four for a two-dimensional array, and consequently have limitations in terms of dynamic range and spatial resolution. Thus, although these systems are highly efficient for applications where low signal levels are obtained, such as galactic x-ray astronomy, they are not suitable for use with the high signal levels obtained from laboratory EUV and soft x-ray sources or from telescopes for solar studies at EUV and soft x-ray wavelengths. Accordingly we have set out to develop photon-counting detector arrays in which each image element is connected to an individual amplifier and counting circuit. A low-resolution detector array of this type has been described in the

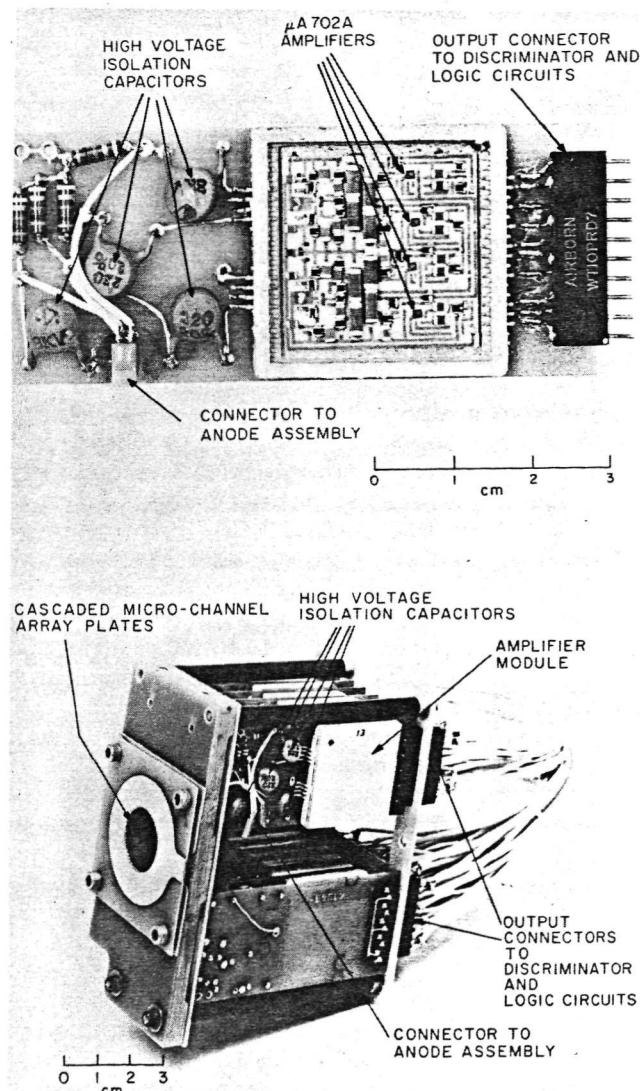

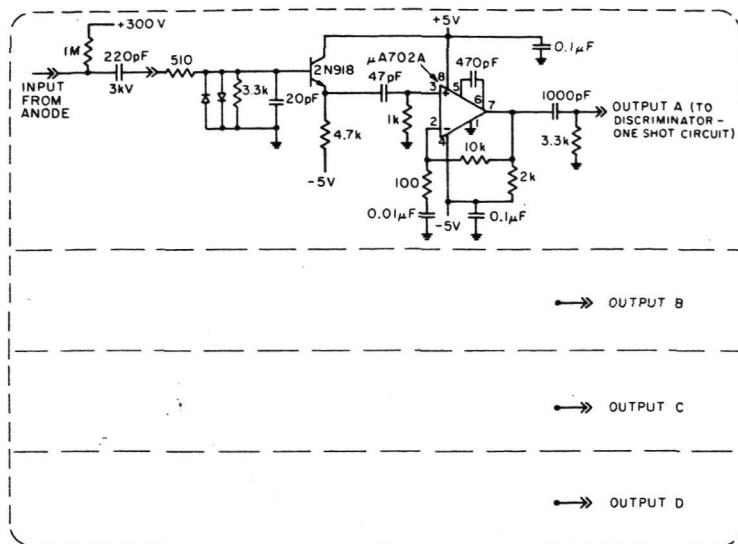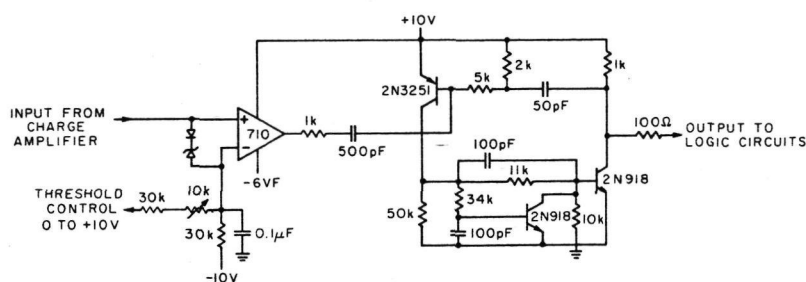Fig. 4. (a) Amplifier module; (b) assembled sixty-four-element array.

Fig. 5. (a) Amplifier circuit; (b) discriminator circuit.

C. Amplifiers and Discriminators

The sixty-four individual charge-sensitive amplifiers for the breadboard array were produced in a thick-film hybrid format (Fig. 4) with four amplifiers mounted in a flat pack having dimensions of 3.2 cm × 3.2 cm × 0.6 cm deep. The μ 702A operational amplifiers [Fig. 5(a)] are held to a closed-loop gain of 100 with the output charge from the MCP integrated on a total input capacitance of 30 pF, consisting of a 20-pF integrating capacitor plus 10 pF of stray and diode capacitance. The pulse-pair resolution of the amplifier is 300 nsec. An input charge of 10^{-12} C (equivalent to a gain of 6.3×10^6 in the MCP) produces a 1-V output pulse from the amplifier. Since the total capacitance between adjacent electrodes in the anode array, including the capacitance of connectors and cables, is 2 pF, the cross coupling between adjacent electrodes is approximately 7% of the output charge from the MCP. No attempt was made to limit the total power dissipation of the amplifiers for the breadboard unit, each operational amplifier dissipating about 120 mW for a total output of 480 mW/ package. However, the total power consumption of the amplifier is considerably less than that required by a conventional charge-sensitive amplifier of equivalent bandwidth employing a feedback capacitor to integrate the charge. The use of a feedback charge-sensitive amplifier would have significantly reduced the effects of capacitative cross coupling between adjacent electrodes. However, the practical difficulties associated with such an amplifier prevented its implementation in the breadboard unit. Heat sinks [not shown in Fig. 4(b)] on each package maintained a maximum operating temperature of 48°C during operation under vacuum. More sophisticated amplifiers, having a greatly reduced size and power dissipation, will be required for larger arrays and are currently being developed. During the initial evaluation of the system it was necessary to study the operating characteristics of the MCP with either a high negative potential at the microchannel input or a high positive potential at the microchannel output. Consequently, high-voltage isolation capacitors were required at the inputs to the amplifiers (see Fig. 4).

The output from each amplifier is fed to a separate discriminator and one-shot circuit [Fig. 5(b)] which generates a 10-V logic pulse, 300 nsec in width, compatible with the C-MOS data-handling and display circuits. The discriminator circuits are constructed from discrete components and are mounted in a rack in the vacuum system adjacent to the detector array. The discriminator threshold can be varied from outside the vacuum system over the range 8×10^{-13} C (5×10^6 electrons pulse^{-1}) to 1.1×10^{-11} C (7×10^7 electrons pulse^{-1}).

DETECTOR SYSTEM   DISPLAY ELECTRONICS
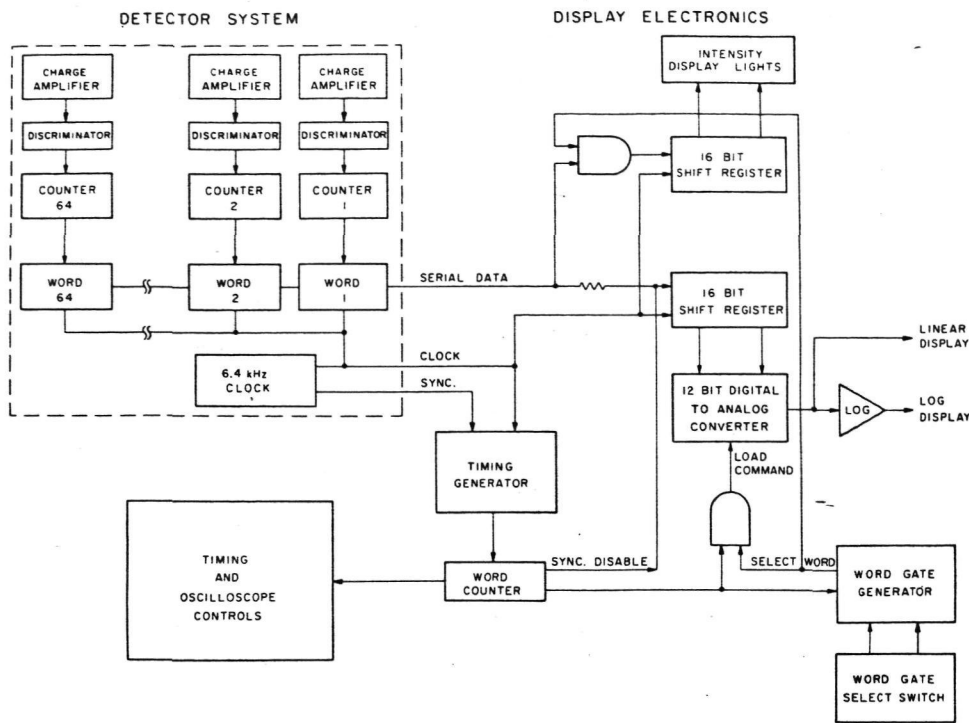

Fig. 6. Schematic of data handling and display circuits.

D. Data handling system

The digital data from the sixty-four amplifiers and discriminators can be read out in serial format directly to an on-line digital computer and can be presented simultaneously in a number of different formats for immediate display on an oscilloscope or an analog plotter. A block diagram of the display electronics is shown in Fig. 6. The data from each amplifier are accumulated in a counter and read out as a 16-bit serial word to two 16-bit shift registers in a time of 166 μsec. The first register shifts the count from any selected amplifier to a set of binary-coded intensity display lights. The second register transfers the count to a 12-bit digital-to-analog converter, the output being displayed in linear or logarithmic format on an oscilloscope or recorded on an analog plotter. A total of ten different integration periods may be selected over the 0.32–164-sec range. The accumulated counts recorded by all sixty-four amplifiers can be presented simultaneously in analog format, while the intensity level from any selected amplifier is presented on the intensity display lights, both displays being updated automatically at the end of each integration period.

III. Results

The performance of the sixty-four-element array was evaluated in the laboratory over the wavelength range from 461 Å to 1216 Å with particular emphasis on the following parameters:

(A) MCP output pulse-height distribution;
(B) spatial resolution;
(C) dynamic range;
(D) uniformity of response;
(E) detection efficiency.

In order to carry out this evaluation, the array was mounted with the front face of the MCP on the Rowland circle of an EUV spectrometer and the sixty-four elements distributed along the plane of dispersion (see Fig. 7). A Skylab two-stage CEM[5] was mounted in the normal location behind an exit slit and employed as a reference standard in the determinations of the dynamic range and the detection efficiency of the array. Three different types of MCP were employed in the initial evaluation of the array, namely, Galileo[13] model BX3040 (38-μm channels on 50-μm centers), Mullard[14] model G40-25 (40-μm channels on 50-μm centers), and ITT[15] model 115 (11-μm channels on 14-μm centers). All MCP's employed in this initial evaluation had a conventional geometry with straight microchannels set at bias angles in the 0–20° range to the face of the plate. High voltages were applied to the microchannels by means of conducting electrodes evaporated on the faces of the MCP. The conducting electrodes on the ITT plates penetrate the microchannels to a depth equal to half of a microchannel diameter at the input and one diameter at the output. This end-spoiling improves the spatial resolution of the MCP when used in proximity focus by collimating the output electron
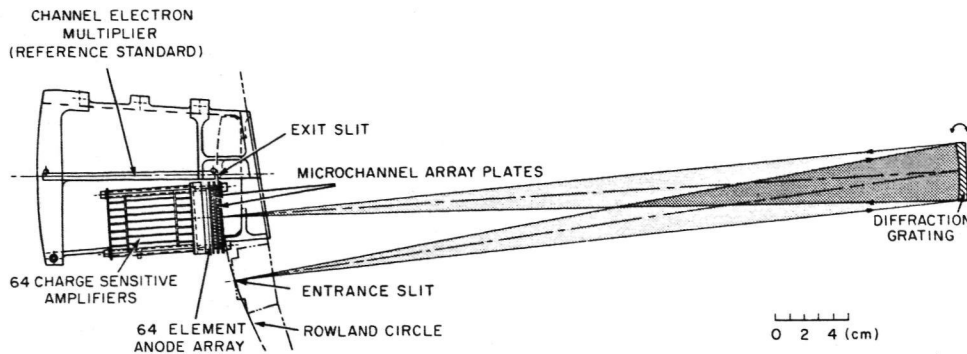
Fig. 7. Assembly of sixty-four-element array in a normal-incidence EUV spectrometer.

beam.[16] Initial studies of MCP performance were carried out with a single 10-mm diam anode in order to eliminate the effects of charge spreading between the output of the MCP and the anode array.

A. MCP Output Pulse-Height Distribution

Initial tests with two MCP's in cascade quickly confirmed our earlier findings[5,8] that the chevron configuration produces a multiplier with a performance greatly inferior to that of a conventional CEM. The trapping of positive ions at the interface between the two plates is not as effective as that in a conventional curved CEM, and, consequently, it is not possible to raise the over-all voltage to a level at which a true saturated distribution is obtained without inducing the onset of ion-feedback instabilities at any reasonable operating pressure ($<10^{-6}$ Torr). Furthermore, the very large number of low-amplitude feedback pulses produced in the second stage of the chevron multiplier reduces the standing charge in the walls of the microchannels and hence lowers the dynamic range of the multiplier. An additional problem in employing the chevron configuration in an image-recording array is the loss of spatial resolution because of charge spreading at the interface between the two plates.

The optimum pulse-height distributions obtained with two Galileo BX3040 plates in cascade are shown in Fig. 8. These distributions are typical of those obtained with both Mullard and Galileo MCP's having microchannel diameters of the order of 40 μm stimulated by EUV photons. The distributions are broader and have lower values of the modal gain than those obtained with the same plates stimulated by charged particles. This is because there is a high probability for the reflection of EUV photons within the microchannels resulting in the production of photoelectrons at significant distance from the input. It can be seen (Fig. 8—upper curve) that charge spreading at the interface between the plates produces a tail of large-amplitude pulses. Each microchannel in the second MCP is acting as an individual multiplier, and hence the effect of charge spreading at the interface is to broaden the pulse-height distribution, rather than to increase the modal gain value of a saturated distribution. The spreading can be reduced by

applying a bias potential of several hundred volts between the plates, but can only be effectively controlled by reducing the separation of the plates to a distance smaller than the diameter of the microchannels (Fig. 8—lower curve). However, even with the plates in direct contact there will still be some spreading due to the misalignment between individual microchannels.

In an effort to overcome some of the disadvantages of the chevron configuration, we constructed a multiplier with three MCP's in cascade. The output pulse-height distributions for three ITT 115 plates having 11-μm diam microchannels on 14-μm centers are shown in Fig. 9. It is clear that charge spreading at the two interfaces severely degraded the shape of the distribution even with the minimum practicable separation of 25 μm. However, operating the plates with the faces in direct contact produced a satisfactory distribution when installed in the array (Fig. 10)
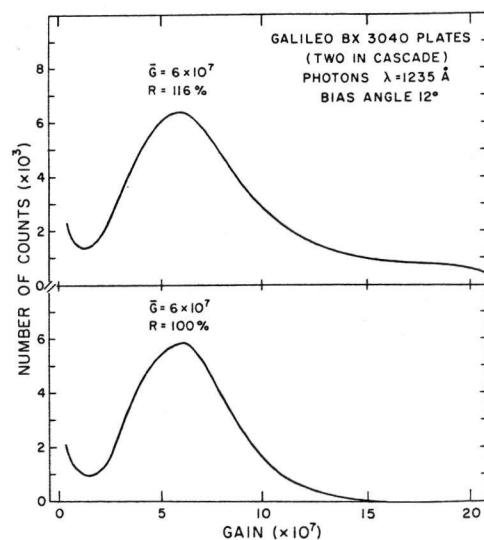

Fig. 8. Output pulse-height distributions for two Galileo BX 3040 plates operated in cascade with 1400-V accelerating potential on each plate at an ambient pressure of 2×10^{-7} Torr. (Upper curve) plate spacing 125 μm. Plate-to-plate bias potential +150 V. (Lower curve) plate spacing 25 μm. Plate-to-plate bias potential 0 V.
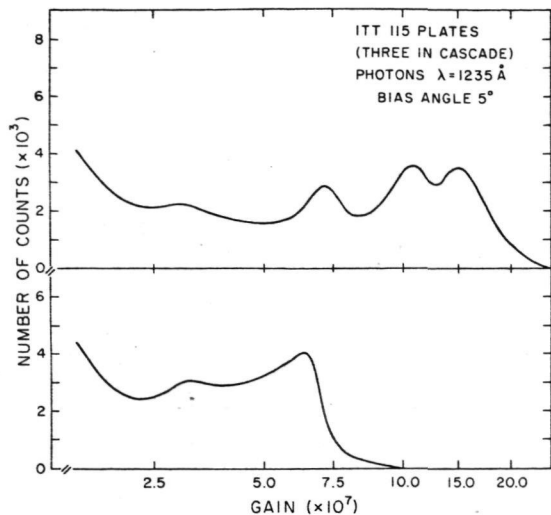
Fig. 9. Output pulse-height distributions for three ITT 115 plates operated in cascade with 1200-V accelerating potential on each plate at an ambient pressure of 2×10^{-7} Torr. (Upper curve) plate-to-plate bias potential 0 V. (Lower curve) plate-to-plate bias potential +50 V.
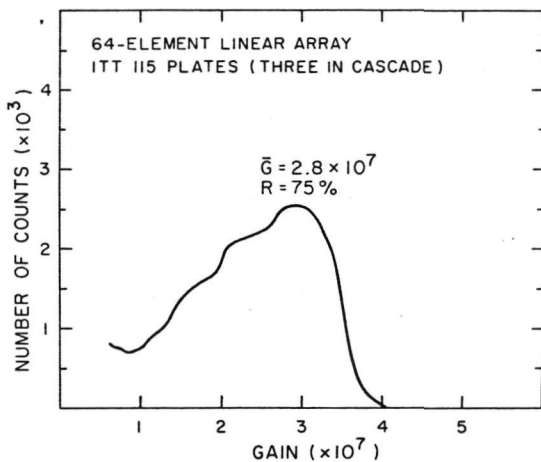

Fig. 10. Output pulse-height distribution for three ITT 115 plates operated in cascade in the sixty-four-element array. Accelerating potential 1200 V on each plate at an ambient pressure of 2×10^{-7} Torr.

with a lower accelerating voltage on each plate than that required for two plates in cascade. These plates were accordingly used for the majority of the tests with the array, following a preliminary evaluation with the Galileo BX 3040 plates, since the diameter of the microchannels was small compared to the dimensions of each image element.

B. Spatial Resolution

The output pulse-height distributions obtained when the two Galileo BX 3040 plates were installed in the sixty-four-element array were completely different from those obtained with the single 10-mm diam anode. This was because, first, the output elec-

tron beam from the MCP was repelled by the negative space charge on the insulating substrate of the anode array, and, second, the diameter of the microchannels was comparable to the width of the individual electrodes. In order to reduce the effects of spreading of the electron beam at the output of the MCP (see Appendix), we reduced the MCP-to-anode spacing to the minimum practicable value in the breadboard array of 25 μm. With this separation, an anode-bias potential in the +120–+150-V range was found to be effective in overcoming the combined effects of space-charge repulsion and electron-beam spreading at the output of the MCP (see Fig. 11).

The spatial resolution of the system was, however, directly related to the shape of the output pulse-height distribution. As we have already discussed, capacitive cross coupling of the signal between adjacent electrodes is an intrinsic factor in the operation of the array. In the breadboard array the total cross-coupled signal on an electrode had an amplitude approximately 7% of that of the original output pulse. Consequently, in order to reject the cross-coupled signal, it was necessary to set the discriminator threshold in the amplifiers at such a high level that a stable operating plateau in the high voltage characteristic could not be obtained at any reasonable operating voltage [see Fig. 12(a)]. The problem is illustrated in Fig. 1 for an array with 10% capacitive cross coupling. It can be seen (Fig. 1—upper curve) that it is possible, with the typical pulse-height distribution from a conventional CEM, to set the discriminator threshold almost an order of magnitude below the level of the modal gain while still rejecting all cross-coupled pulses. However, with the wide distribution obtained from two MCP's in cascade (Fig. 1—lower curve), it is necessary to set the discriminator threshold at such a high level that the low-amplitude signal pulses are rejected. The full potential of the array can accordingly not be realized with currently available MCP's.

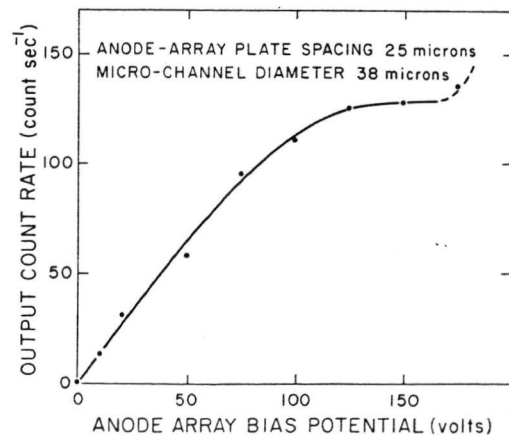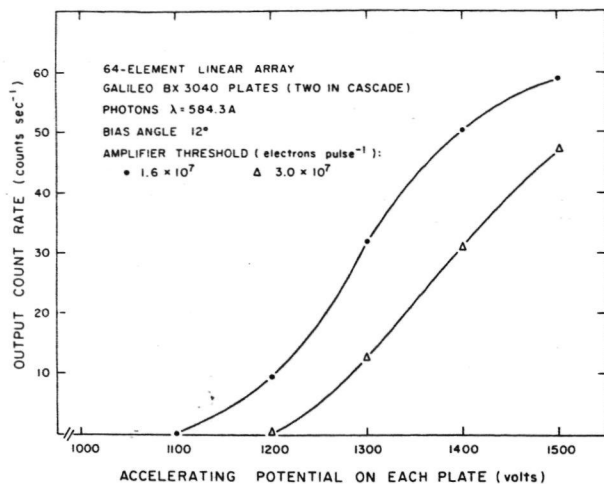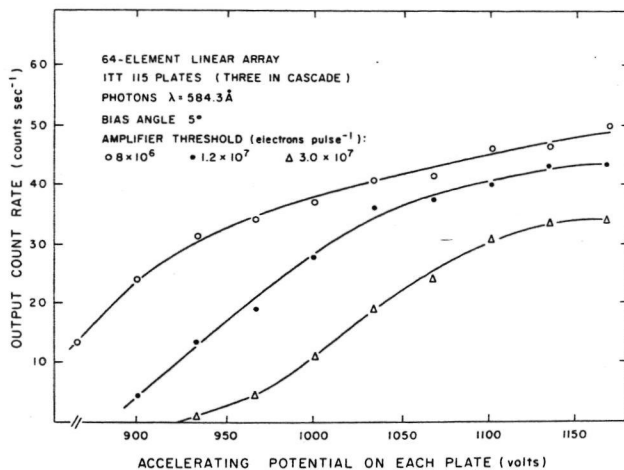The high-voltage characteristics for one element in

Fig. 11. Variation in the output count rate from a single element in the anode array as a function of the anode bias potential. Discriminator threshold 3.0×10^7 electrons pulse^{-1}.

(a)

(b)

Fig. 12. High-voltage characteristics with MCP-to-anode spacing of 25 μm at an ambient pressure of 2 $\times$ 10^{-7} Torr: (a) two Galileo BX 3040 plates in cascade; (b) three ITT 115 plates in cascade.

the array with two Galileo BX 3040 plates in cascade and three ITT 115 plates in cascade are shown in Fig. 12. The spatial resolution of the array was degraded by charge spreading at the interface of the Galileo plates even with the discriminator threshold set at 3.0 $\times$ 10^7 electrons pulse^{-1}. Consequently, the detailed analysis of the performance of the array was undertaken using three ITT 115 plates in cascade. Spectra of neon recorded by the array with both the Galileo and ITT sets of MCP's are shown in Fig. 13. The improved spatial resolution obtained with the smaller diameter microchannels can clearly be seen. The effect of lowering the discriminator threshold, and hence increasing the cross-coupled signal, is shown in Fig. 14 for neon spectra recorded with the ITT set of MCP's. The profiles of the exit image of EUV spectrometer obtained, first, by scanning the image with a conventional CEM and slit assembly and, second, by recording the image on the array are shown in Fig. 15. It can be seen that it was possible

to obtain the theoretical system resolution of 50 μm, in spite of the wide output pulse-height distribution from the cascaded MCP's, although other aspects of the system performance were necessarily degraded.

C. Dynamic Range

The need to set the discriminator threshold at a high value in order to reduce the effects of cross coupling severely limited the dynamic range of the array. The variation in the sensitivity of the system as a function of the output countrate is shown in Fig. 16. The high resistance of the microchannels ($\sim$10^{14} Ω) causes the gain of the cascaded MCP's to drop at count rates greater than 1 count sec^{-1} microchannel^{-1}. This coupled with the high discriminator threshold lead to a rapid loss of efficiency at count rates in excess of about 25 count sec^{-1} image element^{-1}. Allowing for the distribution of energy across the exit image of the EUV spectrometer (Fig. 15), we calculate that the sensitivity of the cascaded MCP's, referenced to a discriminator threshold of 1.0 $\times$ 10^7 electrons pulse^{-1}, is reduced by 10% at an output count rate of 0.14 count sec^{-1} microchannel^{-1}. This measured value is in excellent agreement with that calculated from the relaxation time constant of the MCP.
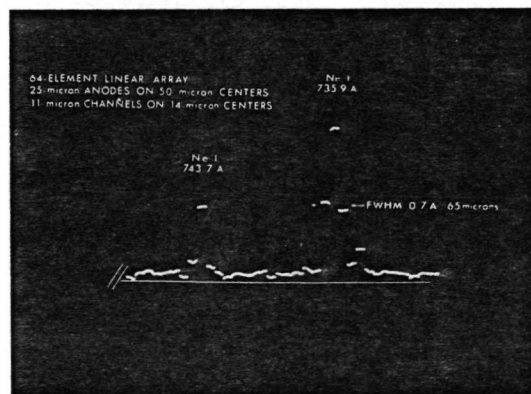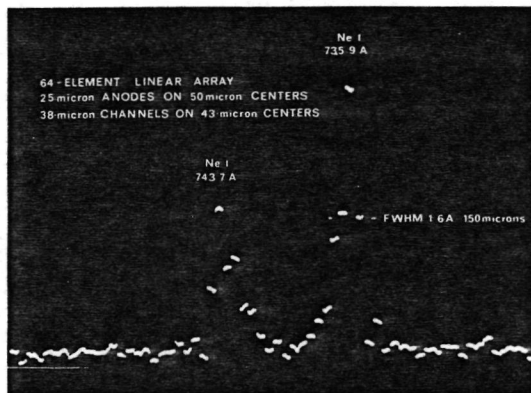

Fig. 13. Spectra of neon recorded with the sixty-four-element array: (a) two Galileo BX 3040 plates in cascade. Discriminator threshold 3.0 $\times$ 10^7 electrons pulse^{-1}. (b) Three ITT 115 plates in cascade. Discriminator threshold 2.0 $\times$ 10^7 electrons pulse^{-1}.
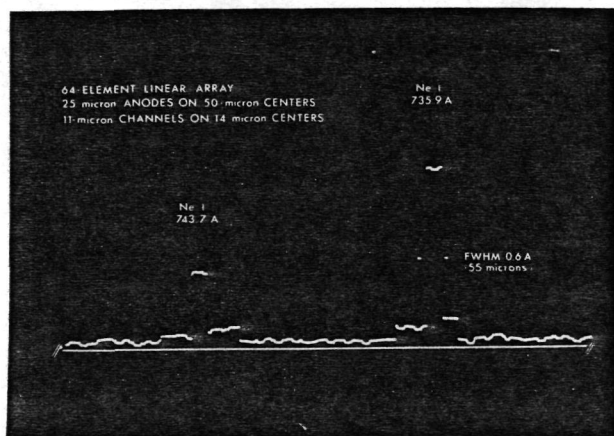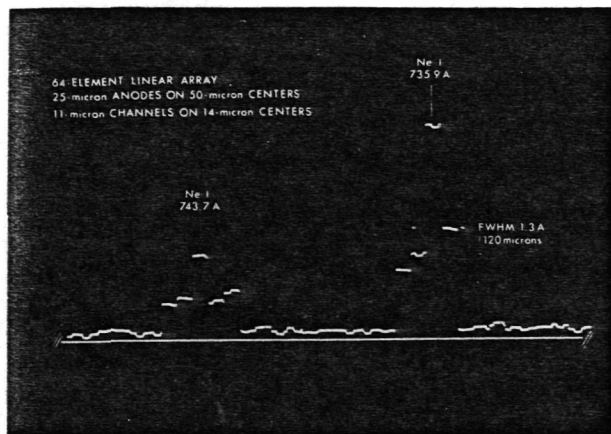
Fig. 14. Spectra of neon recorded with three ITT 115 plates in cascade: (a) discriminator threshold 8×10^6 electrons pulse^{-1}; (b) discriminator threshold 3.0×10^7 electrons pulse^{-1}.

The dynamic range of the cascaded MCP's (10% nonlinear at 1000 count sec^{-1} mm^{-2}) is thus a factor of at least 200 lower than that of a conventional CEM. The dynamic range of the array can be significantly increased by employing high-conductivity MCP's and can be further improved by lowering the discriminator threshold, but only at the expense of spatial resolution. A performance approaching that of a conventional CEM will, however, only be obtained when MCP's having a high gain and a narrow output pulse-height distribution free of ion-feedback effects become available.

D. Uniformity of Response

The uniformity of response across the array was strongly dependent on the form of the output pulse-height distribution. Setting a high discriminator threshold to eliminate the effects of cross coupling produced a system that was highly sensitive to slight variations in gain across the MCP. Such variations are inherent in a system employing a set of MCP's in cascade because of a varying degree of misalignment

between microchannels over the area of the plate. The extreme variations in the response of the array with two Galileo BX 3040 plates in cascade are shown in Fig. 17 (upper curve). These variations can also be observed for the neon spectrum [Fig. 13(a)] recorded with the same discriminator threshold. The greatly improved uniformity obtained with the three ITT plates in cascade can be seen in Fig. 17 (lower curve). The maximum variation in the sensitivity is $\pm 10\%$ with the spatial resolution [Fig. 14(a)] comparable to that obtained with the Galileo plates. Raising the discriminator threshold to obtain the limiting spatial resolution of 50 μm increased the maximum variation to about $\pm 13\%$.

E. Detection Efficiency

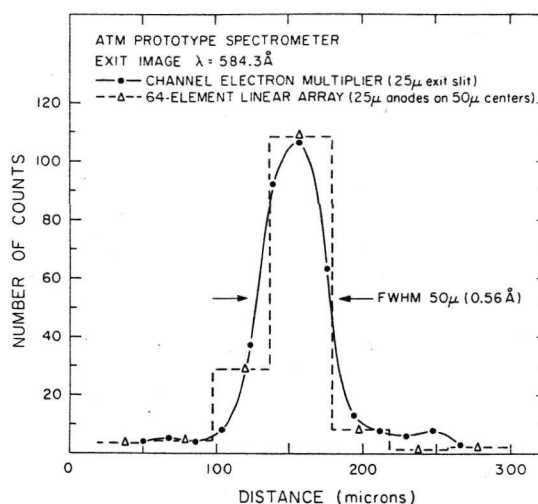The detection efficiency of the array was determined over the wavelength range from 461 Å to 742 Å

Fig. 15. Exit profile of the EUV spectrometer recorded with a CEM mounted behind a 25-μm exit slit and with the MCP array (discriminator threshold 3.0×10^7 electrons pulse^{-1}).
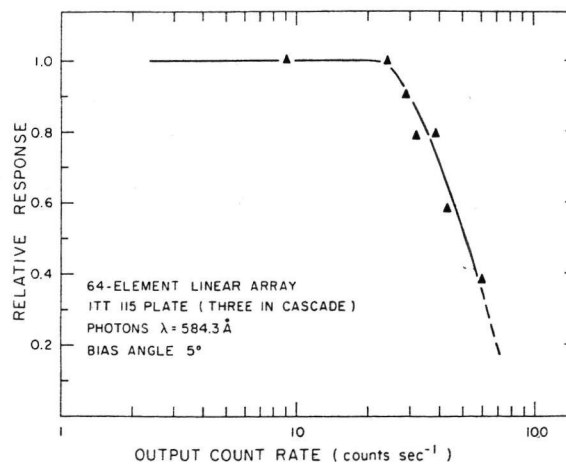

Fig. 16. Variation of sensitivity as a function of count rate with discriminator threshold set at 1.0×10^7 electrons pulse^{-1}.
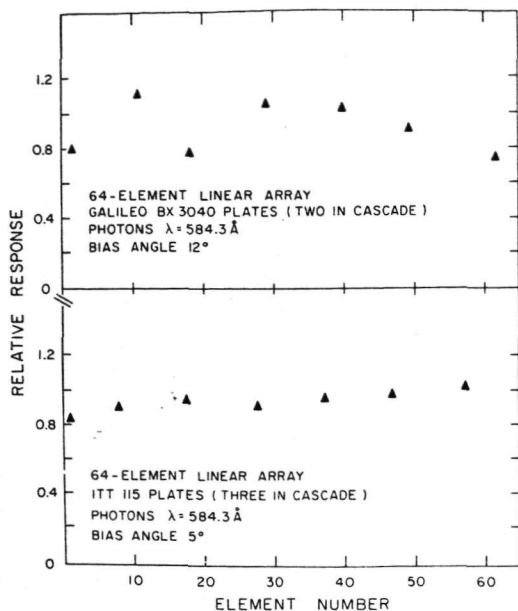
Fig. 17. Variation of sensitivity across the array: (a) Two Galileo BX 3040 plates in cascade. Discriminator threshold 3.0×10^7 electrons pulse^{-1}. (b) Three ITT 115 plates in cascade. Discriminator threshold 1.0×10^7 electrons pulse^{-1}.

IV. Summary

We have successfully constructed and evaluated in the laboratory a one-dimensional photon-counting detector array based on the MCP. The results of these tests show that the breadboard array has achieved the theoretical spatial resolution of 50 μm. Furthermore, the experimental data, together with the theoretical analysis of the charge spreading at the output of the MCP, have revealed no problems in extending the proximity-focused multianode concept to produce a detector array with a spatial resolution better than 10 μm. The construction of arrays having at least 256 image elements is now feasible using miniature, low power amplifiers fabricated with thick-film hybrid techniques. Also, by adding a separate photocathode in proximity focus at the input of the MCP, it will be possible to extend the range of operation of the detector array to uv and visible wavelengths.

The full potential of the breadboard array could not be realized in this initial evaluation because of the problem of ion feedback in the commercially available MCP's. We are currently evaluating the performance of MCP's designed to eliminate this

by comparing the response with that of a Skylab two-stage CEM mounted behind an exit slit. The measured detection efficiencies are shown in Fig. 18, and the ratios of the efficiencies of the MCP array and the CEM are listed in Table I. The open area of the MCP's employed in this investigation was approximately 66%, and detection efficiency was expected to be lower than that of the CEM. However, it can be seen from Table I that the MCP efficiency was greater than that of the CEM at all wavelengths for which measurements were made. The principal reason for this effect is the increase in the quantum yield of the photocathode as a function of the angle of incidence at wavelengths below about 700 Å. The angle of incidence for the ITT plates was 85°, while the CEM was illuminated at normal incidence. This accordingly leads to a progressive increase in the ratio of the MCP-to-CEM detection efficiencies at shorter wavelengths. However, the detection efficiency of the MCP array is significantly greater than 66% of that of the CEM at 742 Å where independent laboratory studies have shown that the value of quantum yield does not have a strong dependence on the angle of incidence. Consequently, it is clear that, even allowing for the possibility of multiple reflections within the microchannel, the emission of photoelectrons from the front face of the MCP has a significant effect on the measured detection efficiency. The detection efficiency of the MCP array may accordingly be expected to remain approximately equal to that of the CEM at wavelengths longer than 800 Å. The effects of photoelectrons produced at the interfaces of the microchannels on the spatial resolution of the array could not be determined in this initial evaluation.
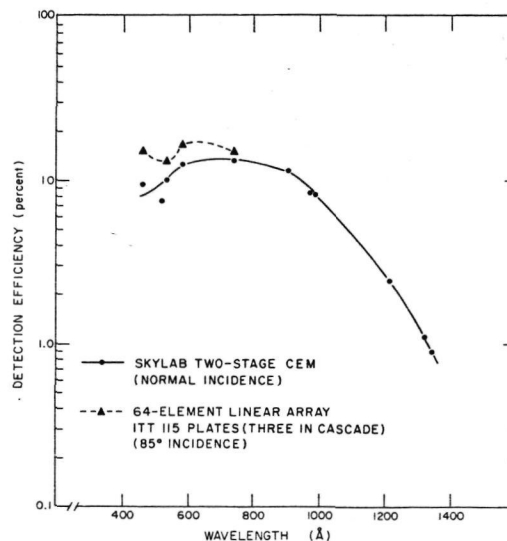

Fig. 18. Variation in the detection efficiencies of CEM, illuminated at normal incidence, and MCP array, illuminated at 85° incidence, with wavelength.

Table I. Detection Efficiencies of Skylab Two-Stage CEM and Sixty-Four-Element Linear Array (Three MCP's in Cascade)

Wavelength (Å)	Detection efficiency (count photon^{-1})		
	CEM (normal incidence)	MCP (85° incidence)	MCP/CEM ratio
742	0.133	0.150	1.14
584	0.130	0.160	1.25
537	0.100	0.134	1.34
461	0.090	0.150	1.70

problem. The results of these tests and the expansion of the multianode array into a two-dimensional format will be described in forthcoming publications.

This study was undertaken as a continuation of the development program for the Harvard College Observatory EUV spectroheliometer on the Skylab Apollo Telescope Mount (ATM). Engineering support for the construction and testing of the breadboard sixty-four-element array was provided by Ball Brothers Research Corporation (BBRC), Boulder, Colorado, as prime contractors for the Harvard ATM program. We wish to particularly acknowledge the outstanding efforts of G. A. Lorman and R. L. Vessel of BBRC throughout the test program. The assistance received both from W. Harby, ATM program manager at Harvard, and D. A. Roalstad, manager of the Harvard program at BBRC, is also greatly appreciated. Finally, we are happy to acknowledge the support and encouragement we received from the personnel of the ATM program office at the NASA Marshall Space Flight Center including the ATM program managers W. C. Keathley and R. Ise.

Appendix: Spreading of the Electron Beam at the Output of the MCP

An analysis of the problem of the spreading of an electron beam in an accelerating field and under space-charge repulsion was first undertaken by Moss.[17] More recently, Vibrans[18] has reproduced the results of Moss in graphical form by means of a computer code. We have calculated the spreading of the electron beam at the output of a set of cascaded MCP's using the method of Vibrans as described by Hutter.[19] In order to carry out the calculations, a number of simplifying assumptions had to be made:

(1) The electron flow between the output of the MCP and the anode array can be represented by a laminar beam.

(2) The output pulse width is 1 nsec. This gives a beam current of 3×10^{-3} A for a gain of 2×10^7 in the MCP.

(3) Initial beam convergence is zero. The beam will actually diverge, however, even without end-spoiling, the worst case would only be a 20° divergence.

(4) The initial mean potential of the electrons at the output of the MCP is 30 V.[20]

(5) The maximum accelerating field at the output of the MCP is 6×10^6 V m^{-1}, corresponding to a bias potential of 150 V with a plate-to-anode spacing of 25 μm (see Fig. 11).

The two equations defining the spreading of the electron beam are

$$z = \frac{e}{m}\frac{E}{2}t^2 + \dot{z}_0 t$$

and

$$\frac{d^2 r}{dt^2} = \frac{eI}{\epsilon_0 2\pi r m \left(\frac{e}{m} Et + \dot{z}_0 \right)},$$

where

r = beam radius = $r(z)$;
z = the coordinate along the beam axis;
t = the flight time of the electron;
E = the axial electrostatic field;
$\dot{z}_0$ = the velocity of the electron at $z = 0$, $t = 0$;
I = the beam current;
e = the charge on an electron;
m = the mass of the electron;
ϵ_0 = 8.85×10^{-12} A sec V^{-1} m^{-1}.

We can obtain a physical solution for these equations by employing the method and results derived by Vibrans. We first compute in succession the following functions:

$$\dot{z}_0 = \left(2U\frac{e}{m} \right)^{1/2},$$

$$W_0 = r_0 \frac{e}{m} E_z \left(\frac{\epsilon_0 2\pi m}{\dot{z}_0 eI} \right)^{1/2},$$

$$\dot{R}_0 = r_0' \left(\frac{\dot{z}_0^3 \epsilon_0 2\pi m}{eI} \right)^{1/2},$$

$$C = \dot{R}_0^2 - W_0 R_0 - 2 \ln W_0,$$

$$\dot{W}_0 = R_0 - \tfrac{1}{2} W_0,$$

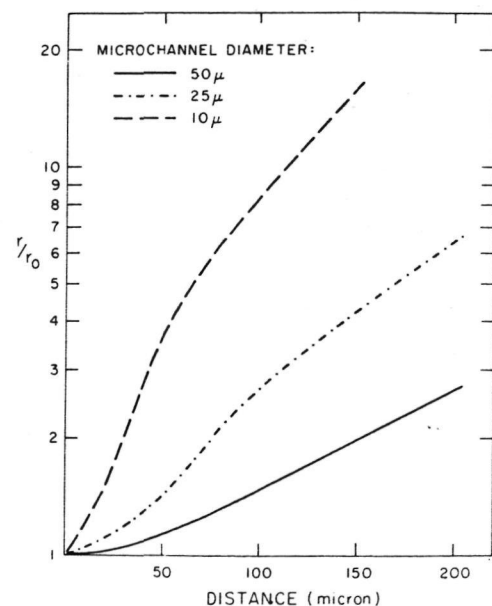$$Z = z \frac{E_z (e/m)}{z_0^2},$$

where

Fig. 19. Variation in the radius of the electron beam as a function of the distance between the MCP output and the anode array for a MCP gain of 2×10^7 and a MCP-to-anode bias potential +150 V.
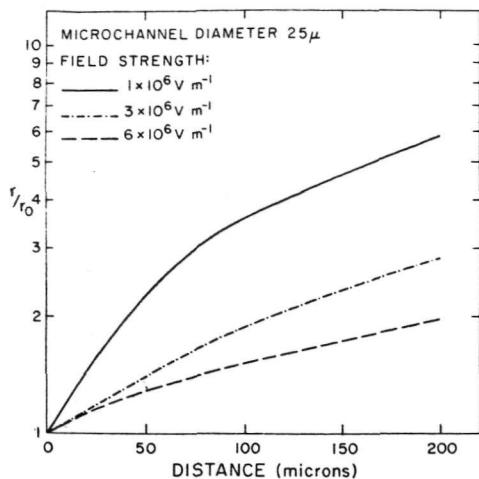
Fig. 20. Variation in the radius of the electron beam as a function of the accelerating electrostatic field for MCP with 25-μm diam microchannels and a gain of 2×10^7.
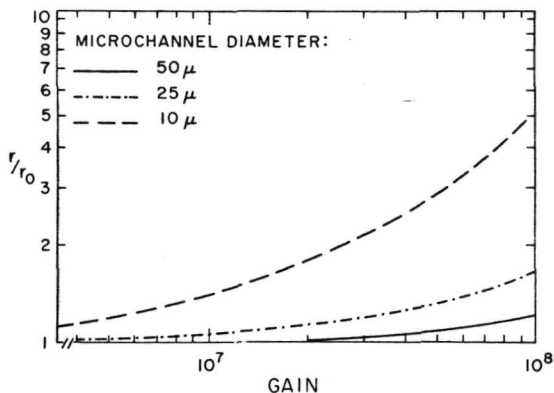

Fig. 21. Variation in the radius of the electron beam as a function of the gain of the MCP. MCP-to-anode spacing 25 μm and MCP-to-anode bias potential +150 V.

U = initial potential of electrons;
E_z = accelerating electric field;
r = initial beam radius, $Z = 0$;
$r_0{}'$ = $(dr/dz)_0$;

and other symbols are as before. The calculation for the output of the MCP is simplified by assuming that the initial convergence is zero. Hence the function R_0 will be zero, and the expressions for C and $\dot{W}_0$ reduce to

$$C = -2 \ln W_0$$

and

$$\dot{W}_0 = -\tfrac{1}{2} W_0.$$

Depending on the sign of C, the function $|F(W_0,C)|$ is determined from the graphs of Vibrans (Fig. 2 or Fig. 3)[18] reproduced in Hutter (Fig. 5 or Fig. 6).[19]
The function $F(W,C)$ is then calculated from

$$F(W, C) = \ln(1 + 2Z)^{1/2} + \frac{\dot{W}_0}{|W_0|} |F(W_0, C)|$$

and the function W obtained by reinserting the value of $|F(W,C)|$ into the appropriate graph of Vibrans.
The electron beam spreading is then given by

$$\frac{r}{r_0} = \frac{W}{W_0}(1 + 2Z)^{1/4}.$$

We have calculated the electron-beam spreading at the output of the MCP for a number of different conditions using the simplifying assumptions already defined. The spreading of the output beam from three MCP's, having different microchannel diameters and a constant gain of 2×10^7, as a function of the MCP-to-anode spacing is shown in Fig. 19. The effect of varying the accelerating electrostatic field is shown in Fig. 20, and effect of varying the gain is shown in Fig. 21.

The calculated results shown in Fig. 20 are in good agreement with our experimental data from the sixty-four-element breadboard array, even though no allowance was made for the effects of charge spreading at the interface between the plates. Furthermore, we may infer from the experimental data that a spreading of up to 20% between the output of the MCP and the anode array will have no significant effect on the spatial resolution of the system. Thus, the principal conclusions from this analysis are:

(1) The spatial resolution is directly proportional to the distance between the output of the MCP and the anode array.

(2) The spatial resolution can be improved by increasing the value of the accelerating electrostatic field; however, the degradation of resolution produced by a large MCP-to-anode spacing cannot be corrected with any reasonable value of the electrostatic field strength.

(3) Attempts to improve the spatial resolution of the system by employing very small microchannels (10 μm or less in diameter) will only be effective if the MCP-to-anode spacing is kept comparable to the MCP diameter. This is particularly important for high-gain systems (see Fig. 21) and imposes strict requirements on the flatness of both the output face of the MCP and the anode array.

References

1. D. S. Evans, Rev. Sci. Instrum. **36,** 375 (1965).
2. J. Adams and B. W. Manley, Trans. IEEE Nucl. Sci. **NS-13,** (3), 88 (1966).
3. G. Eschard and B. W. Manley, Acta Electron. **14,** 19 (1971).
4. A. W. Woodhead and G. Eschard, Acta Electron. **14,** 181 (1971).
5. J. G. Timothy and L. B. Lapson, Appl. Opt. **13,** 1417 (1974).
6. D. Washington, Mullard Ltd., London, E.C.2, England. British Patent 1,352,732 (1974).
7. U. S. Patent 3,374,380 (1968).
8. J. G. Timothy, Rev. Sci. Instrum. **45,** 834 (1974).
9. G. R. Riegler and K. A. More, Trans. IEEE Nucl. Sci. **NS-20,** (1), 102 (1973).
10. J. M. Morton and W. Parkes, Acta Electron. **16,** 85 (1973).
11. M. Lampton and F. Paresce, Rev. Sci. Instrum. **45,** 1098 (1974).
12. C. E. Catchpole and C. B. Johnson, Publ. Astron. Soc. Pac. **84,** 134 (1972).
13. Galileo Electro-Optics, Galileo Park, Sturbridge, Mass.
14. Mullard Ltd., Torrington Place, London W.C.1, England. Marketed in U.S.A. by Amperex Electronic Corporation, Hicksville, N.Y.
15. ITT Electro-Optical Products Division, Roanoke, Va.
16. D. J. Ruggieri, Trans. IEEE Nucl. Sci. **NS-19,** (3), 74 (1972).
17. H. Moss, Wireless Engineer (Electron. Technol.) **22,** 316 (1945).
18. G. E. Vibrans, Massachusetts Institute of Technology-Lincoln Laboratory, Technical Report 308 (1963).
19. R. Hutter, in *Focusing of Charged Particles,* A. Septier, Ed. (Academic, New York, 1967), Vol. 2.
20. A. J. Guest, Acta Electron. **14,** 79 (1971).

Two-dimensional photon-counting detector arrays based on microchannel array plates*

J. G. Timothy

Center for Astrophysics, Harvard College Observatory and Smithsonian Astrophysical Observatory, 60 Garden Street, Cambridge, Massachusetts 02138

R. L. Bybee

Ball Brothers Research Corporation, Boulder, Colorado 80302

The production of simple and rugged photon-counting detector arrays has been made possible by recent improvements in the performance of the microchannel array plate (MCP) and by the parallel development of compatible electronic readout systems. The construction of proximity-focused MCP arrays of novel design in which photometric information from ($n \times m$) picture elements is read out with a total of ($n + m$) amplifier and discriminator circuits is described. Results obtained with a breadboard (32×32)-element array employing 64 charge-sensitive amplifiers are presented, and the application of systems of this type in spectrometers and cameras for use with ground-based telescopes and on orbiting spacecraft discussed.

INTRODUCTION

The microchannel array plate (MCP) possesses a number of major advantages over conventional discrete-dynode electron multipliers. In particular it produces a high gain with a low applied potential and has an image-intensifying capability. In order to exploit the full sensitivity, dynamic range, and photometric stability of the MCP, it is necessary to employ pulse-counting readout systems working directly at the output of the plate. A number of systems of this type have been described in the literature[1-3]; however, these systems have been designed to employ a limited number of amplifiers, two for a one-dimensional array and four for a two-dimensional array, and consequently have significant limitations in terms of both dynamic range and spatial resolution. Although these systems are highly efficient for applications where very low signal levels are obtained, such as galactic x-ray astronomy, they are not suitable for use with the high signal levels obtained from laboratory ultraviolet and soft x-ray sources or from telescopes for solar or stellar observations at uv and visible wavelengths. In order to overcome these limitations in dynamic range and spatial resolution, we have already developed a photon-counting detector array of high dynamic range, employing discrete anodes in proximity focus at the output of the MCP, in which each anode (i.e., picture element) is connected to an individual amplifier and counting circuit.[4] This type of system, however, has its own limitations in that the total number of picture elements (pixels) is limited to about 500 by the currently available electronic and ceramic technologies. To overcome this limitation we have recently designed a novel readout system, which can be produced in a variety of two-dimensional and extended one-dimensional formats, and with which photometric data from ($n \times m$) pixels are read out with a total of ($n + m$) amplifier and discriminator circuits. The readout system employs two sets of orthogonal linear anodes (row and column), insulated from each other, but exposed to the output face of the MCP. The output charge from the MCP is divided between the row and column anodes at the intersection where the event occurs, allowing the spatial location to be identified by the coincident arrival of pulses on the appropriate row and column anodes. This paper will describe the performance of a breadboard two-dimensional (32×32)-pixel array, employing 64 charge-sensitive amplifiers, and having a spatial resolution of $50\,\mu$. The use of this type of photon-counting detector array, with greater than 10^4 pixels, at ground-based telescopes and on orbiting spacecraft will also be discussed.

MICROCHANNEL ARRAY PLATES

The performance characteristics of the continuous-channel electron multiplier (CEM) have been well documented in the literature[5-8] and will not be considered further here.

It should be noted, however, that the performance of a CEM depends basically on the length-to-diameter ratio of the channel and not on the absolute physical dimensions. Consequently, the CEM can be reduced in size to a limit set by the available glass technology (currently about $8\,\mu$ in diameter), and large numbers of these microchannels can then be assembled in a billet to form a microchannel array plate (MCP). Since each channel is an independent photomultiplier, the MCP is a detector with an imaging capability similar to that of a photographic plate, but with sufficient gain to permit photon counting.

However, a basic problem exists with the operation of presently available MCPs; namely ion-feedback instabilities at high operating potentials and high ambient pressures. These problems arise from the straight geometry of
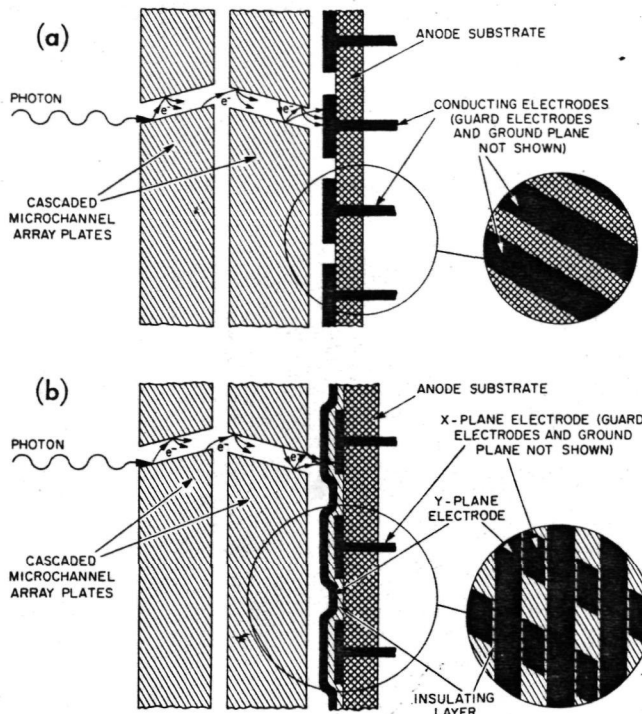
FIG. 1. Proximity-focused MCP detector arrays. (a) Discrete-anode array; (b) coincidence-anode array.

the microchannels. To prevent ion feedback in a straight-geometry microchannel the gain of a single MCP is generally limited to about 10^4, and the device can be operated only at pressures below 10^{-6} Torr. In order to achieve higher gains it is, however, possible to couple two MCPs in cascade, as shown in Fig. 1. This configuration can be constructed with suitable bias angles and plate orientations so that positive ions are trapped at the interface between the two plates. The total voltage across the plates can then be increased to the level at which a saturated output pulse-height distribution is obtained.

COINCIDENCE-ANODE ARRAYS

The coincidence-anode array is a direct descendent of the discrete-anode array which was our first development.[4] Both types of array are shown in Fig. 1. The coincidence-anode array [Fig. 1(b)] consists of two sets of orthogonal linear electrodes (row and column), insulated from each other, but exposed to the output face of the MCP. The output charge from the MCP is divided between the row and column anodes at the intersection where the event occurs, the spatial location being identified by the coincident arrival of pulses on the appropriate row and column anodes. It is thus possible with this system to obtain photometric information from $(n \times m)$ pixels using only $(n+m)$ amplifier and discriminator circuits. The construction of the breadboard anode array, produced using thin-film technology by Raytheon, Inc.,[9] is shown in Fig. 2. The first set of aluminum electrodes, 25 μ in width and 1.6 mm in length, set on 50-μ centers, was sputtered onto a quartz substrate that was polished flat to better than 2 μ. The fanout of the electrodes to the connector pads at the edges of the 5×5 cm² substrate was arranged

so that the interelectrode capacitance was kept below 2 pF. The first set of electrodes was then completely covered by an evaporated quartz film 2500 Å thick. The second set of aluminum electrodes was then sputtered orthogonally to the first set on the insulating quartz film. In order to keep the exposed areas of the two sets of electrodes approximately equal, the upper set was 15 μ in width and 1.6 mm in length, set on 50-μ centers. Following the deposition of the second set of electrodes the entire array was inserted in a plasma discharge with photoresist-masking to protect the upper electrodes. The quartz insulating film in the spaces between the upper electrodes was then etched away to expose the lower electrodes (Fig. 3).

The complete array was mounted on a printed-circuit connector card on the front face of the amplifier module, the MCPs being held in proximity focus against the array by means of a 25-μ thick Mylar spacer and a spring loaded support structure (Fig. 4).

ELECTRONICS

The block diagrams of the data-handling and display electronics are shown in Fig. 5. As noted earlier, the output pulses from the MCP are collected by the 32 row and
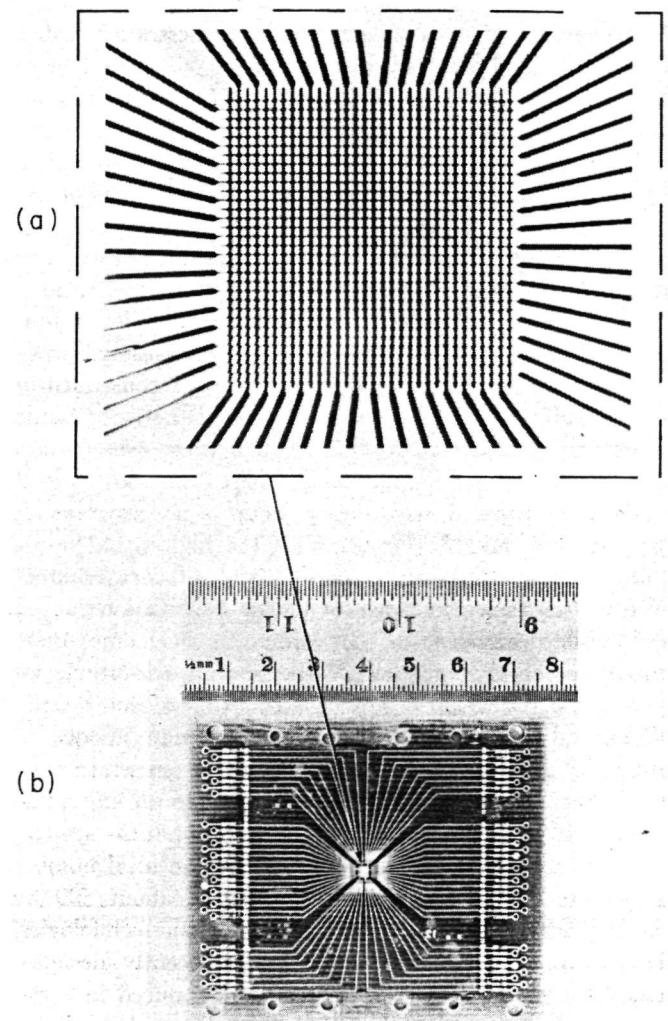

FIG. 2. Breadboard (32×32)-element array. (a) Photomask; (b) assembled array of aluminum electrodes on quartz substrate.

32 column anodes and detected by a total of 64 charge-sensitive amplifier and discriminator circuits. An output charge packet of 10^{-12} C (equivalent to a gain of 6.3×10^6 in the MCP) produces a 1-V output pulse from the charge-sensitive amplifiers. The output from each amplifier [Fig. 6(a)] is fed to a separate discriminator and one-shot circuit [Fig. 6(b)] which generates a 10-V logic pulse, 300 nsec in width, compatible with the C-MOS data-handling and display circuits when the discriminator threshold is exceeded. The discriminator threshold can be varied over the range 8×10^{-14} (5×10^5 electrons·pulse^{-1}) to 1.1×10^{-11} C (7×10^7 electrons·pulse^{-1}) from outside the vacuum system.

In operation the digital data from the 32 column amplifiers and the 32 row amplifiers are fed to two 32-line-to-5-line binary encoders [Fig. 5(a)]. These encoders generate two 5-bit binary address words in addition to row and column event pulses which are fed to a coincidence detection circuit. If a row and a column pulse occur within 150 nsec of each other the detection circuit generates an event pulse to initiate the storage cycle of a 10-bit×1024-word random access memory (RAM). In this cycle the 10-bit location address word is first loaded into the memory address register. The data stored in the addressed register are then read and loaded into the external register. This register is then incremented by one event and loaded back into memory. The total cycle time of the coincidence-detection and memory-address circuits is 1 μsec, allowing a total count rate of 10^5 counts·sec^{-1} (Poissonian arrival) to be detected with the anode array.

The data stored in the memory are read out by a separate timing control circuit [Fig. 5(b)] into a second 10-bit ×1024-word RAM after any one of 15 selectable integration times ranging from 0.25 to 4096 sec. The readout time for each data frame is 0.76 sec for video display and 256 sec for plotting. The second RAM stores the data to allow refreshing of the display circuits and to produce a serial biphase output to an on-line digital computer. The count in any selected address in the memory may be dis-
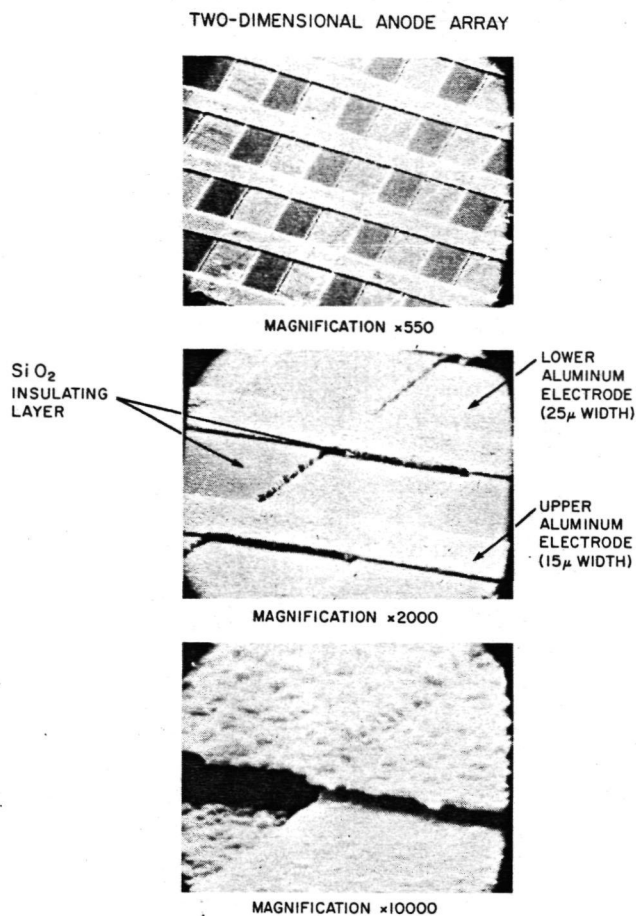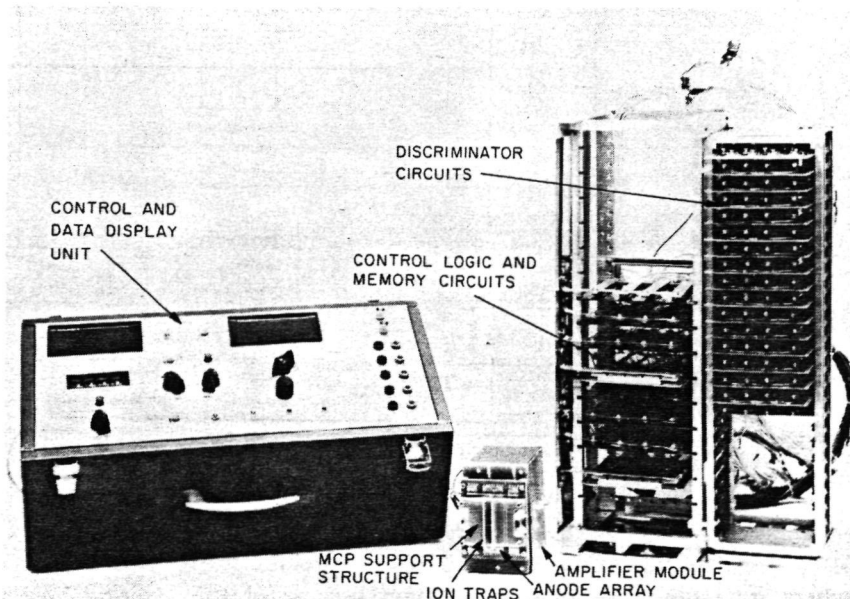
played in digital format, while the intensities in all 1024 pixels are presented in analog format on a CRT or plotter.

RESULTS

We have evaluated cascaded MCPs at extreme ultraviolet (euv) wavelengths[4,8] and have found the performance to be greatly inferior to that of a conventional CEM. Consequently we have also investigated techniques to

TWO-DIMENSIONAL ANODE ARRAY

MAGNIFICATION ×550

SiO$_2$ INSULATING LAYER

LOWER ALUMINUM ELECTRODE (25μ WIDTH)

UPPER ALUMINUM ELECTRODE (15μ WIDTH)

MAGNIFICATION ×2000

MAGNIFICATION ×10000

Fig. 3. Scanning electron micrographs of assembled anode array.

DISCRIMINATOR CIRCUITS

CONTROL AND DATA DISPLAY UNIT

CONTROL LOGIC AND MEMORY CIRCUITS

AMPLIFIER MODULE

MCP SUPPORT STRUCTURE

ION TRAPS ANODE ARRAY

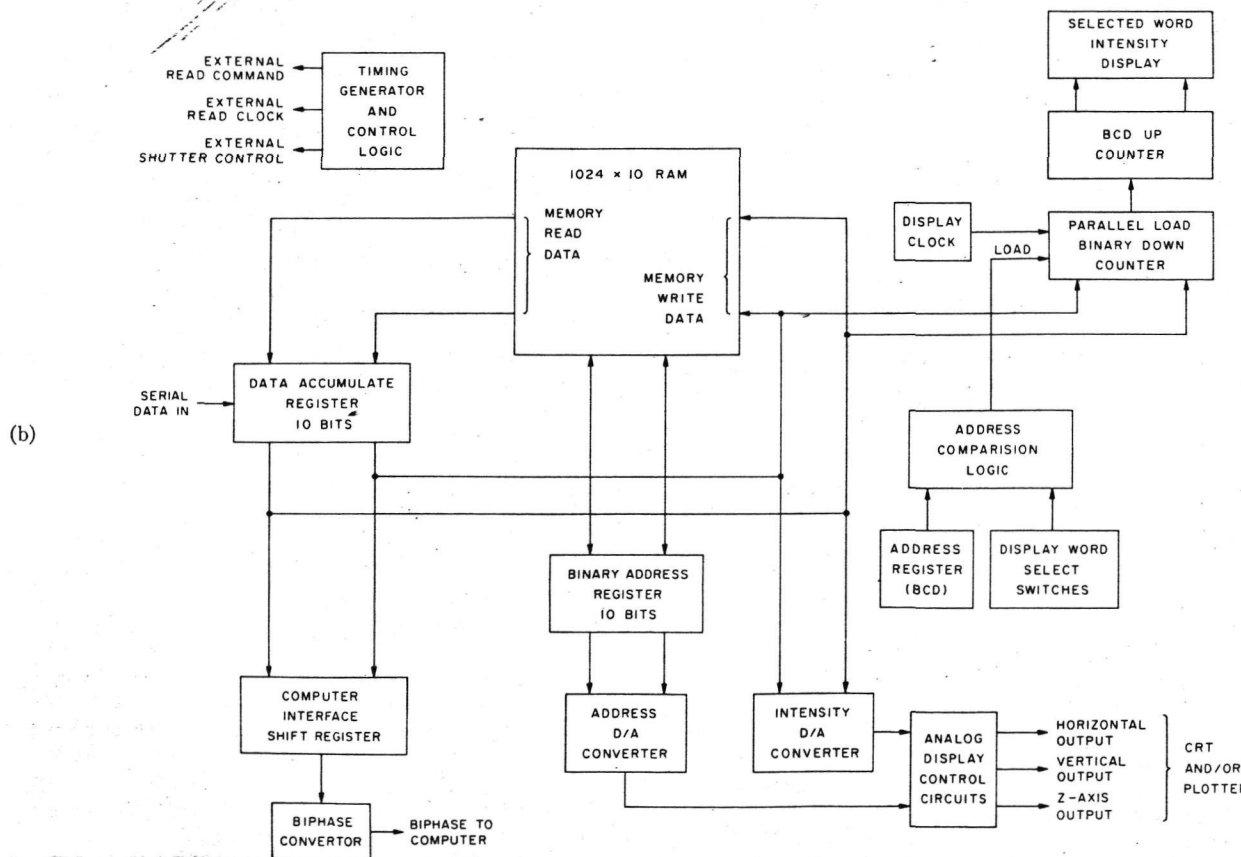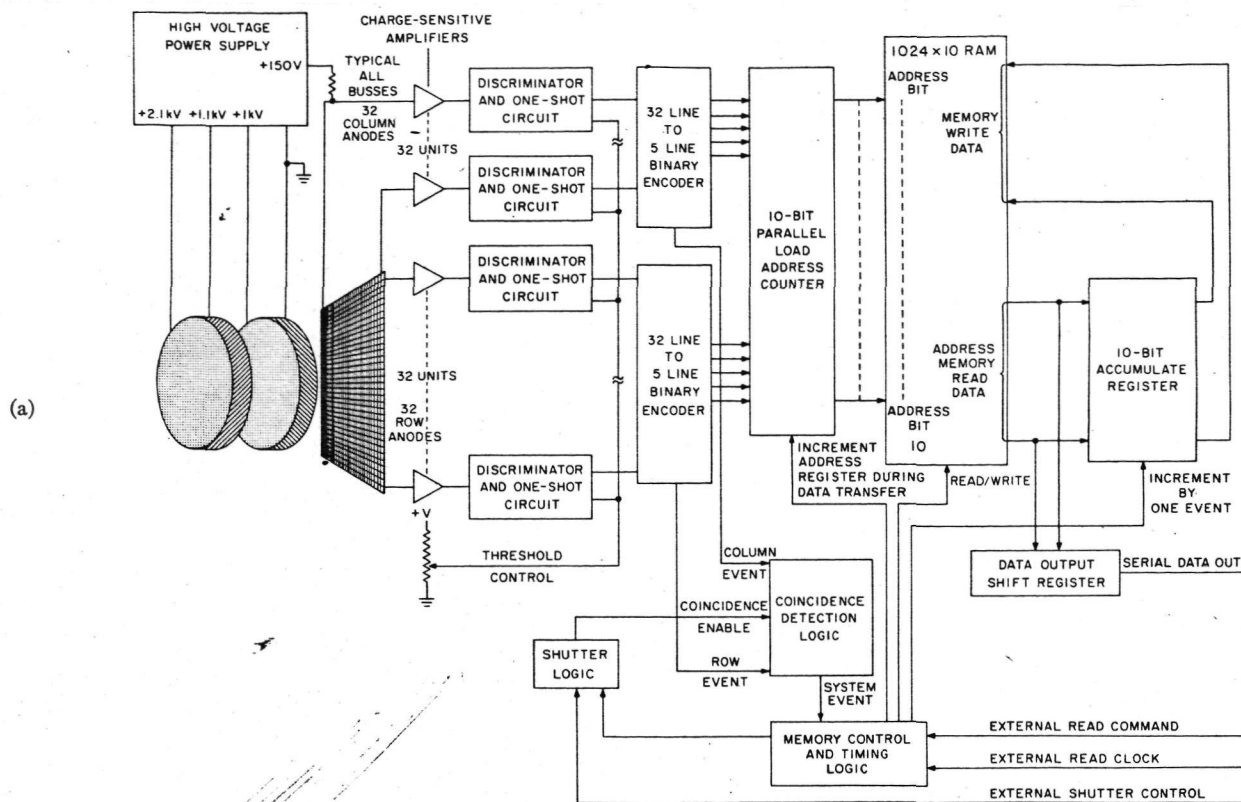Fig. 4. Assembled (32×32)-element detection system.

(a)

(b)

FIG. 5. Block diagram of data-handling and display electronics. (a) Pulse-counting and coincidence-detection circuits; (b) digital and analog display circuits.

eliminate the problem of ion feedback. The angled-field MCP produced by Galileo, Inc.,[10] shows promise but suffers from problems of gain reduction because of the accumulation of space charge on the insulating strips in the channel wall used to establish the angled electrostatic field.[11] We are currently evaluating the performance of

development-model MCPs supplied by Amperex, Inc.,[12] which employ curved microchannels to inhibit ion feedback. The initial results of these tests have proved highly successful, and data will be presented in the literature shortly. However, since MCPs employing curved microchannels are still in the development stage, the initial evaluation of the breadboard two-dimensional array described in this paper was undertaken using two Galileo BX 3040 straight-geometry MCPs (38-μ channels on 50-μ centers) in cascade. The limited performance of the cascaded MCPs in the "chevron" configuration[4,8,11] prevented the full potential of the system from being attained, but did permit a thorough analysis of the basic characteristics of the array.

The high-voltage characteristic for one pixel in the array is shown in Fig. 7. As expected, no stable counting plateau was obtained for any practical value of the applied accelerating potential. This is the direct result of the broad output pulse-height distribution of the cascaded MCPs which causes low amplitude pulses to be lost below the discriminator threshold. Increasing the gain by in-

creasing the value of the accelerating potential on each MCP above 1450 V is not possible because of the onset of ion-feedback instabilities at any practical operating pressure. Decreasing the threshold is also not possible since the wide range of amplitudes in the output pulses causes significant capacitative crosstalk between adjacent electrodes at lower discriminator thresholds.

We have noted an additional effect that further reduces the gain of an MCP in a proximity-focused array, namely the collection of charge by the electrode on the output face of the plate. The electrode is allowed to penetrate the microchannels to a depth of about one diameter ("end-spoiling"[13]), in order to improve the collimation of the output electron beam when the MCP is operated at low gain in a linear mode. The collection of charge by this output electrode when the MCP is operated in the saturated mode can be reduced by increasing the bias potential between the output face and the anode array as shown in Fig. 8. Increasing the bias potential also reduces the effects of charge spreading due to space-charge repulsion in the electron cloud and to repulsion
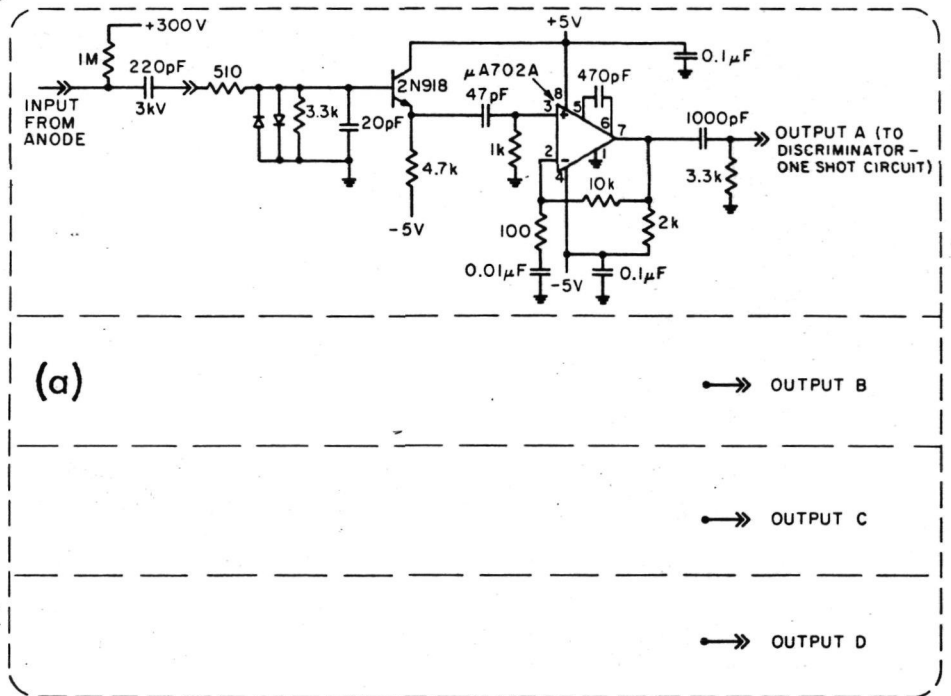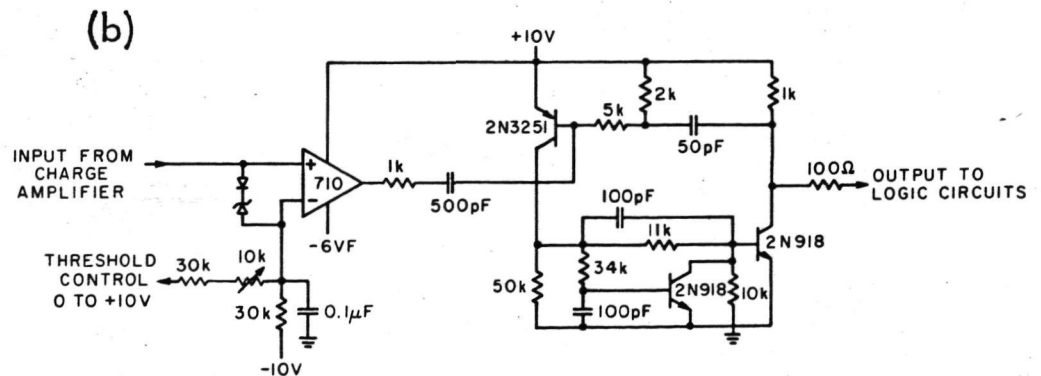

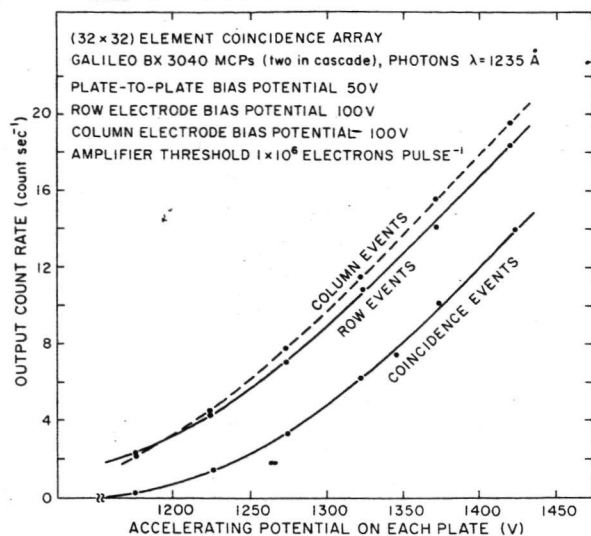FIG. 6. (a) Amplifier circuit; (b) discriminator circuit.

FIG. 7. High-voltage characteristic for a single pixel. MCP-to-anode spacing 100 μ, pressure 2×10^{-7} Torr. Column electrodes are closest to the output face of the MCP.

effects from space charge on the insulating substrate between the anode electrodes.

The operating characteristics shown in Figs. 7 and 8 are essentially identical to those obtained with cascaded MCPs in a discrete-anode array.[4] Consequently, it is clear that the addition of the second, orthogonal, set of anodes did not have any detrimental effect on the basic system performance. However, the division of charge between the row and column anodes was dependent on the bias potential between the two sets of anodes. The best performance was obtained with the same value of the bias potential on the row and column anodes (Fig. 9), a potential difference of about ±3 V from nominal, having no effect on the collection efficiency in spite of the low mean energy of the electrons (about 30 V)[14] in the output beam.

It can be seen in Figs. 7, 8, and 9 that the number of events detected on the row anodes and on the column anodes greatly exceeds the number of coincidence events for the selected pixel. This is because of the mismatch between the dimensions of the microchannels and the
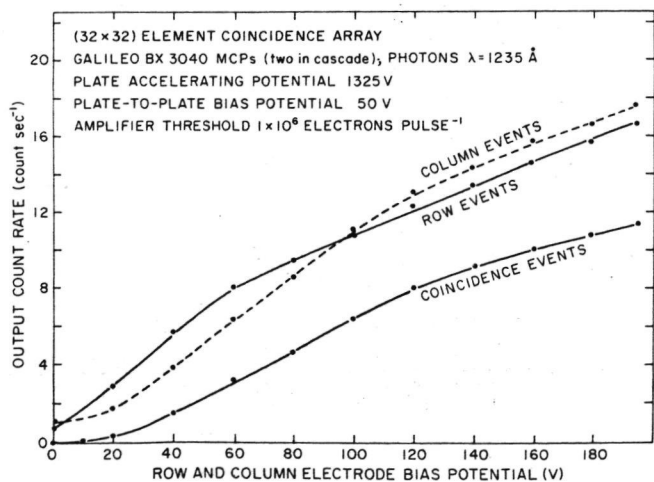

FIG. 8. Variation of the output count rate from a single pixel as a function of the anode-array bias potential. MCP-to-anode spacing 100 μ, pressure 2×10^{-7} Torr.
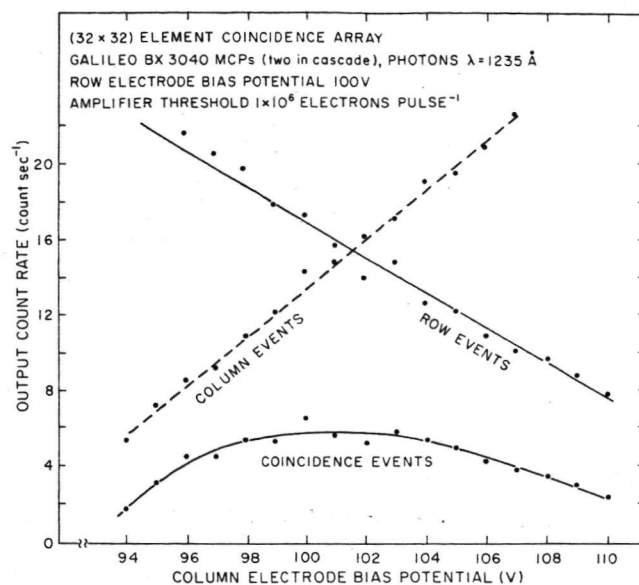
FIG. 9. Variation of the output count rate from a single pixel as a function of the bias potential between the row and column anodes. MCP-to-anode spacing 100 μ, pressure 2×10^{-7} Torr.

anodes in the breadboard array which allowed the output charge from certain microchannels to be collected uniquely by either a row or a column anode. Also the distribution of charge can be such as to result in a row or column event pulse having an amplitude below the high discriminator threshold used in these initial investigations.

In order to evaluate the imaging properties of the detector, the array was illuminated with 1235 Å radiation through a 20-μ pinhole. The output data as recorded on the video display are shown in Fig. 10. It can be seen that the theoretical system resolution of (50×50) μ^2 was achieved, although a high discriminator threshold of 2×10^6 electrons·pulse^{-1} was required to eliminate the effects of capacitative crosstalk. Furthermore, the inherent mismatch between the microchannels and the anodes in the breadboard array caused a degradation of the spatial resolution at certain locations. The image of the 20-μ pinhole, recorded with a lower discriminator threshold of 1×10^6 electrons·pulse^{-1}, is shown in Fig. 11 in the analog plotter
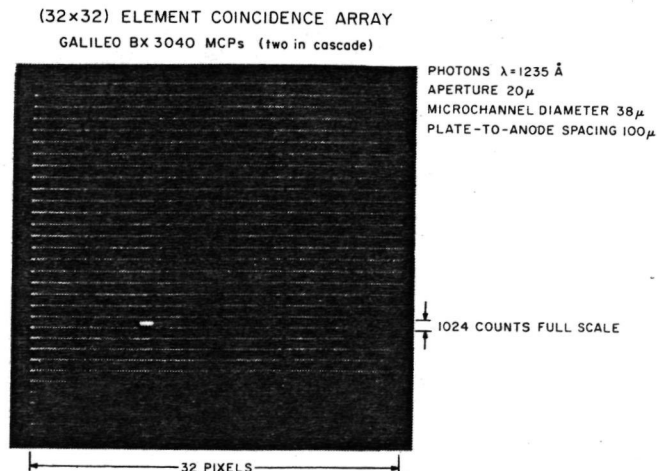

FIG. 10. Image of 20-μ pinhole recorded with breadboard (32×32)-element array. Video display output. Discriminator threshold 2×10^6 electrons·pulse^{-1}.
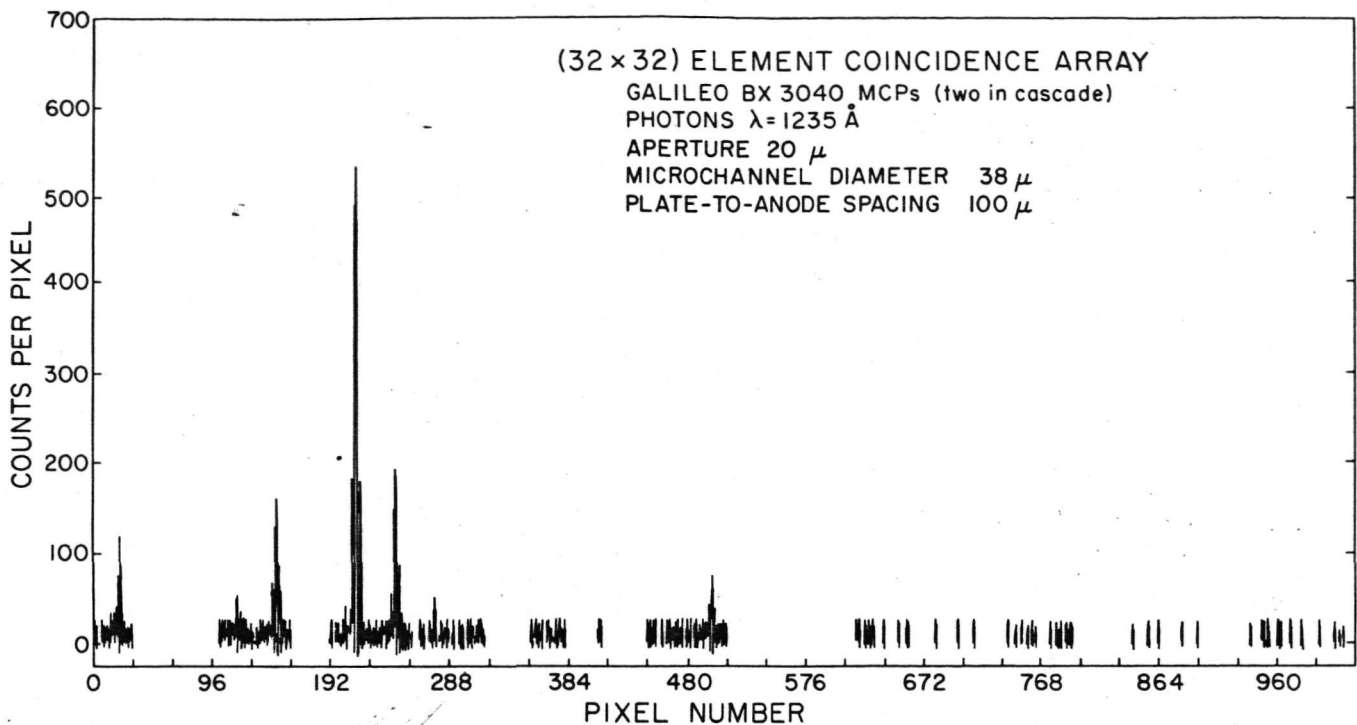
FIG. 11. Image of 20-μ pinhole recorded with breadboard (32×32)-element array. Analog plotter output. Discriminator threshold 1×10^6 electrons·pulse⁻¹.

format. Three effects, arising both from the spatial mismatch between the microchannels and the anodes and from the poor pulse-height distribution of the cascaded MCPs, can be seen in the data. First, the image is broadened over several adjacent pixels because of charge spreading at the interface of the cascaded MCPs. Second, the production of coincident pulses on either two row anodes or two column anodes because of capacitative crosstalk produces incorrect location address words, resulting in the storage of spurious ghost images. Finally, sections of the array produce no output pulses since all the output charge is collected on either a row or a column anode. All these effects arise from the simple geometry of the breadboard array and can easily be corrected in future systems. The operation of a two-dimensional coincidence-anode array in proximity focus with an MCP was thus successfully demonstrated in the laboratory tests.

FUTURE DEVELOPMENTS

The performance data for the breadboard array are now being applied to the production of practical systems of this type for imaging and spectroscopy with both ground-based and spaceborne telescopes. Furthermore, the newly available MCPs which employ curved microchannels have operating characteristics identical to those of a conventional CEM. Consequently, the problems resulting from the broad pulse-height distribution of a set of cascaded MCPs can now be eliminated.

Since the MCP is a high-gain multiplier, we can tolerate a high level of distributed capacitance in the anode array and still maintain a very good signal-to-noise ratio at the output of the charge-sensitive amplifier. Consequently, we can lay out a two-dimensional coincidence array in an

extended linear format as shown in Fig. 12. This array, now under development, employs 160 amplifiers to record photometric information from (2×1024) pixels, each having dimensions of (30×300) μ^2, and is ideally suited for use in high-efficiency spectrometers for faint object spectroscopy. The format of the array can be exactly matched to the dispersion characteristics of the diffraction grating, and in addition, spectra of source and background may be recorded simultaneously. The use of a lattice structure for the upper anodes, as shown in Fig. 12, guarantees the uniform distribution of charge from an 11-μ diameter microchannel at any location. Furthermore, the spacing and separation of adjacent anodes ensures that the amplitude of cross-coupled signals arising both from charge spreading and capacitative crosstalk never exceeds 5% of the initial signal level.

Although the dynamic range of the coincidence-anode array is not as great as that of the discrete-anode array, it is considerably greater than that reported for the resistive-anode readout system.[3] In addition, the coincidence-anode system does not have the pincushion distortion inherent in the two-dimensional resistive-anode array. Furthermore, the dynamic range of the system will adjust automatically to optimize the performance for the type of image being recorded, i.e., the maximum speed of the electronics is either divided uniformly among all pixels for a uniform flat field, or is applied to a particular location to monitor a single bright point source in the field of view. We expect to reduce the data storage cycle time in future units to the order of 200 nsec. Consequently the (2×1024)-pixel array will have a maximum count rate capability for uniform flat-field illumination of 244 counts ·sec⁻¹·pixel⁻¹ (Poissonian arrival).
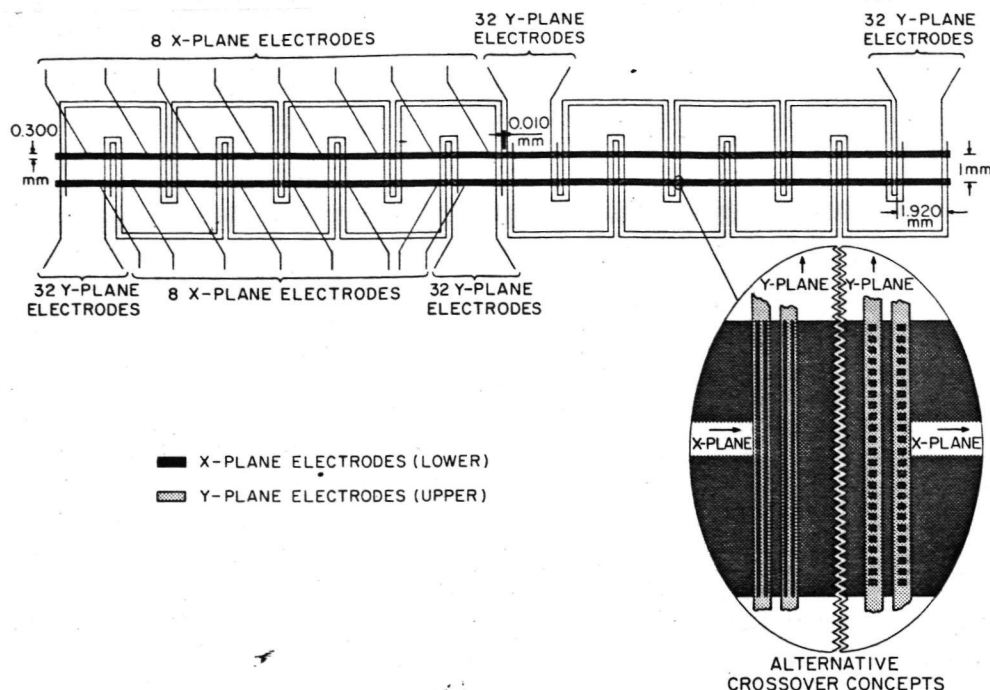
FIG. 12. Schematic of (2×1024)-pixel coincidence array. Sixty-four Y-plane (upper) electrodes cross two sets of eight contiguous X-plane (lower) electrodes to form (2×512) pixels in each half of the array.

Microchannel array plates are constructed from a semiconducting glass which has a work function of about 5 eV. An uncoated MCP can thus be used as an efficient photomultiplier only at euv wavelengths in the range 300–1250 Å. The wavelength range can, however, be extended in a number of ways. First, an MCP can be coated with an opaque MgF_2 cathode at the input of the microchannels to produce a high-efficiency open-structure detector for soft x rays in the wavelength range 20–300 Å. Second, it is possible to integrate the MCP and anode array with either an opaque photocathode, or with a semitransparent photocathode in proximity focus at the input of the

microchannels, in a sealed tube for use at uv and visible wavelengths.

The conceptual layout of sealed MCP "wafer" tubes which we are now constructing is shown in Fig. 13. Two versions of the tube are being produced in the first phase of the development program. The first tube is a (10×10)-pixel discrete-anode array, having an opaque CsI photocathode and a MgF_2 window for operation at wavelengths from 1200 to 1800 Å. The second tube is a (2×1024)-pixel array, employing the coincidence-anode configuration shown in Fig. 12, and a semitransparent trialkali (S-20) photocathode for operation at wavelengths from 3500 to
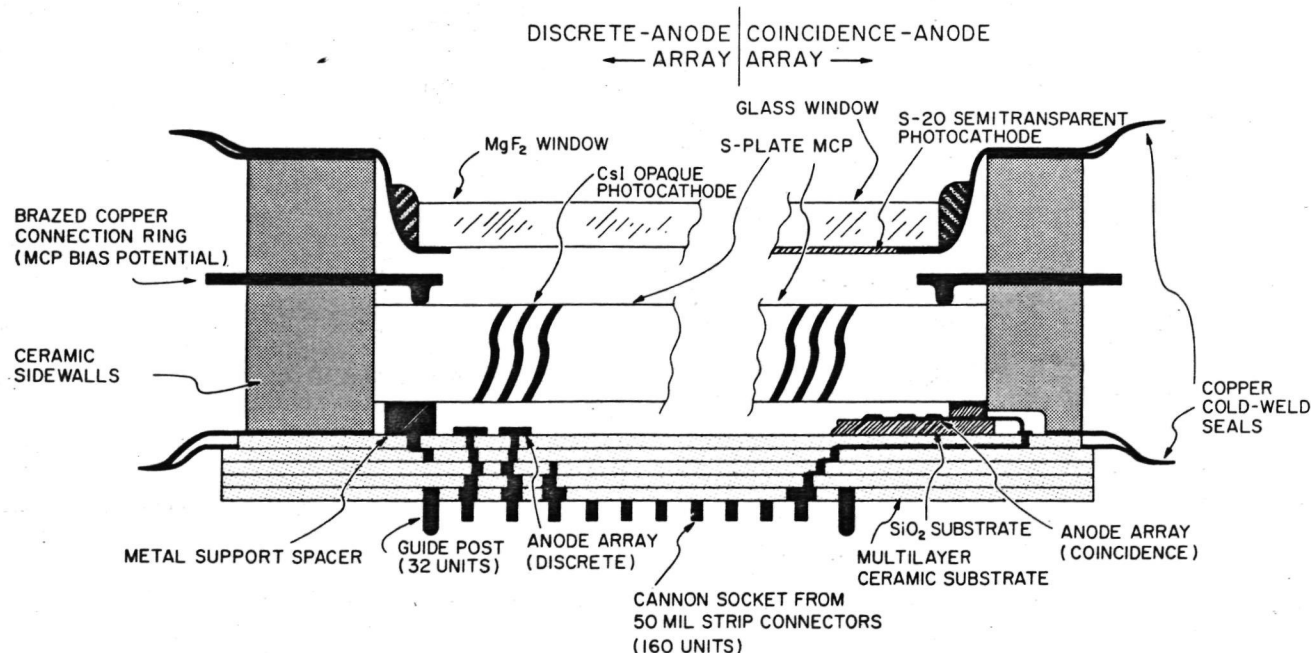

FIG. 13.   Concept of sealed "wafer" tube for use at uv and visible wavelengths (not to scale).

7000 Å. This tube will be used initially for faint object spectrophotometry with the Harvard College Observatory ground-based telescopes; it is, however, ideally suited for spaceborne applications such as the Faint Object Spectrometer proposed for flight on the Large Space Telescope.

The multilayer ceramic header in the wafer tube (Fig. 13) maintains a constant airside pin configuration for different anode formats. The 160-pin header can thus easily be modified to accommodate a wide variety of anode configurations from a (1×160)-pixel discrete-anode array to an (80×80)-pixel coincidence-anode array. Furthermore, the practical upper limit of 500 pins will permit the construction of tubes having greater than 6×10^4 pixels. Details of the performances of these wafer tubes will be presented in the literature as the development proceeds.

ACKNOWLEDGMENTS

*This work was supported by NASA under contract NAS5-3949.

[1] J. M. Morton and W. Parkes, Acta Electron. **16**, 85 (1973).
[2] M. Lampton and F. Paresce, Rev. Sci. Instrum. **45**, 1098 (1974).
[3] G. M. Lawrence and E. J. Stone, Rev. Sci. Instrum. **46**, 432 (1975).
[4] J. G. Timothy and R. L. Bybee, Appl. Opt. **14**, 1632 (1975).
[5] J. Adams and B. W. Manley, IEEE Trans. Nucl. Sci. **NS-13** (3), 88 (1966).
[6] G. Eschard and B. W. Manley, Acta Electron. **14**, 19 (1971).
[7] A. W. Woodhead and G. Eschard, Acta Electron. **14**, 181 (1971).
[8] J. G. Timothy and L. B. Lapson, Appl. Opt. **13**, 1417 (1974).
[9] Raytheon Co., Equipment Development Laboratories, Sudbury, MA 01776.
[10] Galileo Electro-Optics, Inc., Sturbridge, MA 01518.
[11] J. G. Timothy, Rev. Sci. Instrum. **45**, 834 (1974).
[12] Amperex Electronic Corp., Hicksville, NY 11802.
[13] D. J. Ruggieri, IEEE Trans. Nucl. Sci. **NS-19** (3), 74 (1972).
[14] A. J. Guest, Acta Electron. **14**, 79 (1971).